EXPERIMENTAL AND SIMULATED INVESTIGATIONS OF MARINE DIESEL ENGINE PERFORMANCE AGAINST DYNAMIC BACK PRESSURE AT VARYING SEA-STATES DUE TO UNDERWATER EXHAUST SYSTEMS

by

Jaswinder Singh

in partial fulfillment of the requirements for the degree of

Master of Science
In Marine Technology (SDPO)

at the

Delft University of Technology

on 29_{th} August, 2019

SUPERVISORS:

Rear-Admiral (ret.) Ir. K. Visser, TU Delft
Harsh D. Sapra, Phd candidate, TU Delft

THESIS COMMITTEE:

Rear-Admiral (ret.) Ir. K. Visser, TU Delft
Harsh D. Sapra, Phd candidate, TU Delft
Dr.ir. HJ de Koning Gans, TU Delft

Contents

List of Tables

List of Figures

Table 1: **Nomenclature**

Acronymns

IRP	Inlet receiver pressure	temp	temperature
EVT	Exhaust receiver temperature	est	estimator
AER	Air excess ratio	eV	exhaust valve
ERT	Exhaust receiver temperature	a	air
IRT	Inlet receiver temperature	s	simulations
FFR	Fuel flow rate	m	measurement
MVEM	Mean value estimated model	min	minimum
IRT	Inlet receiver temperature	max	maximum
BP	Back pressure	e	exhaust
WP	Wave period	d	discharge
DE	Diesel engine		
NBP	No external back pressure		

Symbols

p	pressure (bar)
T	temperature (K)
M	torque (Nm)
α	area correction factor
β	power correction factor
$\dot{m}$	mass-flow rate (kg/s)
W	work (J)
C_pulse	pulse correction factor
Π	pressure ratio
τ	temperature ratio
η	speed (rpm)
χ	ratio of specific heats of air and exhaust gas
afr	air-to-fuel ratio
λ	air-excess ratio

Units

s	second
kg/s	kilogram per second
mbar	millibar
m	meter
mWC	meter water column
rpm	revolutions per minute
KW	kilowatt
ppm	parts per million

Subscripts

com	compressor
tur	turbine
ac	air-cover
cac	charger-air cooler
cyl	cylinder
eng	engine
Turbo/TC	turbocharger
OR	outlet-receiver
IR	inlet receiver
exh	exhaust
sv	silencer volume
amb	ambient
const	constant pressure turbocharger system

ABSTRACT

The innovation of underwater exhaust systems on ships increases onboard space, reduces noise emission and allows for zero direct emissions. For defense vessels, stealth is increased as the heat signature reduces due to underwater exhaust. However, there is a disadvantage of dynamic back pressure at the exhaust outlet which deteriorates the performance of the engine. The waves at the exhaust outlet are dynamic consisting of different wave heights depending on sea state and period. These waves cause dynamic back pressure at the exhaust outlet. Experimental and simulation investigations on the effect of externally applied static back pressure due to submerged exhaust is already carried out. It was found that there is an increase in fuel consumption and thermal loading with an increase in static back pressure. But, the sea waves acting at the exhaust outlet is dynamic with fluctuating amplitude and wave period. No experimentally validated research is available in the public domain to understand the effect of externally applied dynamic back pressure due to sea waves on the diesel engine performance. Thus, in this master thesis, the effect of the externally applied dynamic back pressure due to underwater exhaust on the performance of the diesel engine is investigated. Experiments are performed on a pulse turbocharged 4-stroke marine diesel engine at the Netherlands Defence Academy. Effects of dynamic back pressure on engine performance at different sea-states are investigated. The impact of wave significant height and wave period on the performance of the diesel engine is examined separately. Along with the performance of the diesel engine, the effect of back pressure on the emissions are also investigated. In this research experiment, the diesel engine under selected load points is subjected to single and continuous waves of back-pressure with changing amplitudes of 45 mbar, 35 mbar and 25 mbar(Gauge) while the periods were varied between 2, 4, 6, and 8 seconds. The back pressure is replicated with the help of an electronically controlled butterfly valve turbine outlet placed after which controls the resistance to exhaust gas flow to the atmosphere. A Diesel Engine - B model developed at TU-Delft is adopted and verified with the help of measured data from the experiments. The adopted model is a mean value engine model implemented in MATLAB/Simulink environment. Current literature lacks studies on experimental validation of the effects of dynamic back pressure on a marine diesel engine. The verified model is used to simulate the performance with higher sea states which may not be possible to simulate on a test bench.

This research showed that exhaust side parameters (e.g Exhaust receiver temperature) are more critical than the inlet side parameters (e.g. Inlet receiver temperature). Moreover, there is an increase in parameters progressively with increase in the amplitude of back-pressure. Above a wave period value, the engine performance parameters changed by approximately equal values irrespective of varying periods above it. The impact of steady state back pressure is found more severe on the diesel

engine's parameters and fuel consumption compared to externally applied dynamic back pressure of the same amplitude. The recorded emissions show an increase in the concentration of carbon monoxide (CO), carbon di-oxide (CO_2), nitrous oxide (NO) and sulphur di oxide (SO_2) in the exhaust with an increase in back pressure. On the other side, the oxygen concentration decreases with increase in the applied steady state and dynamic back pressure. Simulations suggested that the governor plays a crucial role in tackling the effects of dynamic back pressure by controlling the fuel flow to the diesel engine. The simulation results are also used to provide the applied back pressure ceiling limits in terms of air excess ratio and exhaust valve temperature for the test engine.

.

Chapter 1

INTRODUCTION

Diesel engines are used as the primary power system for main transportation and are still in common use today. They are being widely used in the maritime sector for power generation to meet auxiliary and propulsion power requirements. Low fuel consumption, more space, better efficiency, and low emissions are some of the key driving forces for innovation in diesel engine technology. For e.g, to address the emission concerns, the International Maritime Organization (IMO) has set up strict and urgent emission regulations that must be met by the ship operators [7]. For instance, the IMO TIER-III regulations for NOx emissions are applicable from January 2016 in Emissions Control Areas (ECA) [8]. Similarly, a global sulfur cap will be applicable from 2020, which will require the sulfur content in maritime fuels to be below 0.5% [8]. To meet these emission regulations, current marine engines are equipped with exhaust gas after-treatment technologies such as scrubbers, and/or selective catalytic reactors (SCR) [9]. However, these after-treatment technologies create a pressure loss in the exhaust line that affects engine performance. This pressure drop is called back pressure. It is defined as the difference between the ambient pressure and average exhaust pressure in the exhaust pipe during the exhaust stroke (mean exhaust pressure) [10] The back pressure due to these after-treatment technologies are static. An extensive public literature is available on the effect of static back pressure due to technologies on diesel engine performance. In this master thesis, the effect on the engine performance due to underwater exhaust is carried out. The waves acting at the submerged exhaust outlet is dynamic with varying amplitude based on sea states and varying wave period due to the geographical location. A diesel engine- B model developed at TU Delft is adopted and verified with the experimental results. The model is further used to simulate engine performance with higher sea states and wave period which is not possible to perform on the test engine for the safety of the engine. The detail description about externally applied dynamic back pressure and diesel engine model can be seen in the later sections.

1.1 UNDERWATER EXHAUST

The underwater exhaust is an innovation used in small boats to reduce noise and odor from exhaust. For large boats exhaust escapes from funnel directly into the atmosphere through after treatment plants. In some cases, an alternating solution is used, in which an exhaust pipe escapes near or under the water surface.

The various advantages of the underwater exhaust are listed below [3]

- Reduced noise
- Prevention of direct emission into the atmosphere.
- Saves space when compared to funnel exhaust.
- Increases stealth for naval vessels by reducing infrared detection
- Elimination of bulky and unappealing vertical exhaust funnel with better aesthetics of luxury ships.

The major drawback for such design is the resistance to the flow of the exhaust gases at the outlet which increases the back pressure. The pressure exerted on a moving fluid by obstructions against its direction of flow is called back pressure [11]. In addition to the static back pressure due to after-treatment technologies, diesel engine with submerged exhaust experiences an additional externally applied back pressure due to waves acting at the outlet. This back pressure consists of a steady state back pressure due to the constant sea water head above the exhaust outlet and dynamic back pressure due to pulsating sea waves. The experimental and simulated research is already conducted for the steady state back pressure due to underwater exhaust by Sapra et. al. [3]. In this research study, the effect of the dynamic back pressure due to underwater exhaust is investigated experimentally. The sea waves acting at the exhaust outlet are dynamic with different significant wave height amplitude depending on sea state and varying amplitude depending on the geographical location on the globe. Therefore, back pressure exerted by these waves is also dynamic. This dynamic back pressure imposes high and fluctuating resistance to the exhaust gas flow of the engine. This flow resistance in an underwater exhaust is like the fluctuating flow resistance experienced by a submarine diesel engine at snorkeling depth [12]. At this depth, the pressure loss in the exhaust piping plus the static pressure due to the water head above the snorkel and the dynamic back pressure due to sea waves at the water surface accumulate to form a high and fluctuating pressure loss or back pressure, which is felt at the turbine outlet of the turbocharged engine. From the previous research on static back pressure effects on the diesel engine, it is found that steady state back pressure reduces the operating limits for the diesel engine and deteriorates engine performance [13] [3]. With an increase in back pressure, there is an addition in the pumping work to remove the exhaust gases from the cylinder to atmosphere. This lead to an increase in fuel consumption and exhaust temperature. Apart from this, it may affect the performance of the turbocharger, causing changes in the air-to-fuel ratio. In this research, the dynamic effects of the back pressure is examined experimentally on the 4 stroke pulse turbocharged marine diesel engine. The effect of wave height amplitude and wave period on the performance of the diesel engine is also the part of the exploration. Along with performance, the emissions from the exhaust is also measured and examined. The emission analyzer measured carbon dioxide, carbon monoxide, sulphur dioxide, oxygen and nitrous oxide. From the experimental data, an adopted DE-B model is verified to simulate the engine performances with higher sea states and wave periods which could not be tested experimentally. The model helps in the better understanding and prediction of the performance of the diesel engine at higher sea states. Moreover, the back pressure ceiling limits are also plotted in the engine envelope in which the engine limits are shown in terms of air

excess ratio and exhaust valve temperature. Before this, the previous literature on the topic is discussed in the next section.

1.2 PREVIOUS LITERATURE

Effects of steady state back pressure on engine performance have been investigated by many researchers. Bolt et. al. [14] gave the theoretical relationship between engine air consumption and exhaust pressure by experimenting on 1971 Ford with 0.5-1.5 atmospheric back pressure at different speeds and loads. He stated that air consumption varies with the ratio of absolute back pressure to the absolute inlet manifold. Patil et. al. [15], Joardder et. al. [16] performed an experimental investigation on the effect of back pressure due to after-treatment devices fitted on the exhaust side of naturally aspirated compression ignition (C.I.) engine for performance and emission. The former observed an increase in fuel consumption and an increase in pumping work with an increase in back pressure at the same operating conditions. The latter executed the study at different loads and speeds. He found that there is no significant effect of back pressure at low engine speed on the brake specific fuel consumption (bsfc). At medium and high speed the performance remains constant up to 53.3 mbar (gauge) and over 53.3 mbar, it deteriorates (increase in bsfc). Burnete et. al. [17] also discovered a reduction of torque and power at high rpm with an increase in back pressure but, no significant impact noted at low speed. He stated that in addition to increasing pumping work, exhaust back pressure affects the quantity of post-combustion gases retained in the cylinder from one cycle to next. In another research, Cong et. al. [18] developed an engine model from the experimental data of high speed naturally aspirated engine using Ricardo Wave to predict the Residual Gas fraction at different exhaust back pressure values. By estimating trapped residual gas fraction, the links between the exhaust back pressure and the engine combustion performance and emissions were examined. The above researches were carried out experimentally on a naturally aspirated engine. However, the effects of back pressure on a naturally aspirated engine are different from the effects on a turbocharged engine due to the difference in air-intake, fuel-intake, inlet receiver pressures, exhaust receiver temperatures. Mittal et. al. [19] conducted an experiment on turbocharged, after-cooled diesel engine coupled with a generator rated. The two values for low and high back pressure corresponded to 45 mbar (gauge) and 90 mbar (gauge). He found that the emission of NO_x was cut down at all operating loads whereas soot and particulate matter (PM) increased with increment in back-pressure. All of the above researches are carried out experimentally for steady state back pressure.

Some of the researchers used models to replicate the diesel engine performance and simulate the effect of back pressure on the diesel engine. Michos et. al. [20] used commercial software Ricardo Wave to analyze the effect of back pressure due to Organic Rankine Cycle evaporator as a waste heat recovery system on turbocharged (fixed turbine) marine diesel engine. The model demonstrated an increase in pumping work resulting in an increment in bsfc. Deteriorating performance with a reduction in air-fuel ratio (AFR) and increase thermal loading was also detected. Furthermore, he simulated the performance of diesel engine using two turbocharger strategies namely: waste-Gate and variable geometry turbine. The air-fuel ratio is maintained with both strategies but bsfc is less with VGT. Therefore, the author

concluded that VGT turbocharger is the best solution strategy to curtail the effects of high back-pressure. But, this research lacks the experimental validation of the model. Sapra et. al. [3] performed a combination of experiments and simulation to investigate the effect of externally applied static back pressure on the performance of the diesel engine. The experiments were performed on pulse turbocharged diesel engine at 9 different loads and speeds with back pressure values 25 mbar (gauge) and 50 mbar (gauge). A mean value engine model (MVEM) with compressor and turbine sub-models are calibrated and matched with the assistance of experimental data. The validated model is used to predict and compare constant turbocharged engine performance (with two values of valve overlap) with pulse turbocharged engine. The response of engine with pulse turbocharger engine in handling the exhaust back pressure was found better than constant pressure turbocharged engine with the same valve overlap. In addition to this, the author defined the engine envelope in terms of air excess ratio and exhaust valve temperature to find the thermal overloading and smoke limit. The acceptable back pressure boundaries are also defined based on the exhaust valve temperature and air excess ratio values. The results demonstrated the serious effects of back pressure on air-excess ratio, exhaust receiver temperature, and exhaust valve temperature

All the above-mentioned studies analyzed engine performance against static back-pressure, and none of the research examined the effects of dynamic back pressure on engine performance. Tauzia et. al. [21] used model simulations to provide a general understanding of the effects of dynamic back pressure due to a partially submerged exhaust on the performance of a marine diesel engine. He simulated performances with back pressure ranging from o to 600 mbar. Peter Hield [12] explained in his research that the diesel electric-submarine with turbocharged diesel engine experiences the fluctuating back pressure at snorkeling depth. He used Ricardo Wave software to simulate the performance of a turbocharged diesel engine in such operating conditions. The mean part of water pressure head on the exhaust is considered 1.45 bar. The values for varying part (sinusoidal) with varying amplitude and time period is taken from Bretschneider spectra. He notices that the response of varying back pressure was highly non-linear with dependency on back pressure amplitude, and period fluctuations. Swain et. al. [22] along with predicting engine system performance with fluctuating back pressure also examined the use of variable nozzle geometry turbocharger to counter the dynamic back-pressure. Distinguished improvements in maximum allowable power with variable geometry turbine (VGT) compared to supercharging and fixed nozzle area were noted in their research. It is important to notice that no experimental investigations on the effect of externally applied dynamic back pressure is carried out. The various models used for simulating the engine performance with dynamic back pressure is not validated with experimental results. The literature highlights a lack of experimentally validated research on qualitative and quantitative effects of dynamic back pressure on the performance of a marine diesel engine due to dynamic back pressure.

The research topic for this master thesis is a sub-topic of the project "GasDrive: Minimizing emissions and energy losses at sea with LNG combined prime movers, underwater exhausts and nano hull materials" (project 14504) of the Netherlands Organisation for Scientific Research (NWO), domain Applied and Engineering Sciences (TTW). Out of such a vast research topic, a sub topic discussing under water exhaust is studied in this master thesis. The study regarding the effect of steady

state back pressure is already conducted and analyzed by Sapra et. al. [3]. With a motivation to support the gas drive project, this master thesis research is conducted on the sub-topic "experimental and simulation investigation of the marine diesel engine performance against the dynamic back pressure of varying amplitudes and time periods due to an underwater exhaust system operating in different sea-states" .

1.3 RESEARCH OBJECTIVE

The main objective in this master thesis is to perform experiments on pulse turbocharged 4 stroke diesel engine at The Netherlands Defence Academy to investigate the effect of externally applied dynamic back pressure on the performance of the engine and simulate the engine performance using the adopted DE-B model developed at TU Delft.

The following questions and sub-questions will be answered by the end of the research project.

1. How to set-up the experiment on pulse turbocharged diesel engine with dynamic back pressure.
    - What input is required to be given to the already constructed Arduino in python environment to rotate the electronic controlled butterfly valve to replicate the back pressure created by waves?
2. What are the effects of the externally applied dynamic back pressure on the engine parameters at different load?
    - Which engine parameters are critical to the dynamic back pressure and why?
    - How the wave amplitude and wave period affect the engine parameters?
    - What is time lag for parameters to respond to the dynamic back pressure?
    - How emissions are changing with dynamic back pressure for different loads?
3. How to verify the adopted DE-B model from the experimental results?
    - What is the percentage error between the measured and simulated performances?
    - What is the effect on the fuel consumption of the engine?
    - Defining the allowable limits of dynamic back-pressure in terms of sea state?
    - Which diesel engine component controls the engine performance when external dynamic back pressure is applied?

1.4 STRUCTURE OF THESIS

The basic introduction of the master thesis topic is already presented in the previous sections of this chapter. Next chapter provides the necessary information regarding the test set up and methodology used for the experiments. In this chapter, the load set points along with the wave data used for the various experiment is discussed in detail. It also includes a description of the adopted diesel engine model (DE-B). The equations regarding the modeling of various section of the DE-B model are briefly explained in the same chapter. Chapter 3 consist of the results measured from the experiments performed on the diesel engine. The results for a static, step change, amplitude change (single and multiple waves) and wave period change (single and multiple waves) are analyzed in detail. The experimental results are compared with the simulated results for verification of the model in chapter 4. In chapter five, the discussion is carried out regarding the ceiling limits of back pressure to avoid thermal loading and smoke from the exhaust. The critical wave period and a comparison between static and dynamic back pressure is also done briefly. This is followed by the chapter discussing the emission results measured during the experiments. Lastly, the conclusion and recommendations for future work are provided followed by the appendices.

Chapter 2

TEST SET-UP AND METHODOLOGY

2.1 TEST SET-UP

The test set up for the back pressure experiment is discussed in detail in the upcoming sub-sections. It is initiated with the test engine specification followed by the discussion on the selected load points. The operation of an electronically controlled butterfly valve to replicate the back pressure by the sea waves on the diesel engine is also included.

2.1.1 ENGINE SPECIFICATION

Experiments were performed on a 4-stroke, pulse turbocharged marine diesel engine with a rated power output of 360 kW at 1000 rpm to study the effects of dynamic back pressure on marine engine performance. Table 2.1 provides the engine specifications of the test engine.

Table 2.1: **Engine Specifications**

Engine model	MAN4L2027
Number of cylinders	4
Bore	0.20 m
Stroke	0.27 m
Rated speed	1000 rpm
Rated power	360 KW
Compression ratio	13.4
Fuel injection system	Plunger pump, direct injection
Turbocharger system	Pulse
Maximum back pressure	25 mbar

In this experimental study, the engine measurements are restricted to the maximum set point of 340 kW at 981 rpm to avoid damage to the turbocharger due to thermal overloading. Therefore, the 100% load point presented in this thesis corresponds to 340 KW at 981 rpm. The test engine was connected to a water-brake to

apply the required load, which allowed the engine to run at the required set-point of load and speed.

2.1.2 LOAD SET POINTS

Engine performance against dynamic back pressure was studied at four set-points along the propeller curve as designated in figure 2.1. The experiments are performed twice at each set-point for every back pressure. Table 2.2 shows the load percentage with the corresponding rpm for each set point.

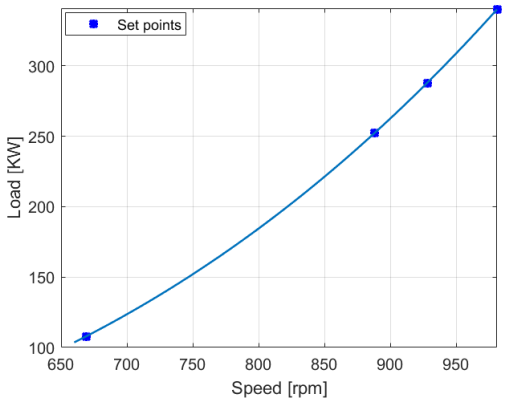

Figure 2.1: **Measurement set-points along propeller curve**

Table 2.2: **Load set-points**

Set Point number	Load [%]	Speed [%]	Load [KW]	Speed [RPM]
1	31.76	68.19	108	669
2	74.11	90.51	252	888
3	84.7	94.59	288	928
4	100	100	340	981

The lowest set-point is limited to 31.7% load where as the highest set point is selected at 100% load (340 KW at 981 rpm). At low load, there is can be a significant large increase in the in-cylinder and exhaust receiver temperature when engine experiences external back pressure [3]. This can increase thermal stresses and cause serious damage to the turbocharger. Moreover, excessive exhaust temperatures can damage seals and grooves causing unintended oil and exhaust gas leakage [23]. At high loads, the absolute exhaust gas temperatures can reach very high values when subjected external back pressure. This can lead to a coked center housing, which will affect turbocharger performance and life [24]. Therefore, the highest set point is restricted to 340 KW at 981 rpm.

2.1.3 ELECTRONICALLY CONTROLLED BUTTERFLY VALVE

In order to replicate the back pressure due to sea waves, an electronically controlled butterfly valve was installed downstream of the turbine in the exhaust line. Figure 2.2 gives the schematic representation of the engine test set up along with the location of the butterfly valve along with different pressure and temperature sensors. The rotation of the electronic controlled butterfly valve can be controlled by Adruino programmed in Python environment. The operation of the butterfly valve is programmed and tested by Marcel Robert Scheuten at NLDA.

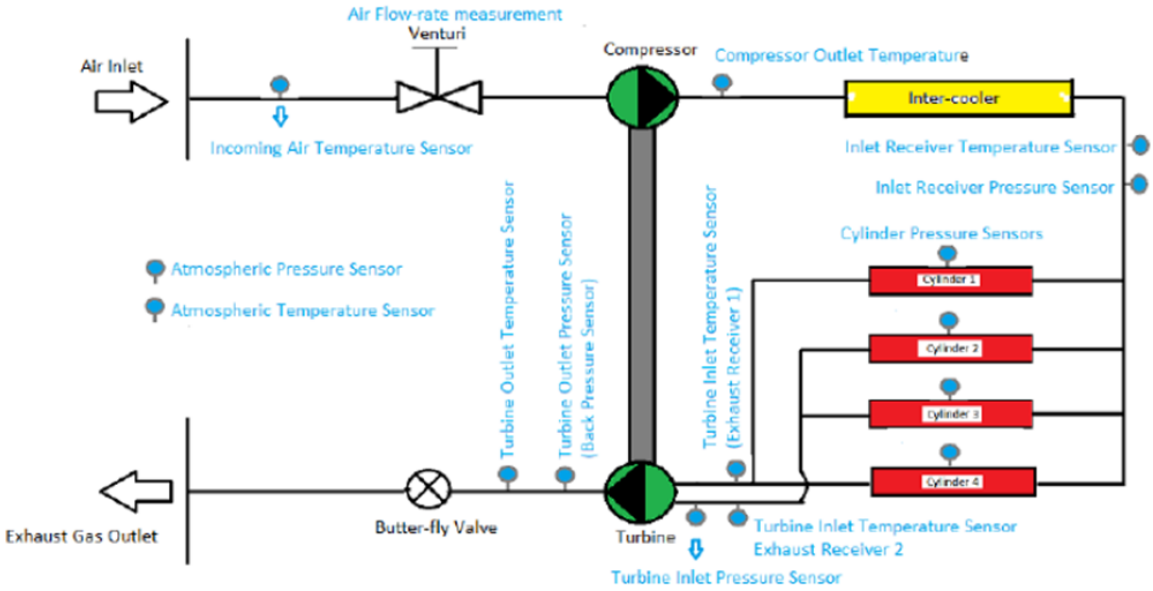

Figure 2.2: **Outline of test set-up and sensor placement [3]**

The Adruino is given an i The butterfly valve rotates to the required angle which is given as an input. The partial closing of the valve creates resistance to the flow of the exhaust gasses and thus reaching the required back pressure. The actual experimental sea wave shape is described as a trochoid [25] in shape. When a circle is rolled along a line, the profile traced by a point on a circle forms the trochoid shape as shown in figure 2.3. The Trochoid shape does approach the sine curve in shape for small amplitudes, found in deep water waves. However at transitional water depth the shape is different, with a narrowing of the peaks of the trochoid compared to the sinusoid [26]. It is difficult to mathematically manipulate trochoidal wave as an input to the butterfly valve [25]. Moreover, the type of wave and its mathematical representation changes with the depth of the sea bed from the water line. Therefore, the selected applied wave input has a sinusoidal form, which can be easily simulated.

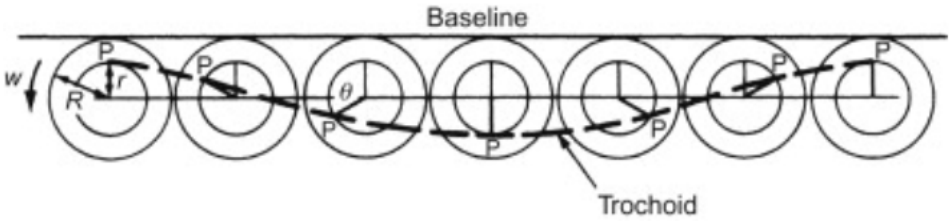

Figure 2.3: **Trochoidal wave [4]**

A single sinusoidal waveform with the valve angle and time is used as an input to the Adruino. The sinusoidal wave input and the corresponding back pressure waveform (output) experienced by the engine is shown in figure 2.4. As depicted in the figure below, the butterfly valve is fully open at 90° valve position whereas 0° corresponds to fully shut valve position. The time on the x-axis represents the wave period of back pressure wave. This matches the average wave period of the sea wave at the exhaust outlet. As seen in figure 2.4 (b), the final applied back pressure wave at the turbine outlet has a square waveform with discrete steps rather than a sinusoidal waveform. This is due to the inertia and the step-wise movement of the butterfly valve in addition to the non-linear effect of the valve movement on the back pressure. Initially, the effect of the butterfly valve on the back pressure, as it starts closing in small steps, is small. However, as it closes further the back pressure increases non-linearly by a higher value. The figure 2.4 (a) shows the butterfly valve input which produced a back-pressure wave (figure 2.4 (b)) of 45 mbar (gauge) amplitude and 6 seconds wave period experienced by the engine running at 100% set point.

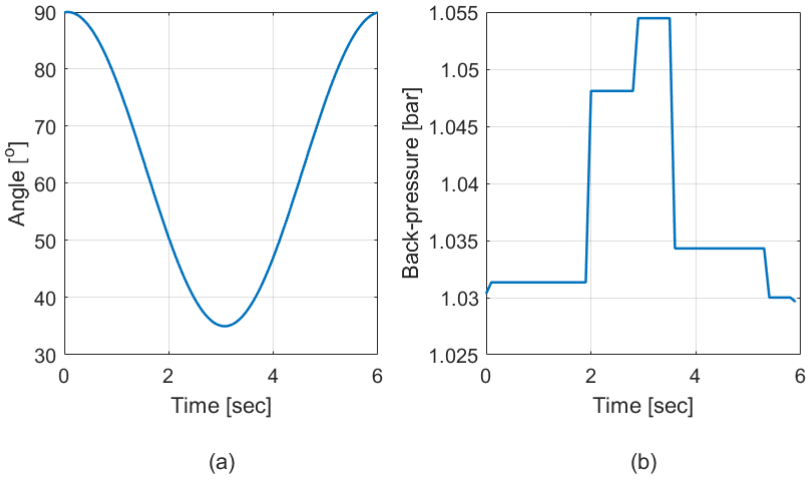

Figure 2.4: **Angle and time input of a sinusoidal waveform for butterfly valve (a) and the corresponding back pressure wave produced (b)**

2.2 METHODOLOGY

A marine diesel engine operating with an underwater exhaust system is exposed to continuous and fluctuating back pressures due to the sea waves at the exhaust outlet.

These waves vary in amplitude or significant wave height (WHT) and average time period (APD) based on the sea-state scales. According to the World Meteorological Organization, the Sea state Scale is described in table 2.3.

Table 2.3: **World Meteorological Organization sea state scale[1]**

Sea State Code	Seaway Description	Lower(m)	Upper(m)	Mean(m)
0	Calm(glassy)	0.00	0.00	0.00
1	Calm (ripped)	0.00	0.10	0.05
2	Smooth(wavelets)	0.10	0.50	0.30
3	Slight	0.50	1.25	0.875
4	Moderate	1.25	2.5	1.875
5	Rough	2.5	4.00	3.25
6	Very rough	4.00	6.00	5.00
7	High	6.00	9.00	7.50
8	Very High	9.00	14.00	11.50
9	Phenomenal	14.00	>14.00	>1400

NOTE - The exact bounding height shall be assigned for the lower code figure; e.g. a height of 4 m is coded as 5.

Along with the code number, the upper and lower limits of significant wave heights are mentioned in the above table. The WMO table only specifies a range of significant wave heights which is defined as the double amplitude of waves. For the experiments, the selected wave amplitude values are closer to the upper range of sea state. Therefore, the amplitude of the selected wave as discussed in next section is kept 45 mbar, closer to the upper value of sea state 2. The engine cannot be subjected to back pressure above 50 mbar, thus, closest value to 50 mbar (sea state 2 upper limit) with a small safety margin is used for the experiments.

2.2.1 WAVE DATA

The waves recorded during real ship operations can be of varying wave amplitudes and wave periods based on the sea states and geographical location of the ship and weather conditions. National Data Buoy Center (NDBC) maintains a network of data collecting buoys and coastal station around the globe measuring the waves and storing the historical data. For experiment purpose, the real wave data is used obtained from the NDBC. The historical meteorological data in the table 2.4 is recorded by a buoy (44066) near the east coast of the United States of America. The significant wave height (WVHT) along with average wave period (APD) recorded by NDBC is shown below.

Table 2.4: **Historical Data from National Data Buoy Center [2]**

Date	Time [hrs	WVHT [m]	APD [sec]	Sea state	Max BP [mbar]
27/01/2018	0250	0.43	3.98	2	43
25/05/2018	0050	0.47	5.58	2	47
24/04/2018	0650	0.37	7.69	2	37

Only 3 of the recorded waves are shown in the table 2.4. The detailed list of the recorded wave data and parameters in the year 2018 is shown in appendix A. The diesel engine can be subjected to a maximum of 50 mbar back pressure (sea state 2) for safety purpose, therefore the experiments cannot be performed with waves with higher sea states. Therefore in table 2.4, wave data for only sea state 2 is mentioned. It is also clear from the recorded wave data in the table 2.4 that sea waves can have different wave periods for the same significant height. For all the experiments performed for this research the applied back pressure wave data were based on the recorded wave data from the NDBC.

2.2.2 POSITION OF UNDER WATER EXHAUST OUTLET

The back pressure felt by the engine depends on the position of the exhaust outlet relative to waterline [12]. The position of the exhaust outlet keeps changing relative to the seawater line due to the interaction between the sea waves, ship motion (rolling, pitching) and waves created by the vessel when moving forward. For simplifying this, the relative interaction between them is neglected and the three possible exhaust outlet positions considered are shown in figure 2.5.

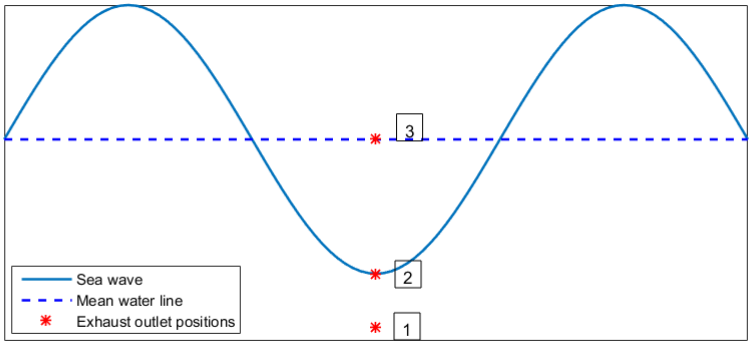

Figure 2.5: **Possible exhaust outlet positions**

For the same wave amplitude and wave period, the back pressure response generated due to different position of exhaust is explained below with the help of respective figures..

- **POSITION 1** - The exhaust outlet at position 1 is below the trough of the propagating wave. The submarine's diesel engine at snorkeling depth faces a

similar scenario [12]. Along with the dynamic back pressure due to propagating waves, an additional static water head pressure always acts on the engine marked by orange color constant BP line in figure 2.6. At this position, the exhaust is always submerged in water at all time with a constant external back pressure acting all the time. For the current test engine, back pressure input cannot exceed 50 mbar. Due to constant back pressure acting on the engine at this position for exhaust outlet, only very small values of back pressure can be tested. For instance, with a constant back pressure of 30 mbar, the engine can be tested with waves having amplitude below 20 mbar. Therefore, to perform experiments with higher back pressure (upto 50 mbar), position 1 is not considered for the experiments.

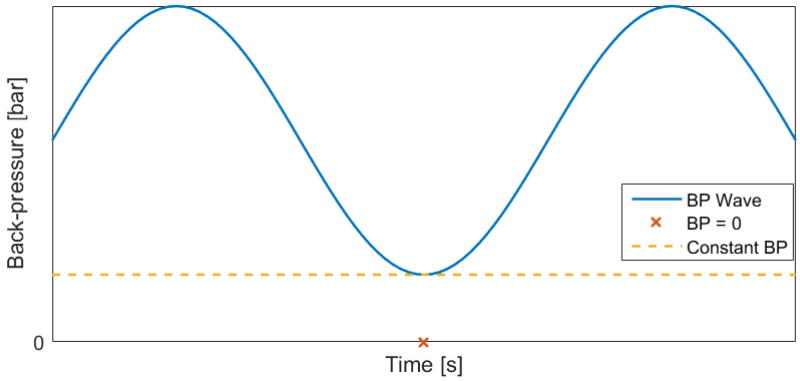

Figure 2.6: **Back pressure experienced for exhaust position 1**

- **POSITION 2** - The position 2 marks the exhaust position below mean water line on the trough of the wave. At this position, the back pressure is maximum at the crest of the wave and reduces to minimum value with no external back pressure at the trough. Thus, diesel engine experiences no external back pressure at the trough of the wave. Figure 2.7 shows the response experienced by the diesel engine. This means that the exhaust outlet reaches the water surface at the trough of the waves. With this position of the underwater exhaust outlet, the engine can be tested with higher amplitude back pressure waves than position 1.

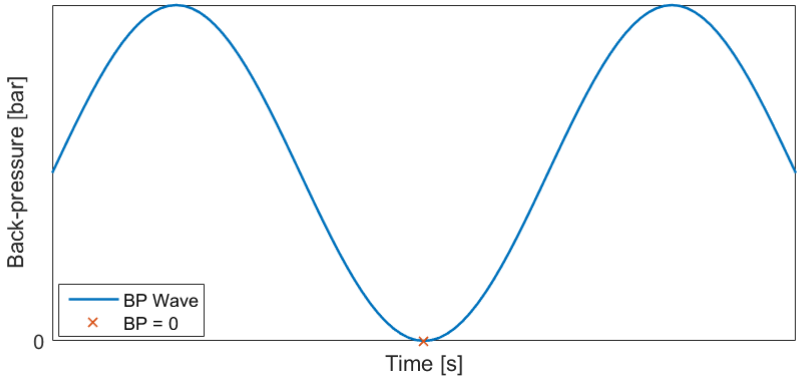

Figure 2.7: **Back pressure experienced for exhaust position 2**

- **POSITION 3** - In this position, the exhaust outlet is partially submerged during the back pressure wave. The engine experiences back pressure only during the positive half of the wave with maximum applied back pressure at the crest of the wave. For the second half the exhaust outlet comes out of the water, therefore no external back pressure for the rest of the half-wave as in figure 2.8. Since, the back pressure is acting only for the first half cycle, the effect of full back pressure wave on the engine cannot be tested at this position. Therefore, this position is also discarded from the experimental point of view.

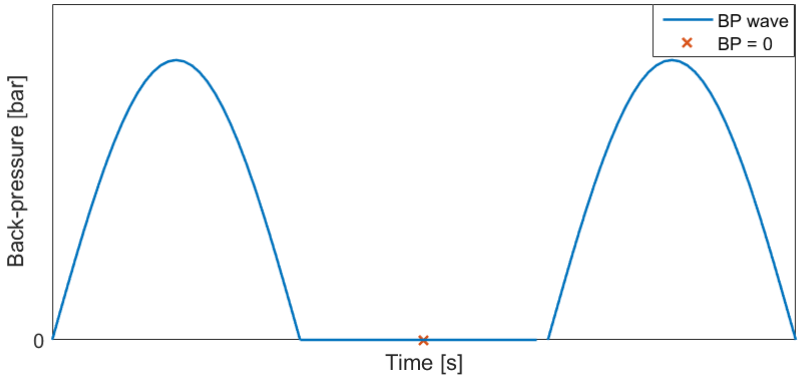

Figure 2.8: **Back pressure experienced for exhaust position 3**

At exhaust position 1, higher back pressure values cannot be tested as the constant back pressure acting on diesel engine due to seawater above the exhaust outlet. On the contrary, at exhaust position 3, higher back pressure values can be tested but the effect of the complete wave on engine performance cannot be captured. Therefore, all the experiments performed on the diesel engine for this master thesis are with an assumption of exhaust outlet is positioned at point 2.

2.3 TYPES OF EXPERIMENTS

The simulated back pressure waves are based on real recorded wave data obtained from the NDBC as explained in the section 2.2.1. The recorded measurements are performed at least twice for each back pressure wave input. For systematic comprehensibility, the experiments were divided into three phases based on the type of back pressure wave input. They are

1. Static (steady state) back pressure
2. Step change of back pressure.
3. Amplitude change of back pressure.
4. Wave period change of back pressure.

2.3.1 STATIC BACK PRESSURE

The detailed experimental and simulation investigation on the effect of steady state back pressure is already performed by Sapra et. al. [3] as a part of gas drive project. For this master thesis, the experiments are again conducted for the static back pressure. These experimental results are compared with the static results from the previous experimental research. The comparison provides an evidence, whether the research is directed in a right direction. The diesel engine is tested with sea state 2 with static back pressures of 30 mbar and 43 mbar. The 30 mbar is the back pressure experienced by the engine when mean value of sea state 2 is acting at the exhaust outlet. The 43 mbar back pressure value is taken from the first data mentioned in table 2.4. The test experiment engine can test only up-to 50 mbar static back pressure, therefore sea states higher than sea state 2 cannot be executed on test engine [3]. This is done to have a safe margin from the smoke and thermal limits of the diesel engine. The smoke limits uses the constant lines of simulated air excess ratio where as thermal limit uses the simulated exhaust valve temperature in a static engine map. This is discussed in detail in section 5.4.1.

The diesel engine is set to the maximum load point (340 KW, 981 rpm) with the help of water brake connected to the diesel engine. After reaching the set point, the back pressure is adjusted to required value by partially closing the butterfly valve. The butterfly valve rotates to partial closing position, depending on the input angle to the valve. After setting the valve to the required angle, diesel engine experiences 43 mbar (gauge) static back pressure continuously. The engine is allowed to run at this point for at-least 15 minutes to allow the engine parameters to stabilize before recording the measurements. The procedure is repeated again for 30 mbar (gauge) back pressure at all the set points. After static back pressure test, the diesel engine is tested with step change in back pressure as explained in next section.

2.3.2 STEP CHANGE OF BACK PRESSURE

In this section, the engine will be tested to a step-change in the back pressure. In step change, the engine is subjected to step-up change and step-down change separately. In step change, the back pressure is increased or decreased in a single step. This helps us in understanding the response of the engine parameters to the only increase or only decrease of external applied back pressure. This is not possible in case of waves in which, the back pressure increases and then decreases back t the original value in the same wave. Table 2.5 shows the initial and final back pressure values. The diesel engine is tested with the same external back pressure values same as static back pressure experiments. The average wave period is independent of the significant wave height [27]. For this experiment, the average period is selected such that half wave period (HPD) is not a fraction .

Table 2.5: **Wave Data - step change of back pressure**

Type [-]	WVHT [m]	APD [s]	Initial BP [mbar]	Final BP [mbar]	HPD [s]
Step up	0.3	4	0	30	2
Step down	0.3	4	30	0	2
Step up	0.43	8	0	43	4
Step down	0.43	8	43	0	4

In step up change, the engine is exposed to a step increase in the externally applied back pressure. The engine runs at a set point from no external back pressure to a new final value shown in table 2.5. For step down, the back pressure is stepped down to a situation when no external back pressure is applied to the engine. Step change Figure 2.9 shows the expected step-up and step-down back-pressure input for the diesel engine. In reality, the change external applied back pressure take place in multiple steps unlike, in single step as shown in figure 2.9. This is due to the inertia and the step-wise movement of the butterfly valve in addition to the non-linear effect of the valve movement on the back pressure. The actual step up wave which is used as an input to the model is discussed in section 3.2.1

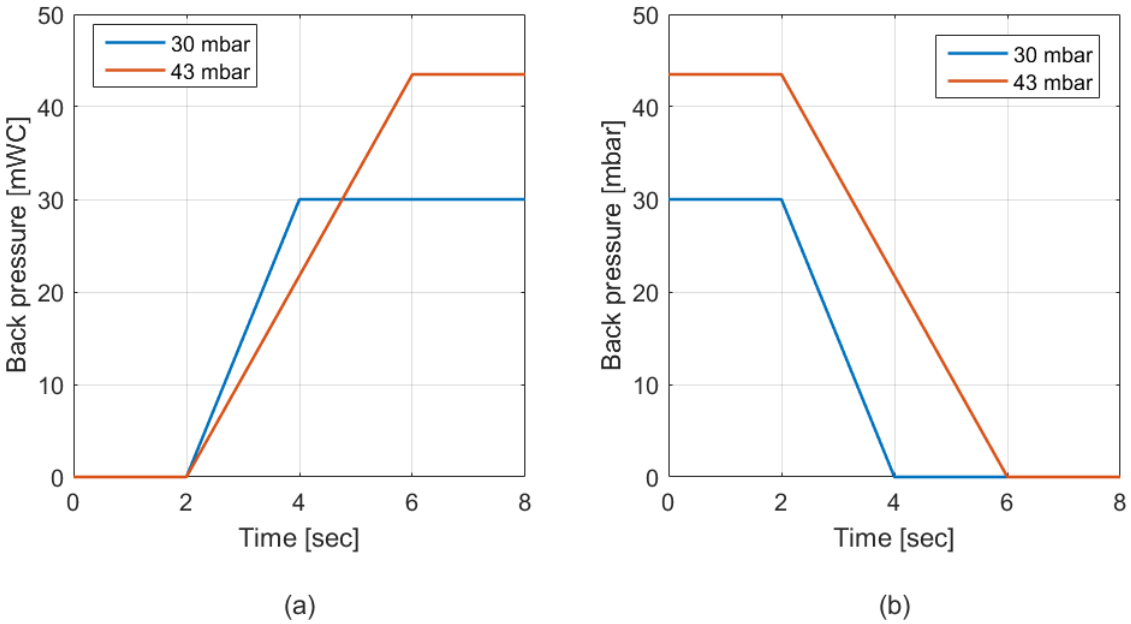

Figure 2.9: **Step change back pressure. Step-up change (a) and step-down change (b)**

In this experiment, the engine made to run at a set load point. The initial position of the butterfly valve is to be set such that the back pressure value is equal to the initial BP. The engine is allowed to run with this setting for at least 15 minutes to stabilize the parameter. Record the parameters at the same point. After recording parameters, the butterfly valve is rotated to a new position such that the back pressure before the valve corresponds to the final BP. The time taken to

change the butterfly valve position or back pressure from the initial value to the final is equal to HPD. The parameters are measured and recorded during the BP change. After completing it, the new setpoint is selected and the experiment is repeated for both step-up and step-down change.

2.3.3 AMPLITUDE CHANGE OF BACK PRESSURE

The sea waves acting at the exhaust outlet of the diesel engine consist of varying amplitude and wave period. The amplitude of the wave acting at the outlet affects the performance of the diesel engine [12]. In these set of experiments, the effect of amplitude on diesel engine parameters is evaluated. The amplitude for the input back pressure wave is changed, keeping the wave period constant (6s in this case). Based on real sea state conditions and wave data, the experiments are performed for -

1. Single wave
2. Multiple waves

For single wave, the measurements are recorded with back pressure wave input consist of one wave whereas for multiple waves, back pressure wave input consist of 8 consecutive waves in a single input. Single waves help in understanding the impact of only amplitude on the performance of the diesel engine as the change and response in the parameters is clearer with single wave input. On the other hand, continuous multiple waves are used as they are closer to the real scenario. The data for the amplitude change experiments are shown in the table 2.6.

Table 2.6: **Wave data - Amplitude change**

Data no.	WVHT [m]	APD [s]	Sea state [-]	max BP [mbar]
Data 1	0.25	6	2	25
Data 2	0.35	6	2	35
Data 3	0.45	6	2	45

In table 2.6, wave with amplitude 45 mbar and wave period 6s is the original wave data obtained from NDBC. The detail discussion on the wave measurements recorded by NDBC is given in appendix A, For the other 2 data set, the amplitude is reduced to 35 mbar and 25 mbar, keeping wave period constant. Figure 2.10 shows the three inputs. It is important to understand that figure 2.10 shows the three applied back pressure waves for the experiments but, the real back pressure wave recorded at the turbine outlet is a square step wave shown in figure 2.4(a) due to valve inertia. The zero back pressure in the figure 2.10 corresponds to diesel engine running with no external applied back pressure. The diesel engine is tested with 25 mbar, 35 mbar and 45 mbar amplitude for single waves. For multiple waves, 35 mbar and 45 mbar amplitude back pressure waves are used for the experiment. In any case, the back pressure is not increased above 50 mbar for the safety of the engine.

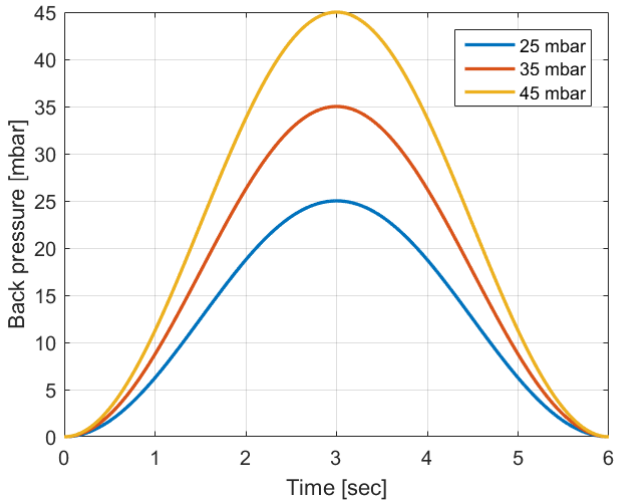

Figure 2.10: **Back pressure waves - Amplitude change**

The diesel engine is allowed to settle for 15 minutes at a load set point before any input. Initially, the engine is running without any external back-pressure. With the butterfly valve input, the butterfly valve starts shutting down to the applied angle and re-opens fully again. The time to partial shut and re-open the valve is equal to the wave period of the wave. In the meantime, the back pressure reaches a maximum applied value at half of the wave period and again drops down to the initial value at the end of the wave period. For single waves, the butterfly valve completes the above movement only once. In multiple waves, the valve continuously shuts and re-opens multiple time (8 times in multiple waves) to simulate continuous waves. This concludes the amplitude change experiment.

2.3.4 WAVE PERIOD CHANGE

After amplitude change experiments, the next aim of the research is to understand the effect of wave period on the performance of the diesel engine. This is done by keeping the amplitude of external back pressure constant and varying the wave period. The data for the experiments are shown in table 2.7. The wave period change experiments are also performed for both single and multiple waves.

Table 2.7: **Wave data - Wave period change**

Data name [-]	WVHT [m]	APD [s]	Sea state [-]	Max BP [m H_2O]
Data 1	0.45	2	2	45
Data 2	0.45	4	2	45
Data 3	0.45	6	2	45
Data 4	0.45	8	2	45

The second data set in table 2.7 is recorded by the NBDC at the eastern coast of the United States of America. The significant wave height of 0.45m includes a

safety margin from 0.5m WC (50 mbar gauge) back pressure limit. Therefore the wave with a significant height of 0.45m is selected. For the other data sets, the wave amplitude is kept constant at 45 mbar and the wave period is changed to 2s, 4s, 6s and 8s as shown in figure 2.11. The experiments are performed for both

1. Single waves
2. Multiple waves

The experiments are performed for single and multiple waves for all the data set in table 2.7. The engine is allowed to stabilize after reaching the set load point. The butterfly valve controls the back pressure such that the time taken by the valve to partially shut and re-opens is equal to the wave period of the back-pressure wave.

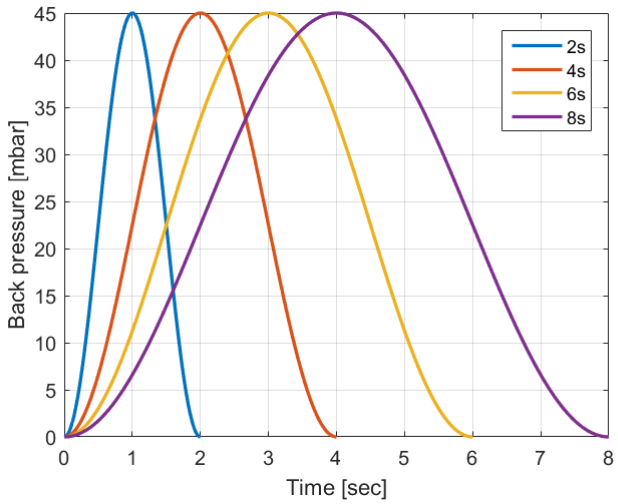

Figure 2.11: **Back pressure waves - Wave period change**

Figure 2.11 shows the applied back pressure waves with single amplitude and multiple wave periods. The original back pressure wave recorded at the turbine outlet is square step wave as shown in fig 2.4(b). This is due to the inertia and the step-wise movement of the butterfly valve in addition to the non-linear effect of the valve movement on the back pressure. After finishing the experiments, the measurements are used to verify the adopted model. The adopted Diesel Engine - B model is a mean value estimated model explained briefly in the coming sub-sections.

2.4 DIESEL ENGINE - B MODEL

With the better technology and powerful computers, detailed modeling of the various complex processes like Gas Exchange, Induction etc. Modelling these process helps in understanding and prediction of the diesel engine performance. Every research project has its fit for purpose model and the selection of the model depends on that objective of the research performed. The categorization of the model based on the level of dynamic and physical details [28]. They are -

- **Zero order models** - A mathematical equation defines the engine torque and fuel consumption without considering dynamics of the turbocharger. They are very simple and does not require any detail.

- **First Oder models** - They are similar to zero-order models but require more extensive measurements because of the variable representing turbocharger speed or pressure which makes it complex compared to zero-order [29].

- **Zero dimensional crank angle models** - It uses mass and energy conservation, gas state equation and solves them in differential form as volume and resistance element [30]. Instead of time, the crank angle is used. The governing equations between the elements are solved at each crank angle. Depending on the detailing, the combustion can be modeled as single zone[31], two zone[32] and three-zone[33] combustion model with the different combination of heat release models.

- **One Dimensional fluid dynamic models** - This model is used to model air flow, temperature, and pressure across the engine. It uses the finite difference method in which the mesh size governs the stability which in turn limits the time step. The models are detailed, complex and need more computing time.

- **Multi-zone combustion model and CFD combustion models** - In CFD the cylinder is divided into small volumes (grid). It requires a powerful computer and long computations to provide detail information about the internal process. The computation time can be reduced by selecting a coarse grid. In addition to continuity, energy and momentum equations, phenomenological equations like reaction rate can also be used. Such models are called phenomenological multi-zone model. Both the models generally include cylinder and /or inlet and outlet ducts but provide detail information of the cylinder process[34].

- **Mean value first principle model** - The models are used in the researches where in-cycle variations are not the primary interest. For instance, when the complete diesel engine model of a ship with external influences (environment) is to be included in a larger system, the in-cylinder details are not the primary concern. Parameters like manifold temperature and pressure, air-fuel ratio, maximum cylinder pressure are the parameters which are focused on when dealing with these models. In these models, the discrete in-cylinder process during a revolution in crank angle models is replaced by mean value models. The Seiliger cycle and gas exchange model can be used to find the exhaust gas conditions [34]. Both 4 stroke [35] [36] and 2 stroke [37] [38] marine Diesel engines can be modeled with it.

MVEM have been used to simulate marine engines operation and predict engine performance parameters but it cannot predict in-cylinder parameters variation. In MVEM, a revolution time scale is used which increases the simulation speed.

2.4.1 Mean Value Model : DE - B Model

The adopted model is the Mean Value First Principle Diesel Engine model (DE-B Model) which has been developed at the Netherlands Defence Academy (NLDA) and Delft University of Technology (TU Delft) since 1998. The model is implemented in an environment of MATLAB/Simulink. In this model, the cylinder volume and inlet/outlet valves are modelled as analytical models. A revolution time scale is used

during simulation, which increases the simulation speed and save time. Despite not providing the information at every crank angle scale, MVEM predicts the same information in terms of number signals. For example mass flow, exhaust receiver temperature and pressure, inlet receiver pressure and temperature etc. The various components of the model are modeled as resistance and volume elements. The concept of mean value model used for the research shown in figure 2.12. The back pressure block is marked by the red square.

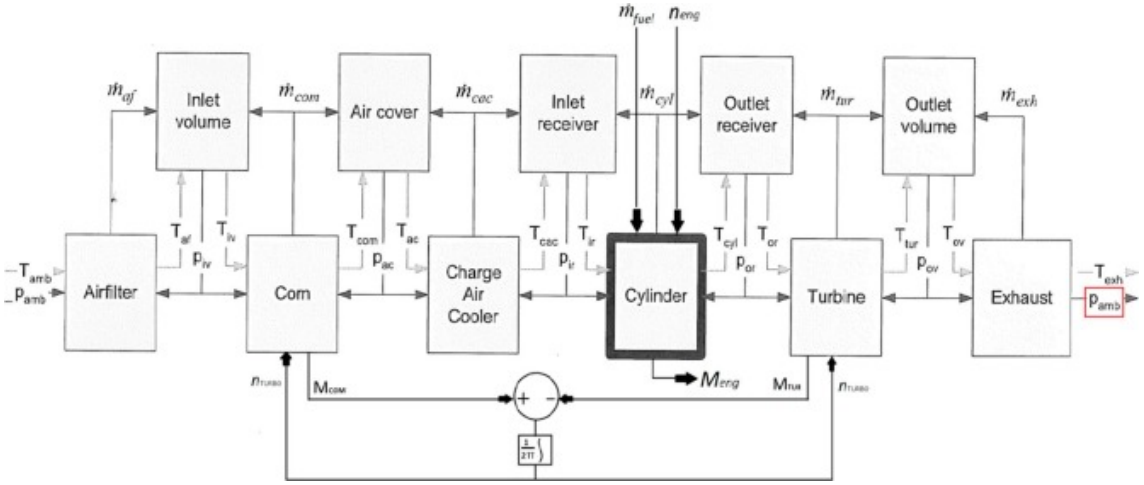

Figure 2.12: **Mean Value Engine Model[3]**

- The inlet volume, the air cover, the inlet receiver, the outlet receiver are modeled as a series of control volumes. By integrating net mass flow (conservation of mass) and net energy flow (conservation of energy), the instantaneous mass and instantaneous temperature is calculated in the control volumes. The instantaneous pressure of the element can be calculated using the ideal gas law. For analytical explanation, please refer to appendix **??**

$$\frac{dT}{dt} = \frac{(c_{p,in} \cdot T_{in} - c_v \cdot T) \cdot \dot{m_{in}} - (c_{p,out} \cdot T_{out} - c_v \cdot T) \cdot \dot{m_{out}} + \dot{Q}}{m \cdot c_v} \tag{2.1}$$

$$p = \frac{m \cdot R \cdot T}{V} \tag{2.2}$$

- The control volumes are connected via resistance elements like air filter, charge air cooler. In a resistance element the mass flow in is calculated as a function of pressure difference using the momentum equation. It is shown in detail in appendix **??**

$$\dot{m} = (\mu \cdot \phi) \cdot A \cdot \frac{p_0}{\sqrt{R_0 \cdot T_0}} \cdot \Psi \tag{2.3}$$

  μ - Contraction factor for the contraction of flow.

  ϕ - resistance factor

  Ψ -function of pressure ratio (depends on type of flow)

- In the back pressure block marked in red colour, the back pressure wave is used as an input to the model. The figure 2.13 shows the user interface for the

back pressure input. The time values at an interval of 0.1 seconds is used in breakpoints 1 row where as the corresponding back pressure values are used in table data. The back pressure wave measured after the turbine during the experiment as shown in figure 2.4(b) is used as an input to the model.

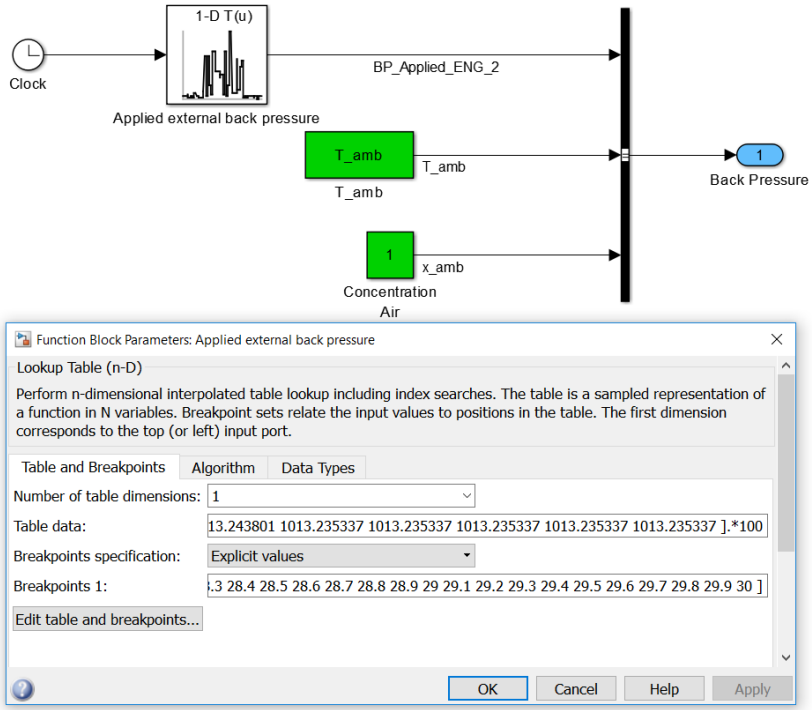

Figure 2.13: **User interface for back pressure wave input to the model.**

After verifyting the adopted model, it is used to simulate sea states which could not be tested on the test engine. Moreover, additional parameters which were not measured or cannot measured during the experiments can be simulated with the help of the verified model. Air excess ratio, fuel flow rate, governor response etc are the examples. DE-B model is successfully used in modeling and simulating the static back-pressure experiment results by Sapra et. al [3]. For detail understanding of the working of the model, it is recommended to read 'Diesel Engines Volumes 1-6' by Professor Stapersma available at TU Delft library. The various components and their modelling are explained in the appendices. After the methodology and experimental set up, we are moving to the experimental results obtained in the next chapter.

Chapter 3

EXPERIMENTAL RESULTS

The results from the back pressure experiment are discussed in detail in this chapter. The experiments are performed on a pulse turbocharged diesel engine rated at 360 KW at 1000 rpm. The back pressure is replicated with an electronically controlled butterfly valve. The amplitude of the back pressure applied is measured from the atmospheric pressure. For instance, if the atmospheric pressure is 1015 millibar, 45 mbar (45 mbar gauge) back pressure increases the back pressure to 1060 millibar. In this chapter, static back pressure results are explained briefly, followed by the results for step change. For both, single and multiple back pressure waves, the effects of amplitude and wave period on engine parameters is also discussed in detail.

3.1 STATIC BACK PRESSURE

The static back pressure experiments are already performed by Sapra et. al. [3] as a part of gas drive project. Since, the experiments are performed on the same test engine, the static results from his research can be compared with the static results obtained for this master thesis. Moreover, the simulated results can be compared to check any deviation from his results. Since, the same model is used for both researches, the deviation in the model response can be pointed out easily. For this section, the 30 mbar and 43 mbar corresponds to the range of significant wave heights for sea state 2 as presented in table 2.3. The back pressure cannot be increased beyond 50 mbar for engine safety, therefore higher sea states wee not tested. For ease of understanding, the pressure and temperature parameters are categorized into inlet side parameters and exhaust side parameters. The inlet side parameters include temperature after the compressor, inlet receiver pressure and temperature. The exhaust side parameters of the diesel engine include exhaust receiver temperature (mean temperature before the turbine), temperature after the turbine.

With increase in static back-pressure value, the resistance to exhaust flow from cylinder to atmosphere through exhaust duct increases. This lead to an increase in the pressures in the exhaust duct of the diesel engine. With an increase in static back pressure before the butterfly valve, pumping work to push out exhaust gasses from cylinder to the atmosphere also increases. To maintain the same load with extra pumping work, fuel flow to the engine increases. More fuel is combusted leading to higher exhaust receiver temperature. The figure 3.1 compares the exhaust receiver temperature for no external back pressure, 30 mbar and 43 mbar at 340 KW and

981 rpm. The parameters shown in the figure 3.1 is minutely fluctuating and precise static values of the temperature is calculated by taking the mean of these fluctuating exhaust eceiver temperature.

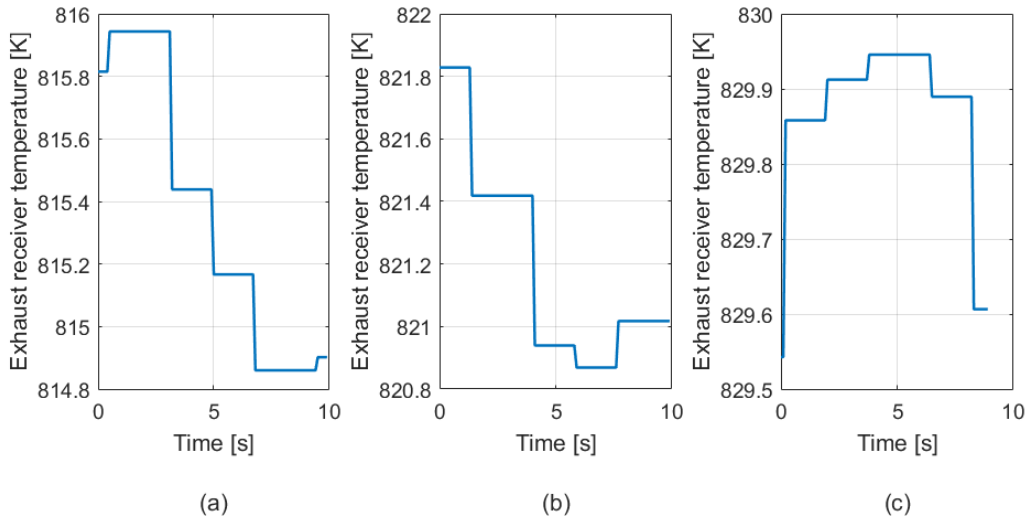

Figure 3.1: **Static exhaust receiver temperature. Load-340KW, RPM-981, BP - no external back-pressure (a), 30 mbar (b) and 43 mbar (c)**

The temperature after the turbine follows the same trend as exhaust receiver temperature. The figure 3.2 shows the temperature after the turbine at 340 KW load at 981 rpm for the same three cases.

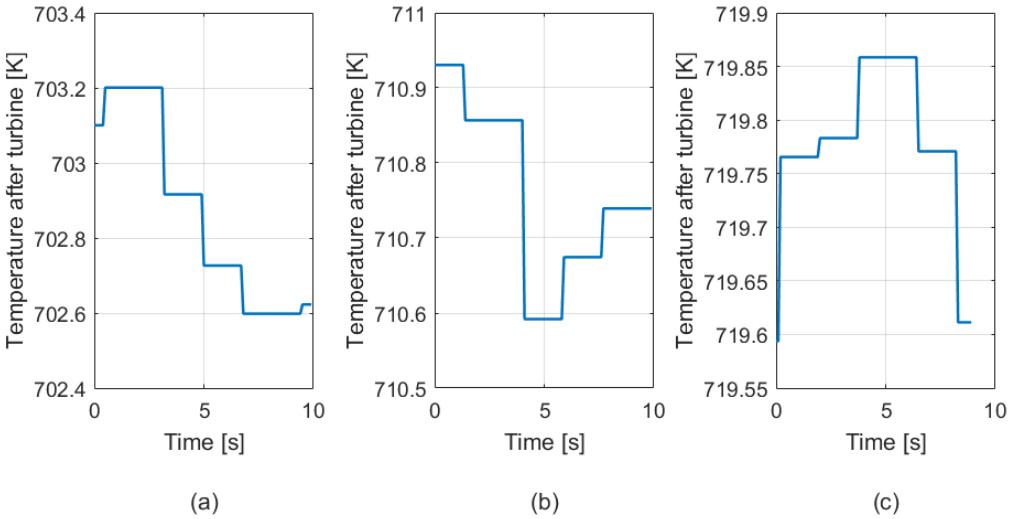

Figure 3.2: **Static temperature after turbine. Load-340KW, RPM-981, BP - no external back-pressure (a), 30 mbar (b) and 43 mbar (c)**

The increased pressure in the exhaust duct increases the exhaust receiver temperature but it also reduces the pressure ratio across the turbine. This leads to a reduction in turbocharger speed which reduces the compressor discharge pressure and eventually, inlet receiver pressure. Therefore, the higher the back pressure,

lower is the inlet receiver pressure. The inlet receiver pressure for the three cases at 340 KW and 981 rpm is shown in 3.3.

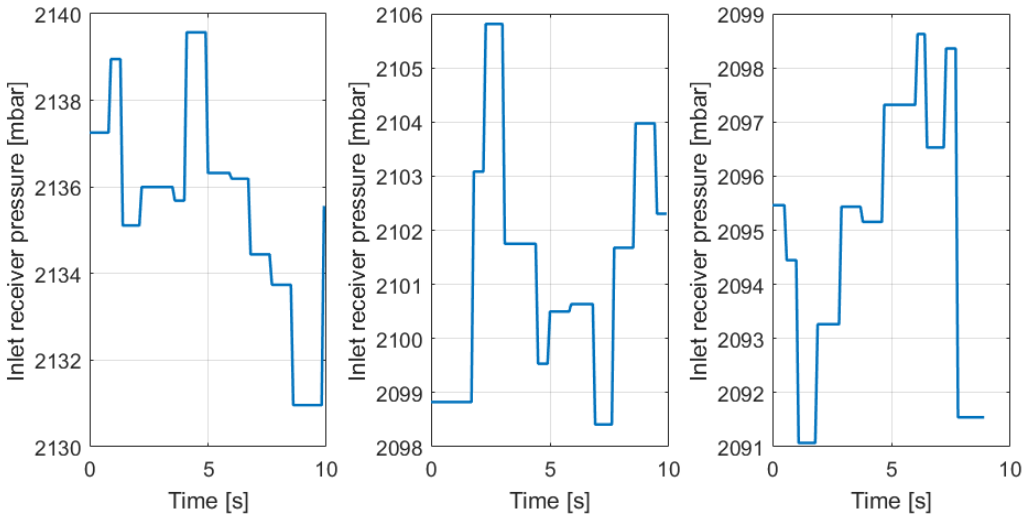

Figure 3.3: **Static inlet receiver pressure. Load-340KW, RPM-981, BP - no external back-pressure (a), 30 mbar (b) and 43 mbar (c)**

The drop in the inlet receiver pressure with an increase in back pressure reduces the inlet receiver temperature. The change in the inlet receiver temperature is very small with the change of static back pressure. On comparing the inlet receiver temperature for the three cases as shown in figure 3.4, it is clear that the inlet receiver temperature is not even changing by 1 kelvin with an increase in static back pressure. Moreover, the inlet receiver temperature for 30 mbar static back pressure is more than 43 mbar. The temperature for different back pressure values are very close to each other, therefore the effect of back pressure on inlet receiver temperature is considered in significant. The static change in the inlet side temperature parameters is also insignificant compared to the exhaust side parameters. Therefore, it can be stated that the exhaust side parameters are more critical compared to the inlet side parameters. This means that exhaust receiver temperature is more susceptible to increase and cause high thermal loading compared to inlet receiver temperatures.

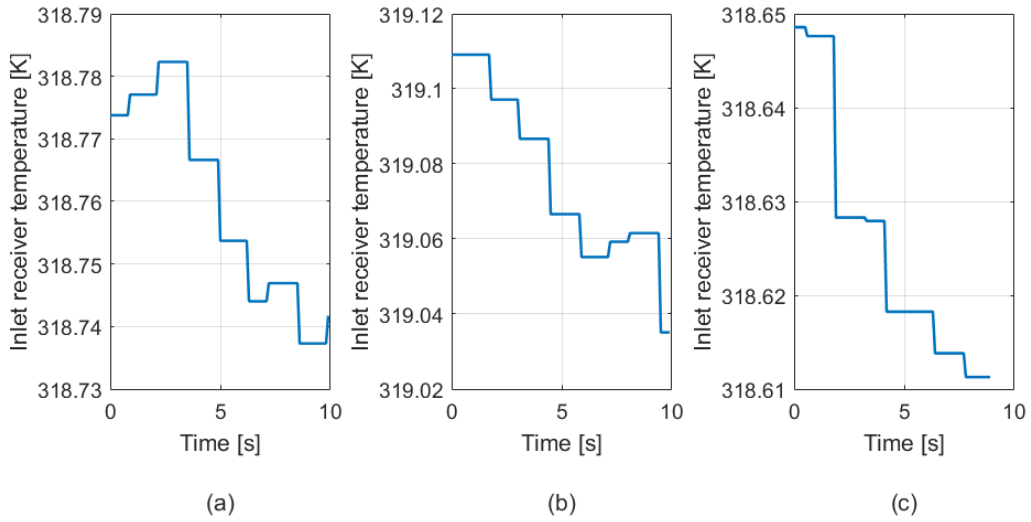

Figure 3.4: **Static inlet receiver temperature. Load-340KW, RPM-981, BP - no external back-pressure (a), 30 mbar (b) and 43 mbar (c)**

Higher the back pressure, higher the exhaust receiver temperature. This is true for all the loads as shown in figure 3.5(a). At any load, the static exhaust receiver temperature is higher for higher back pressure. The inlet receiver pressure reduces with the back pressure and it can be seen at all the set load points in figure 3.5(b).

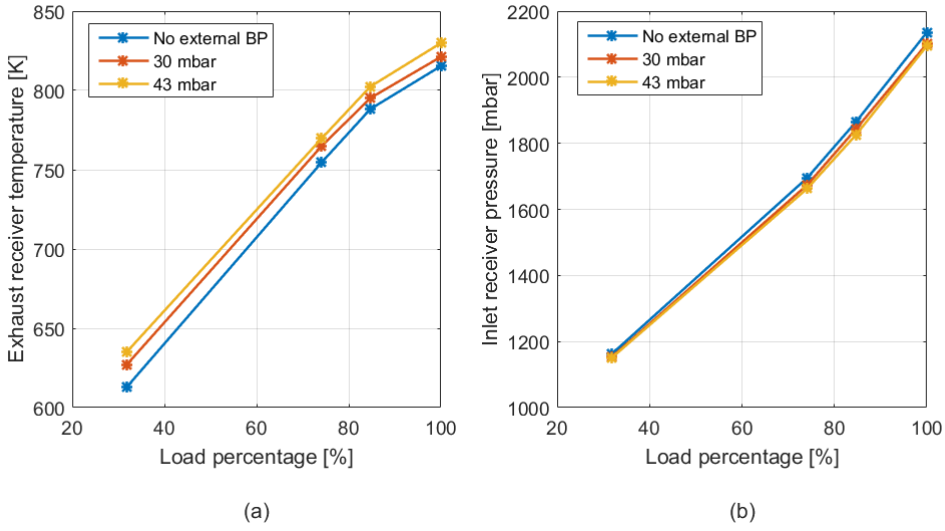

Figure 3.5: **Measured static exhaust receiver temperature (a) and static inlet receiver pressure (b), at all set-points**

The measured fuel flow at all load points is plotted for three back pressure cases in figure 3.6. It is known that higher the external applied back pressure, higher is the required pumping work to remove the exhaust gases from the engine. Thus, more fuel is required for the same load to overcome the pumping which increases fuel consumption with higher back pressure. In figure 3.6, the fuel flow rate for the three cases is shown at all loads. The fuel flow rate is higher for higher back pressure but the increase is very very small at all loads. At 340 KW, the fuel flow rate increases by 0.84% for 30 mbar static back pressure from engine running with

no external static back pressure. For 43 mbar steady state back pressure, the fuel flow rate is increased by 1.9% from engine running with no external static back pressure. Therefore, the increase in fuel consumption is not very significant with an increase in back pressure at any load as shown in the figure below.

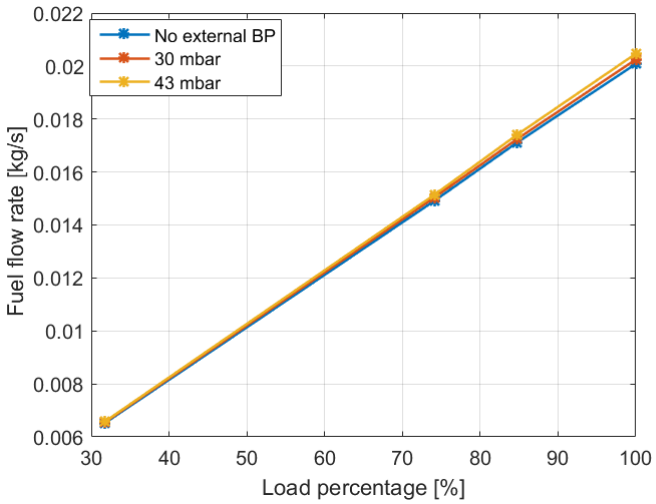

Figure 3.6: **Fuel flow rate. Load-340KW, RPM-981, BP - no external back-pressure (a), 30 mbar (b) and 43 mbar (c)**

3.2 STEP CHANGE

After static back-pressure, the back-pressure is changed in a step manner for this section. During the step change, the effect on the engine performance is evaluated with the dynamic change of the back pressure. The step-change helps in detail understanding of the response of the engine parameters due to the dynamic change of back-pressure. This can be difficult with the fast continuous waves as back pressure increases and decreases very fast. The step change of back pressure can be characterized as -

1. Step up change
2. Step down Change

In step-up change, the back-pressure is increased by partially closing the butterfly valve which is placed after the turbine. Closing the valve increases resistance to the flow of exhaust gasses which in turn creates a back-pressure. For step-down change, the butterfly valve is moved from a partially closed position to fully open. The two step change readings are 30 mbar (gauge) in 2s and 43 mbar (gauge) in 4s.

3.2.1 STEP UP CHANGE

In step-up change, the back pressure is increased in a single step from no external back pressure to the assigned higher value of back pressure. The external back pressure applied to the engine is with respect to the atmospheric pressure. The response time for the diesel engine parameters to the external step-up back pressure

is also evaluated in this section. The engine is allowed to stabilize for at least 15 minutes at maximum set-point (340 KW, 981 rpm). When the butterfly valve starts rotating due to input, back pressure responds first and starts increasing at the same time or with a small lag (less than 1 second). In figure 3.7(a) the input for the butterfly valve is shown for back pressure 43 mbar in 4 seconds. The valve starts partially closing at 14 seconds. The corresponding back pressure response is shown in 3.7(b) with a lag of 0.5 seconds. Despite single step input to the electronic butterfly valve, the step-up back pressure wave consist of multiple steps. This is due to the inertia and the step-wise movement of the butterfly valve in addition to the non-linear effect of the valve movement on the back pressure.

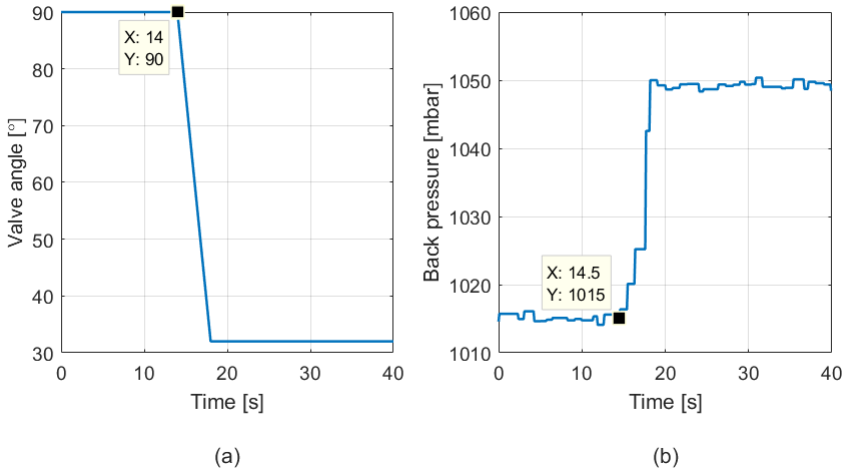

Figure 3.7: **Angle input for butterfly valve (a) and the corresponding step up back pressure response (b). BP- 43 mbar, Time - 4s**

The increase in back-pressure, reduces the pressure ratio across the turbine. With reduction in pressure ratio, turbocharger speed decreases, reducing the compressor discharge pressure and subsequently the inlet receiver pressure. The inlet receiver pressure decreases at the same time or with a small lag (less than 1 sec) to the initial step-up increase in back-pressure as shown in figure 3.8(a). The increased back pressure, increases the engine pumping work to remove the exhaust gasses from the cylinder. Since, more power is required at the same load, the engine slows down due to extra pumping work. To maintain the load at same speed, governor increases the fuel supply to the engine to compensate extra pumping work, increasing exhaust receiver temperature. The governor responds very quickly to slowdown of the engine that the decrease in the engine rpm is not clearly visible in figure 3.8(b). Since the diesel engine fuel flow cannot be measured because of non-availability of flow meters during the experiment, fuel consumption during the dynamic change cannot be measured during the experiment. Therefore, the fuel consumption is simulated with the help of DE-B model and will be discussed in the next chapter.

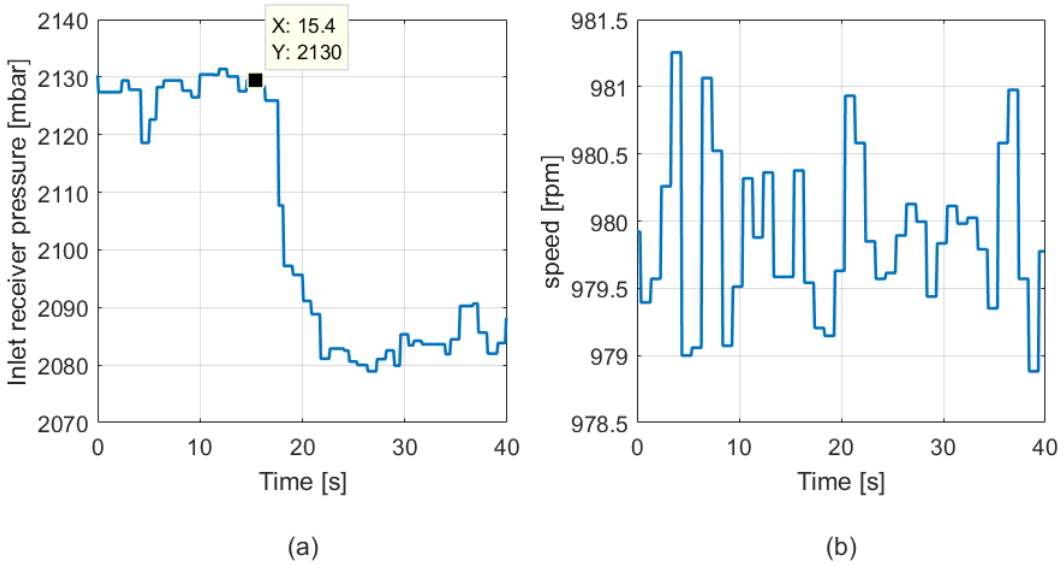

Figure 3.8: **Effect on Inlet receiver pressure (a) and Engine speed (b) due to step-up BP - 43 mbar, Time - 4s, Load- 340 KW, RPM - 981**

The exhaust side temperature and inlet side temperatures respond after a lag to the inlet receiver pressure. After analyzing all the step up measurements, it is not clear whether the temperature parameter from the exhaust side responds first after inlet receiver pressure or the inlet side parameters. The general trend for response time is not clear and there is a probability of selecting the wrong respond point due to human error. But out of exhaust side parameters, it is confirmed that the temperature after the turbine always responds before or together with exhaust receiver temperature as shown in 3.9(b). Moreover, the response of temperature parameter is slow compared to the pressure parameters. This is because of low sampling frequency of the temperature probes.

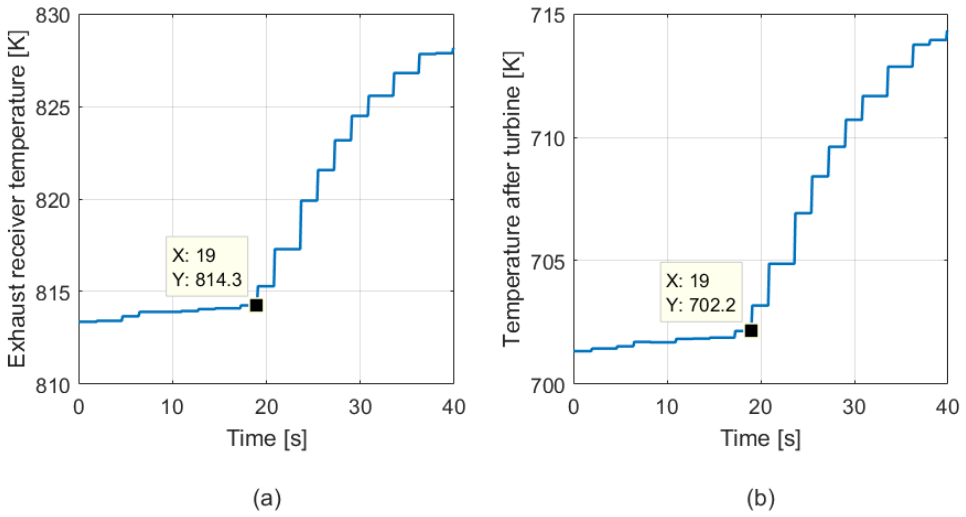

Figure 3.9: **Effect on exhaust receiver temperature (a) and Temperature after turbine (b) for step-up BP - 43 mbar, Time - 4s, Load- 340 KW, RPM - 981**

On the inlet duct side, the inlet receiver temperature and temperature after compressor respond at the same time as shown in 3.9. The sequence of the response of all the parameters to the increased back pressure explained above in this section always the same for any type of back pressure (single wave, multiple waves, step change) at any set load point. The back pressure increases first responding to the rotation of butterfly valve, followed by the inlet receiver pressure at the same time or with a small lag. The temperature after compressor and inlet receiver temperature start reducing next. At last, the exhaust side temperature (exhaust receiver temperature, temperature after turbine) responds to the increase in back pressure.

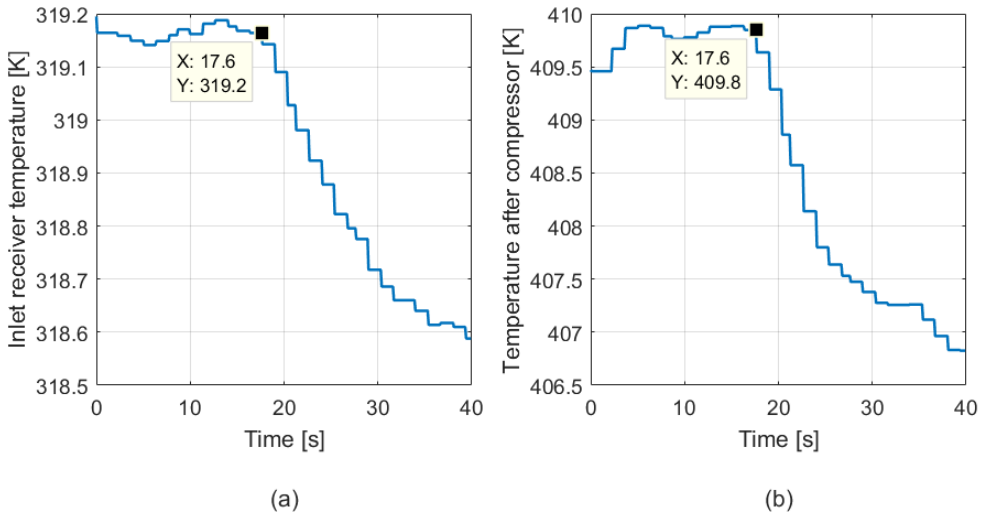

Figure 3.10: **Effect on inlet receiver temperature (a) and Temperature after compressor (b) for step-up BP - 43 mbar, Time - 4s, Load- 340 KW, RPM - 981**

After analyzing the order of response of the parameters, the comparison is made between two different back pressure inputs (30 mbar in 2s and 43 mbar in 4s). In figure 3.11, the 30 mbar step-up back pressure measured at turbine outlet, along with corresponding inlet receiver pressure is shown at 340 KW. As the back pressure started increasing, inlet receiver pressure drops due to low compressor discharge pressure. On comparing it with figure 3.8(b), it can be stated that the drop in the inlet receiver pressure is more for higher back pressure. In figure 3.8(b), the drop in the inlet receiver pressure is 50 mbar for 43 mbar, 4s step up back pressure. The drop is higher compared to 36 mbar drop in inlet receiver pressure for 30 mbar, 2s step up back pressure as shown in figure 3.11(b).

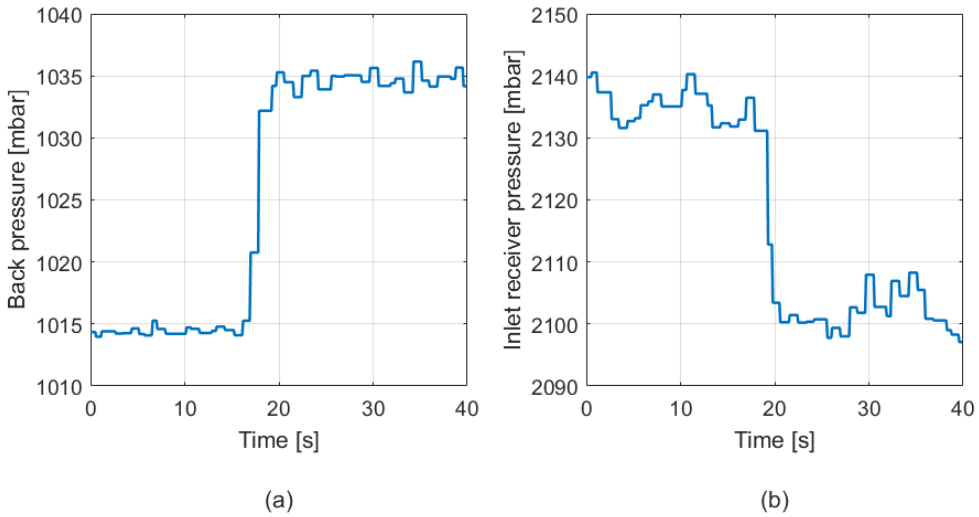

Figure 3.11: **Back pressure (a) and Inlet receiver pressure (b) for BP - 30 mbar Time - 2s**

The increment in exhaust receiver temperature and temperature after turbine is high for higher external applied back pressure. The increase in exhaust receiver temperature in figure 3.9(a) is nearly 13 K for 43 mbar (43 mbar, 4s) step up back pressure. The increment is higher when compared to 9.6 K increment for 30 mbar (30 mbar, 2s) as shown in figure 3.12(a). Therefore, it can be said that higher the change in externally applied back pressure, larger is the change in the exhaust receiver temperature. The temperature after turbine in figure 3.9(b) and 3.12(b) also shows the larger increase in temperature for 43 mbar, 4s step up back pressure.

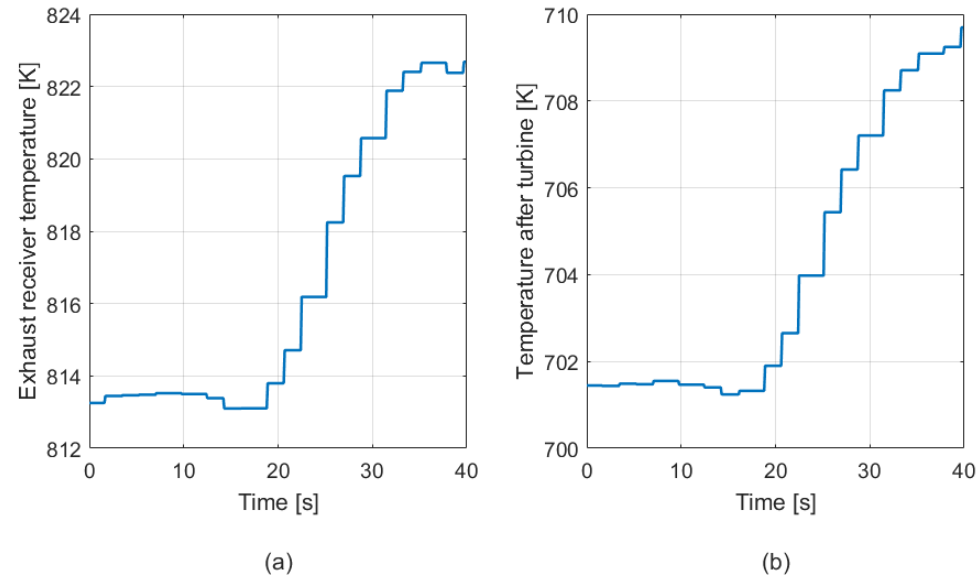

Figure 3.12: **Exhaust receiver pressure (a) and Temperature after turbine (b) for BP - 30 mbar Time - 2s**

For the inlet side parameters, the decrease in inlet receiver temperature for 43 mbar, 4s step back pressure at 340 KW is less than 1 K as shown in 3.10(a). The

change in temperature is insignificant compared to the change in exhaust receiver temperature and temperature after turbine. Therefore, it can be said that exhaust receiver temperature is more critical to engine thermal loading compared to the other temperature parameters. Thus, for future sections (amplitude change, wave period change) only exhaust receiver temperature and inlet receiver pressure is compared for various back pressure waves.

3.3 AMPLITUDE CHANGE

To understand the clear effect of amplitude on diesel engine performance, the engine was tested with back pressure waves of the same wave period but different amplitude. The recorded test data from NDBC used in this section is taken from table 2.6. In this section, the experiments are performed with -

- Single waves
- Multiple waves

3.3.1 SINGLE BACK PRESSURE WAVE

The test engine is subjected to a single back pressure wave at the outlet of the turbine. The wave period of the externally applied back pressure wave is kept constant (6s), with back pressure wave amplitude of 25 mbar, 35 mbar and 45 mbar. For back pressure amplitude 45 mbar and 6 s wave period, the butterfly valve closes partially and re-opens back to the original position in 6 seconds. The time period for which the valve remains at partially closed position is very small. Therefore, the back pressure cannot reach the required value at the same angle again and again as in step change. For instance, the same back pressure single wave of amplitude 45 mbr and 6s wave period is used as input in all the three cases in table 3.1. Despite the same input wave (in terms of angle amplitude and time) to the butterfly valve, the back-pressure values are observed differently. The butterfly valve is subjected to the same input until at least two similar measurements are recorded. For 45 mbar amplitude, wave1 in the table 3.1, the difference between the required and achieved back pressure is smallest. The difference in the other two waves are more as they are not reaching the required back pressure.

Table 3.1: **Different replicated back pressure for same input to the butterfly valve. Load-340 KW, RPM - 981, BP - 45 mbar, WP - 6s**

S. no.	Atmospheric pressure	Required back-pressure	Achieved back-pressure	Difference between required and achieved
[-]	[mbar]	[mbar]	[mbar]	[mbar]
1	1017.5	1061.6	1061	0.628
2	1017.5	1061.6	1056	5.628
3	1017.5	1061.6	1058	3.628

The externally applied back pressure wave (45 mbar, 6s) along with the inlet receiver pressure at 340KW is shown in figure 3.13. When a single wave is exerted

at the exhaust outlet, the back pressure increases initially to a maximum value and decreases back to initial value as in 3.13(a). Again, a sinusoidal wave input to the butterfly valve created a square wave of back pressure due to the inertia and the step-wise movement of the valve in addition to the non-linear response of back pressure to the valve movement. With increasing back pressure the pressure ratio decreases across the turbine, reducing turbocharger speed. It further reduces the compressor discharge pressure, reducing the inlet receiver pressure. As externally applied back pressure drops back to its initial value, the inlet receiver pressure also increases back to the initial state. The back pressure wave along with inlet receiver pressure is shown in figure 3.13.

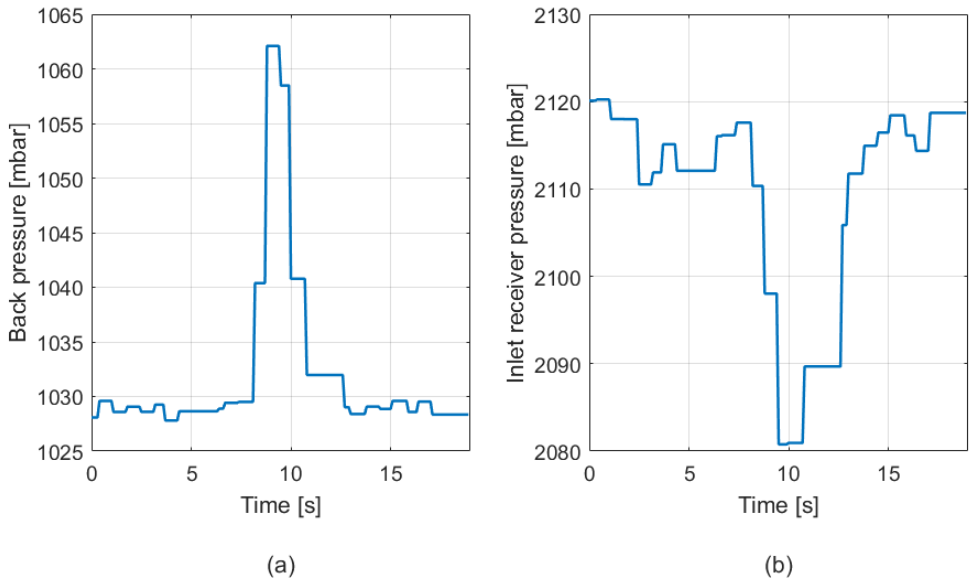

Figure 3.13: **Back pressure (a) and Inlet receiver pressure (b) for BP - 45 mbar WP - 6s**

To understand the quantitative and qualitative effect of externally applied back pressure wave amplitude on the engine, measured engine parameters for 45 mbar back pressure wave is compared with 25 mbar back pressure wave. The exhaust back pressure along with the inlet receiver pressure for 25 mbar is presented in figure 3.14. After analyzing figure 3.13 and 3.14, it can be declared that the inlet receiver pressure drop for 25 mbar, 6s back pressure wav is less compared to 45 mbar, 6s wave. For 45 mbar back pressure wave, the drop in inlet receiver pressure is 35 mbar where as for 25 mbar back pressure wave the drop in inlet receiver pressure is 19 mbar. In other words, higher the amplitude of the externally applied back pressure wave, larger is the drop in the inlet receiver pressure.

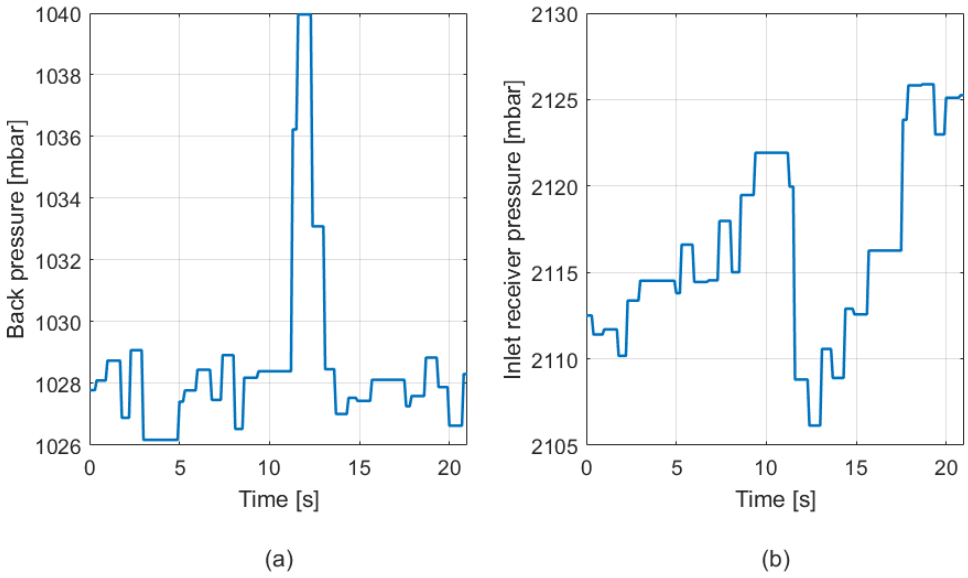

Figure 3.14: **Back pressure (a) and Inlet receiver pressure (b) for BP - 25 mbar WP - 6s**

The decrease in inlet air receiver pressure further decreases the temperature in the inlet receiver. The change in the inlet receiver temperature is insignificant as explained in section 3.2.1. On the other side, the exhaust receiver temperature increases. This increase in temperature is because of the combustion of extra fuel to compensate the extra pumping work to remove the exhaust gasses against the high back pressure. The exhaust receiver temperature and temperature after turbine (Turbine outlet temperature) are plotted in figure 3.15 for 45 mbar, 6s back pressure wave at 340 KW. On analyzing this figure along with figure 3.13(a), it can be spotted that the exhaust side temperatures start increasing after a lag to the back pressure wave. Even, after back pressure returns back to its initial value, the exhaust side temperatures are still close to its maximum value. The exhaust side temperatures also return to its initial value, but it cannot be seen in the figure 3.15 because the measurement is stooped at 20 seconds. This shows that the temperature sensors are slow due to their low sampling frequency.

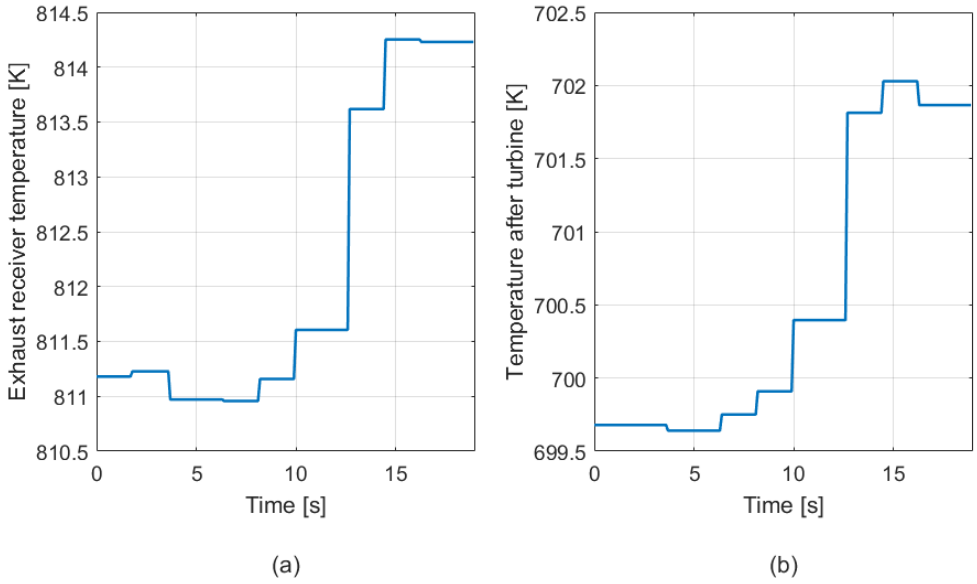

Figure 3.15: **Exhaust receiver temperature (a) and Temperature after turbine (b) for BP - 45 mbar, WP - 6s**

On comparing the above figure with figure 3.16, it is observed that the increment in the exhaust side temperature parameters is more for higher amplitude back pressure wave. The exhaust receiver temperature changed by 1.5 K for 25 mbar, 6s back pressure wave where as, for 45 mbar, 6s back pressure wave, the exhaust receiver temperature increases by 3.2 K. Similar trend was found for the temperature after the turbine as it increases by 2.2 K for 45 mbar (Figure 3.15(b)) and 0.9 K for 25 mbar, 6s back pressure wave (Figure 3.16(b)).

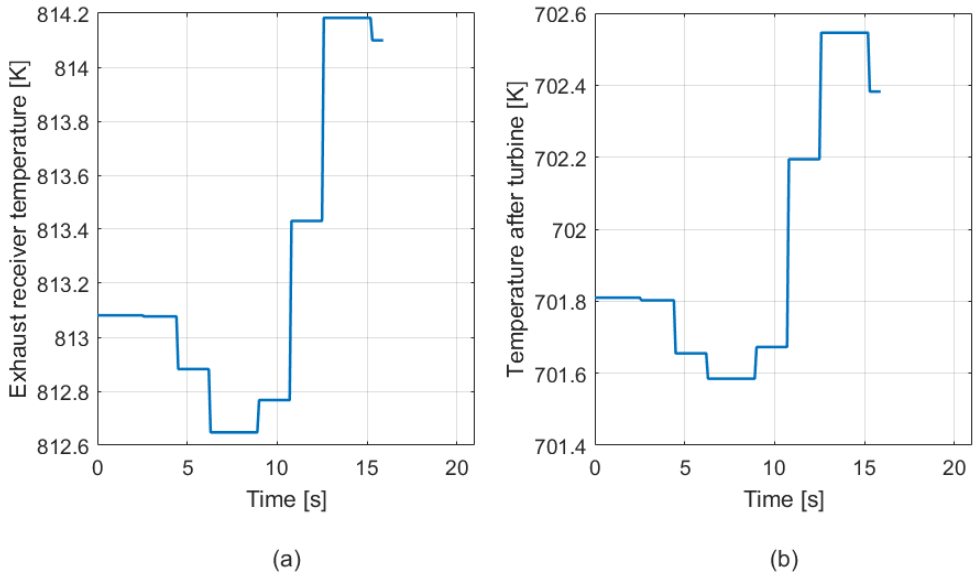

Figure 3.16: **Exhaust receiver temperature (a) and Temperature after turbine (b) for BP - 25 mbar, WP - 6s**

The exhaust receiver temperature for 25 mbar, 6s and 45 mbar, 6s back pressure wave is plotted for all the loads is shown in figure 3.17(a). For all the loads, it can

be seen that the increment in exhaust receiver temperature is always higher for 45 mbar, 6s back pressure wave. This concludes that the change (increase) in exhaust receiver temperature is higher for the higher amplitude of externally applied back pressure wave at all loads.

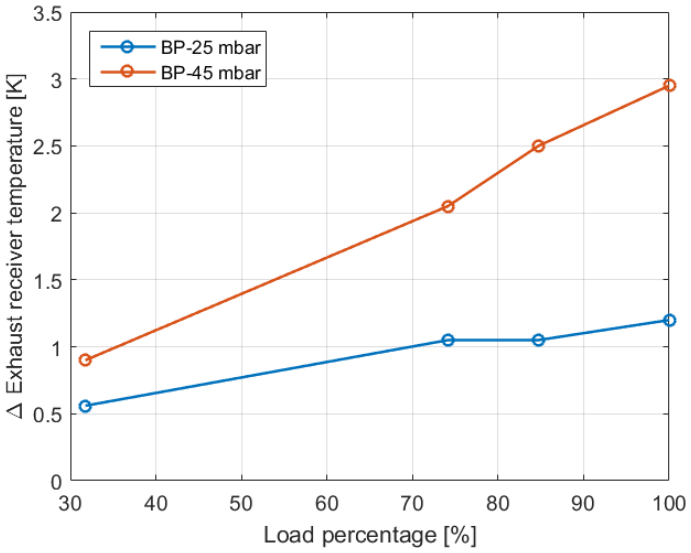

Figure 3.17: **Change in exhaust receiver temperature**

The change in parameters for externally applied single wave back pressure (45 mbar, 6s) input is small compared to the change in parameters for step up change (43 mbar). For instance, the exhaust receiver temperature for externally applied single back pressure wave changes by 1.5 K where as for step-up change, the increment is 13 K. Despite reaching the same back pressure, the change in the exhaust receiver temperature is higher for step change than single back pressure wave. This could be because of the functioning of the governor which changes the fuel flow rate into the engine to tackle the external applied back pressure and maintain constant load and speed. Since, the fuel flow rate cannot be measured during the experiments. Therefore, this is discussed in detail in section 5.3, after analyzing the simulated fuel flow rate and simulated governor response from the model. After analyzing the single back pressure waves, the next section deals with multiple back pressure waves effect on the performance of the diesel engine.

3.3.2 Multiple waves

Underwater exhaust outlet under real condition experiences continuous waves of the varying amplitude depending on the sea state in which ship is sailing. To understand the effect of amplitude of the externally applied back pressure on diessle engine performance, the engine is tested with multiple waves of the amplitude of 35 mbar, 6s and 45 mbar, 6s. The wave period is kept same as 6s for both back pressure waves. In this experiment, the diesel engine is subjected to eight continuous waves. The figure 3.18 shows the externally applied multiple back pressure wave along with the inlet receiver pressure response at 340 KW load and 981 rpm.

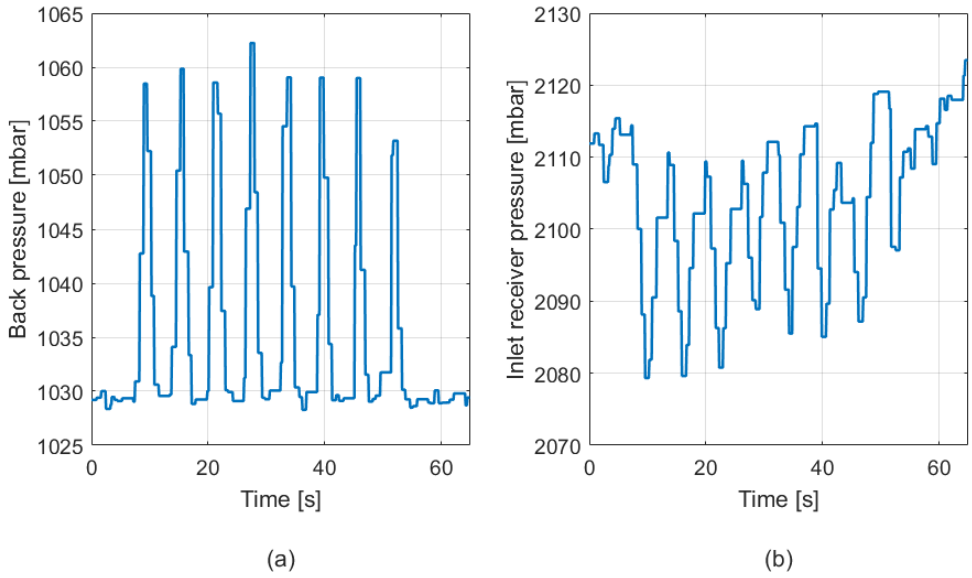

Figure 3.18: **Back pressure (a) and Inlet receiver pressure (b) for BP - 45 mbar WP - 6s**

Correspond to the 8 continuous back pressure wave applied at the exhaust outlet, eight inlet receiver pressure waves are recorded in response to this continuous back pressure wave. It shows that inlet receiver pressure is the first to respond and closely follow the back pressure. The inlet receiver pressure reduces because of the reduction in the turbocharger rpm as the pressure ratio across turbine reduces when back pressure increases. On comparing it to 35 mbar back pressure wave amplitude in figure 3.19 (b) at the same load, it is clear that the drop in inlet receiver pressure is higher for the higher amplitude of back pressure. The maximum drop for 45 mbar, 6s multiple back pressure wave is 38 mbar where as, for 35 mbar, 6s wave the drop in inlet receiver pressure is 29 mbar.

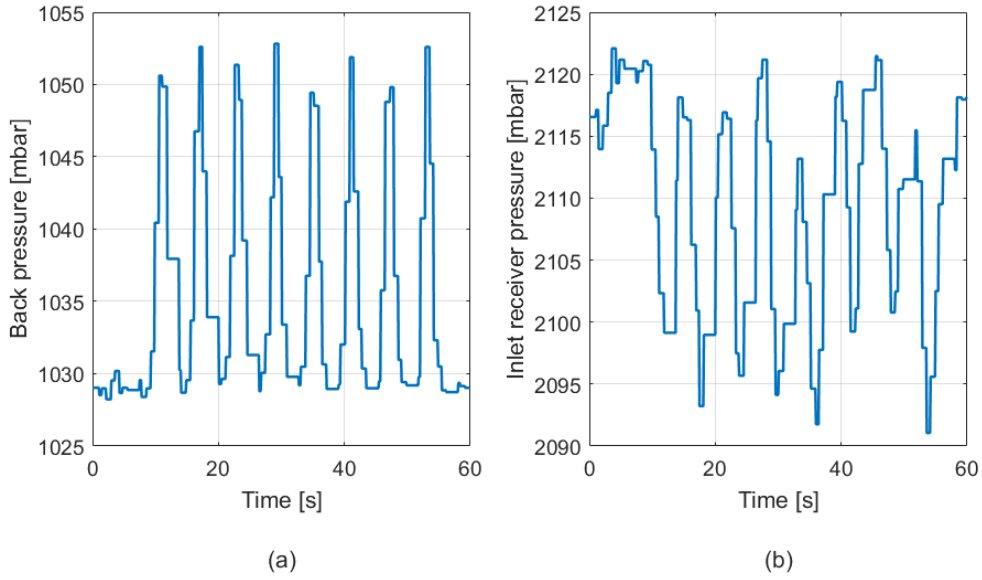

Figure 3.19: **Back pressure (a) and Inlet receiver pressure (b) for BP - 35 mbar WP - 6s**

The exhaust temperatures also respond to the multiple waves after a lag due to slow sampling frequency of the temperature sensors. This can also be see from figure 3.18(a) and figure 3.20. For back pressure wave amplitude 45 mbar, the exhaust receiver temperature and temperature after the turbine is shown side by side in figure 3.20. Unlike inlet receiver pressure in figure 3.18 (b) which follows the external applied back pressure wave, the temperature parameters in the figure below respond after a lag. Moreover, the clear crest and troughs for inlet receiver pressure is missing for the temperature parameters. This is because the exhaust receiver temperature sensor has a low sampling frequency. Therefore, it records the fluctuations in exhaust receiver temperature close to the crests and is unable to capture the troughs. This can also be seen for 35 mbar, 6s back pressure wave in figure 3.21.

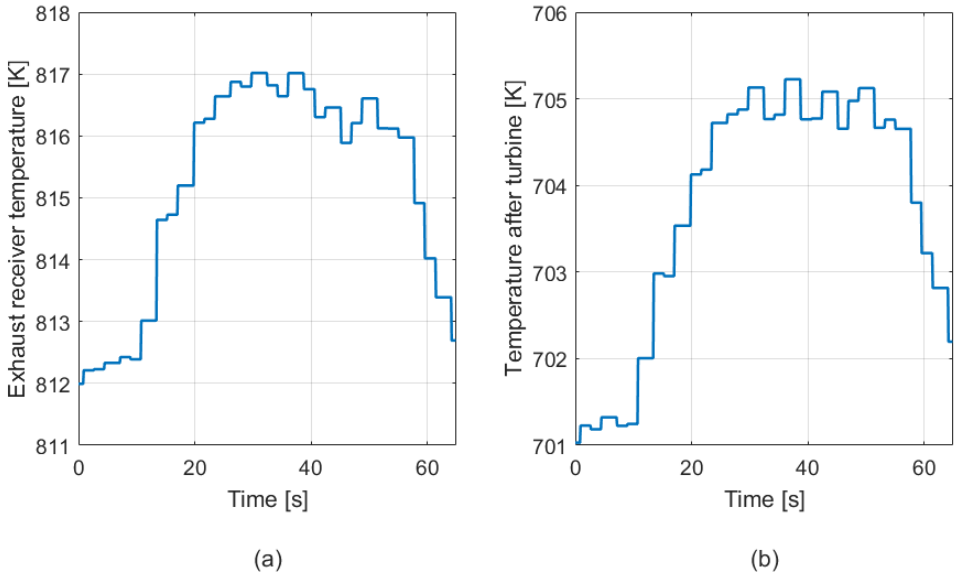

Figure 3.20: **Exhaust receiver temperature (a) and Temperature after turbine (b) for BP - 45 mbar, WP - 6s**

These temperature parameters are analyzed and compared with temperature parameters in figure 3.21. It shows the exhaust side temperatures for 35 mbar, 6s back pressure wave at 340 KW. The maximum increase in exhaust receiver temperature at 340 kW is about 5.50 K for 45 mbar, 6s back pressure wave. The increment in exhaust receiver temperature for 35 mbar, 6s back pressure wave is 4.25 K. Therefore, it can be concluded once again that the exhaust receiver temperature increases with increasing wave amplitude.

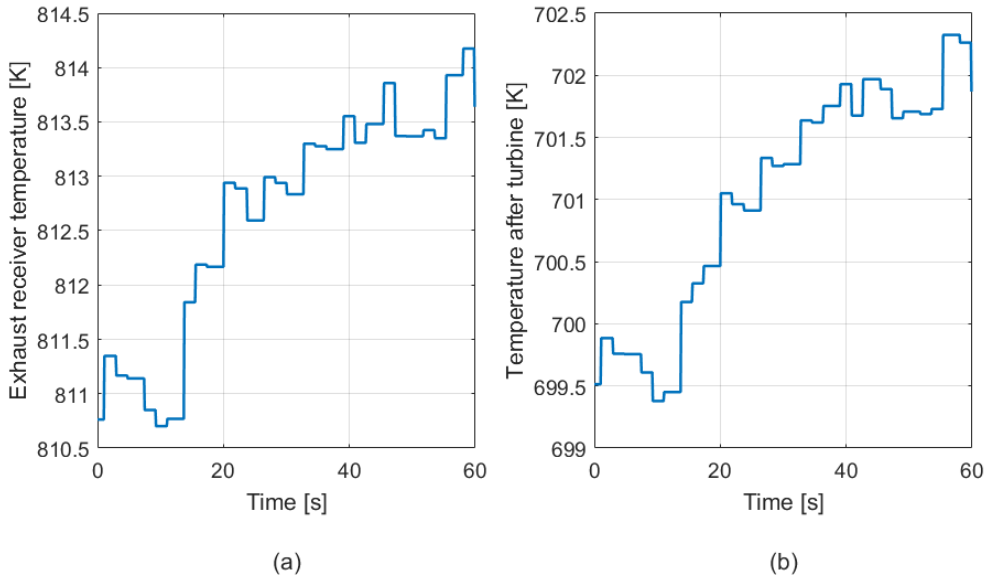

Figure 3.21: **Exhaust receiver temperature (a) and Temperature after turbine (b) for BP - 35 mbar, WP - 6s**

The exhaust receiver temperature change in response to 45 mbar, 6s and 35 mbar, 6s back pressure wave are plotted for all the set points in figure 3.17. At all loads, the exhaust receiver temperature for high back pressure (45 mbar) is always above the blue line of 35 mbar. This state that the increase in exhaust receiver temperature is higher for higher back pressure wave or significant height of the wave at all loads.

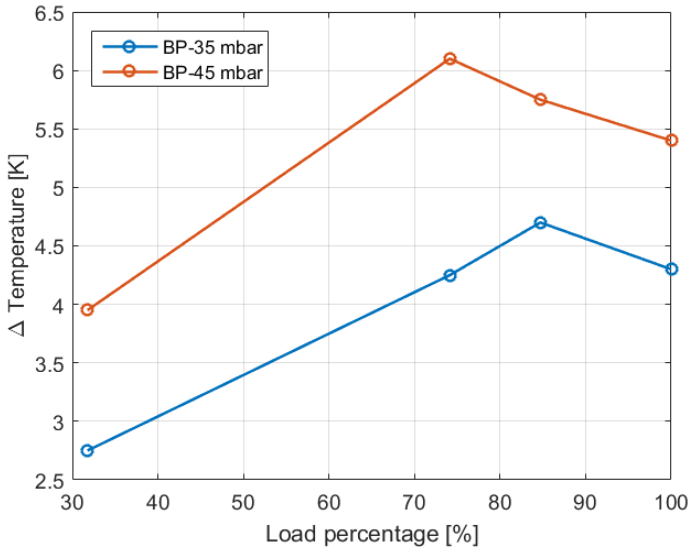

Figure 3.22: **Change in exhaust receiver temperature**

The maximum increase in exhaust receiver temperature for continuous waves is higher than that recorded for a single wave with the same wave amplitude. This increase due to multiple back pressure waves is about 5.5 K while the increment for a single wave was 2.8 K. As explained earlier, the increase in exhaust temperature

arises from the increased fuel-intake. Since the fuel flow is controlled by the governor, the governor may respond to the pulsating waves of back pressure with an overshoot and undershoot in fuel flow due to a Proportional Integral derivative (PID) controller for the governor. A continuous trend of overshooting and undershooting fuel-intake could contribute to the higher increase in exhaust receiver temperatures caused by multiple back pressure waves. The governor response and fuel flow rate cannot be measured during the dynamic experiments, therefore this is discussed in detail after discussing and analyzing the simulated results in section 5.3. This concludes the amplitude change back pressure experiments. In next section, the effect of varying wave period of the externally applied back pressure wave on the diesel engine performance is discussed in detail.

3.4 WAVE PERIOD CHANGE

The effect of change of wave period on diesel engine performance is evaluated in this section. This is done by keeping the amplitude constant and using different wave period for each input. The amplitude of externally applied back pressure wave is kept same at 45 mbar. The wave period used in these experiments are 2s, 4s, 6 and 8s. The test engine is again subjected to

- Single waves
- Multiple waves

To understand the effect of wave period, it is important that the amplitude of all back-pressure wave should be the same for all inputs. At any load, the back-pressure is not reaching 45 mbar for 2 second wave period. This is because 2 second is a very short interval in which the butterfly valve first partially closes and then opens again. The fast movement of the butterfly valve allows very less time to built up the required back pressure. Moreover, the diameter of the exhaust pipe is very large which increases the required time to built the back pressure. Thus, the back pressure value of 45 mbar cannot be reached. Therefore, waves with a wave period of 2 seconds cannot be compared with other back pressure waves with wave periods 4s, 6s and 8s. The effect of 2s wave period back pressure wave is also discussed separately in section 5.1. For a clear understanding, the comparison is carried out between the response of 4s ad 8s wave period back pressure waves in this section.

3.4.1 SINGLE WAVES

The diesel engine is subjected to single back pressure waves of different wave periods and same amplitude. Similar to the previous section in which, higher the wave amplitude, higher is the change in engine parameters. This trend holds true for the wave periods experiment also. Figure 3.23 and 3.24 shows the back pressure wave along with its effect on inlet receiver pressure for back pressure wave amplitude and a wave period of 45 mbar, 8s and 45 mbar, 4s respectively.

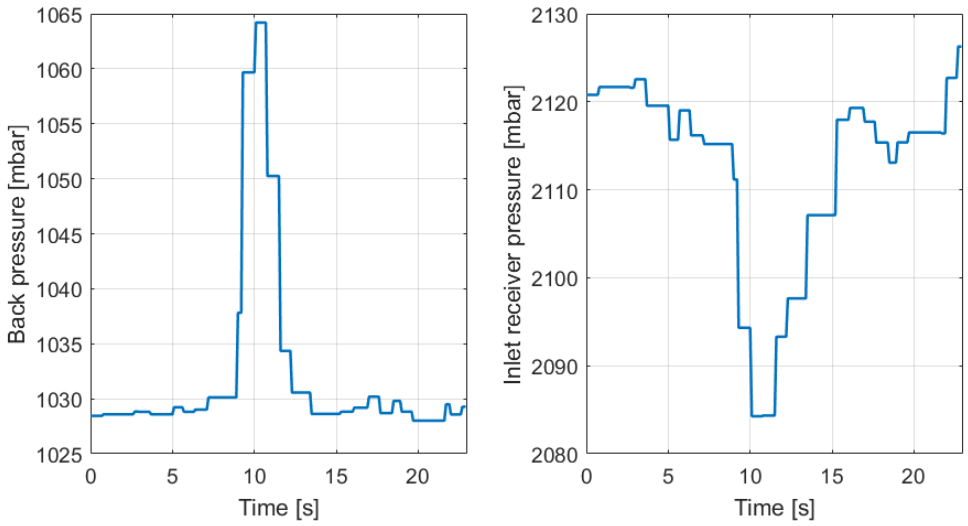

Figure 3.23: **Back pressure (a) and Inlet receiver pressure (b) for BP - 45 mbar WP - 8s**

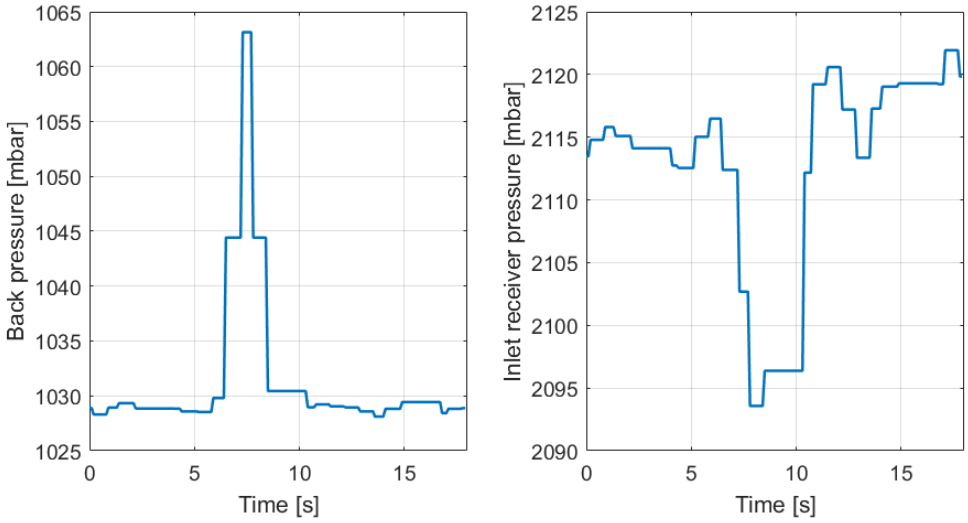

Figure 3.24: **Back pressure (a) and Inlet receiver pressure (b) for BP - 45 mbar WP - 4s**

The inlet receiver pressure can be seen dropping in both the above cases due to the increase in back pressure. The increasing back pressure reduces pressure ratio across turbine, slowing down turbine and thus, compressor. This reduces compressor discharge pressure and eventually, inlet receiver pressure. The drop in the inlet receiver pressure is more for the 8s wave period back pressure wave compared to 4s wave period. For 8s wave period, the drop in inlet receiver pressure is 31 mbar where as for 4s wave period back pressure wave, the inlet receiver pressure reduces by 24 mbar. For higher wave period, the butterfly valve gets more time to reach its required angle or back pressure and come back to the initial value. This leads to diesel engine experiencing same back pressures for more time for 8s wave period wave when compared to 4s back pressure wave. A similar trend also found for the exhaust side temperature parameters. Figure 3.25 and 3.26 show the

exhaust receiver temperature and temperature after the turbine for 8s and 4s wave period back pressure waves respectively. It is clear that the temperature parameters increment for 8s wave period wave is more than 4s wave period back pressure wave.

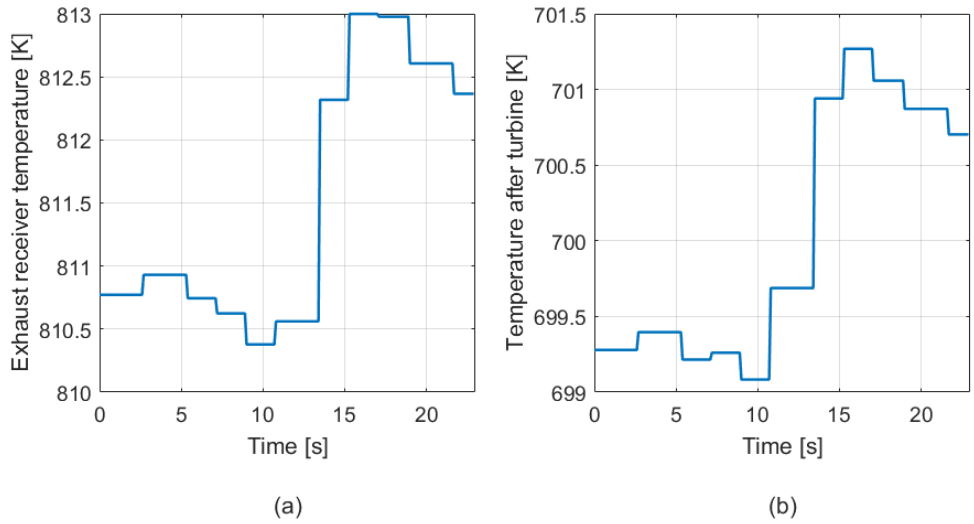

Figure 3.25: **Exhaust receiver temperature (a) and Temperature after turbine. (b) for BP - 45 mbar WP - 8s**

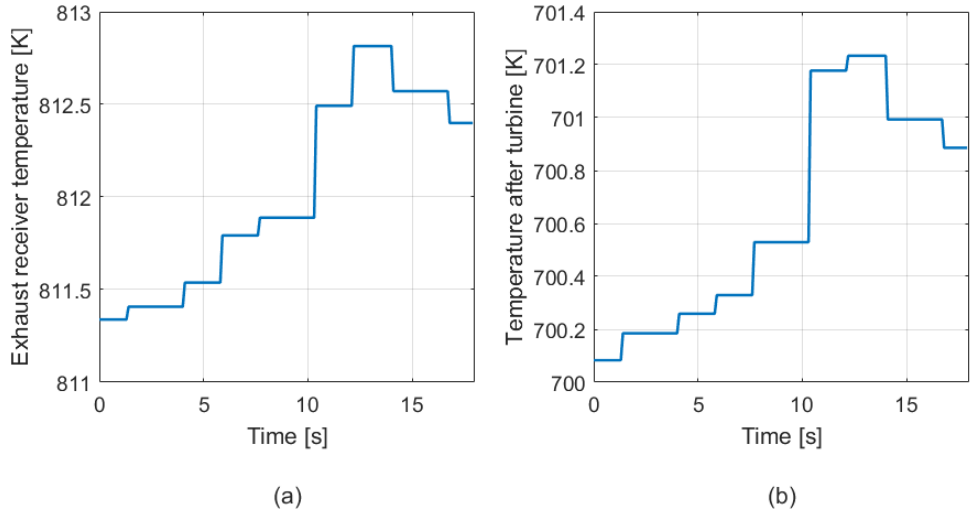

Figure 3.26: **Exhaust receiver temperature (a) and Temperature after turbine. (b) for BP - 45 mbar WP - 4s**

The maximum increment in exhaust receiver temperature is 3 K for the 8 second wave period wave while, it is about 1.25 K for the 4 second wave period. These values of increment in turbine inlet temperature are very close to the ones found for amplitude variations. As the wave period reduces below 4 seconds, the fluctuations and the rise in exhaust receiver temperature could go on reducing. This could be due to the finite response time of the governor to react to the fluctuations in back pressure. The back pressure wave period 2s is discussed separately in the sections 5.1. The increase in the maximum exhaust receiver temperature can be seen at all

loads in figure 3.27. The red line of 8s back pressure is always above the blue line of 4s wave period at all the set load points.

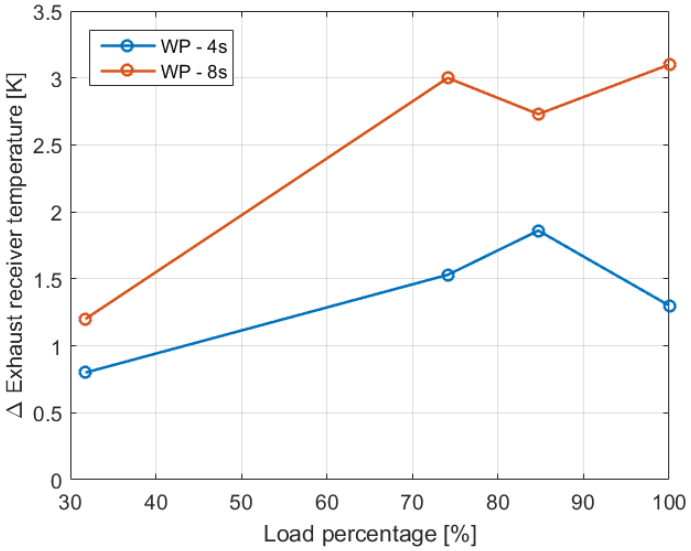

Figure 3.27: **Change in exhaust receiver temperature**

After discussing the experimental results for single wave input for wave period change experiments, the next section deals with the effect of changing wave period of multiple waves on the performance of the diesel engine.

3.4.2 MULTIPLE WAVES

In this section, the diesel engine is subjected to multiple waves (8 continuous waves). The amplitude is kept constant at 45 mbar (gauge) with different wave periods of 2s, 4s, 6s and 8s.For understanding a clear cut difference in the response of wave period on engine parameters, the comparison is carried out between 4s and 8s wave period back pressure waves. The back pressure wave and the corresponding response of inlet receiver pressure is shown in figure 3.28 (45 mbar, 8s) and figure 3.29 (45 mbar, 4s).

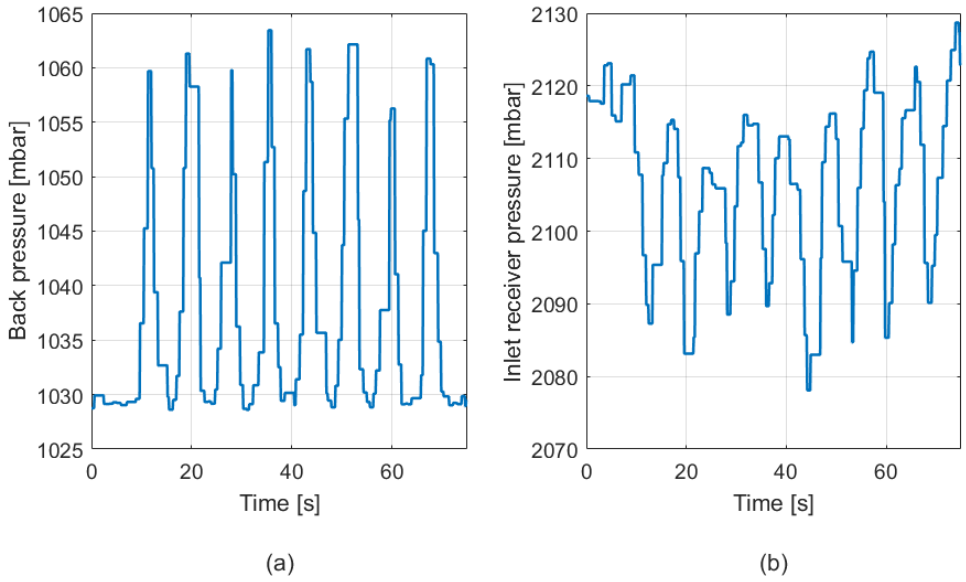

Figure 3.28: **Back pressure (a) and Inlet receiver pressure (b) for BP - 45 mbar WP - 8s**

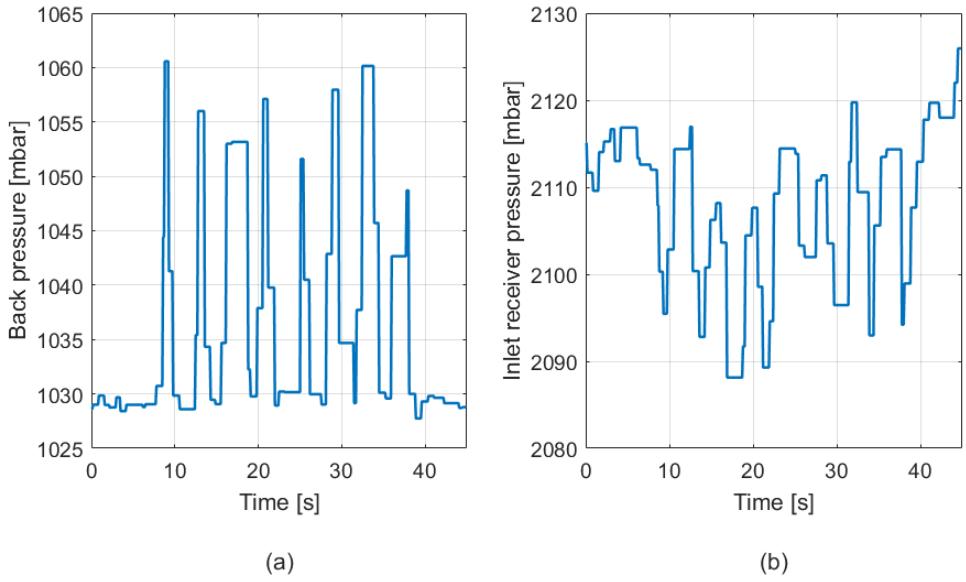

Figure 3.29: **Back pressure (a) and Inlet receiver pressure (b) for BP - 45 mbar WP - 4s**

The inlet receiver pressure drop is again found higher for higher wave period. For 8s wave period back pressure wave, the drop in inlet receiver pressure is 43 mbar where as, for 4s wave period, the inlet receiver pressures falls by 29 mbar. A similar trend for exhaust side parameters is measured in which the temperature after the turbine and exhaust receiver temperature increment is higher for 8s wave compared to 4s wave at 340 Kw load. For 8s back pressure wave the exhaust side temperature parameters can be seen in figure 3.30 whereas figure 3.31 shows temperature parameters for 4s wave period. For 8s wave period back pressure wave, the increase in exhaust receiver temperature is 6.2 K compared to the increment of 4.2

K for 4s wave period back pressure wave.It is important to note that the maximum amplitude for both back pressure is kept constant at 45 mbar.

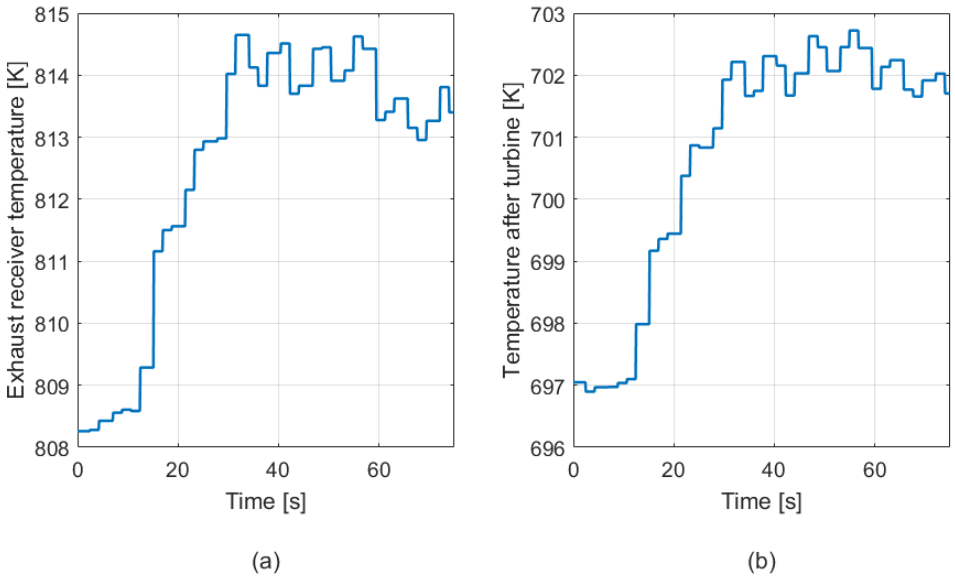

Figure 3.30: **Exhaust receiver temperature (a) and Temperature after turbine. (b) for BP - 45 mbar WP - 8s**

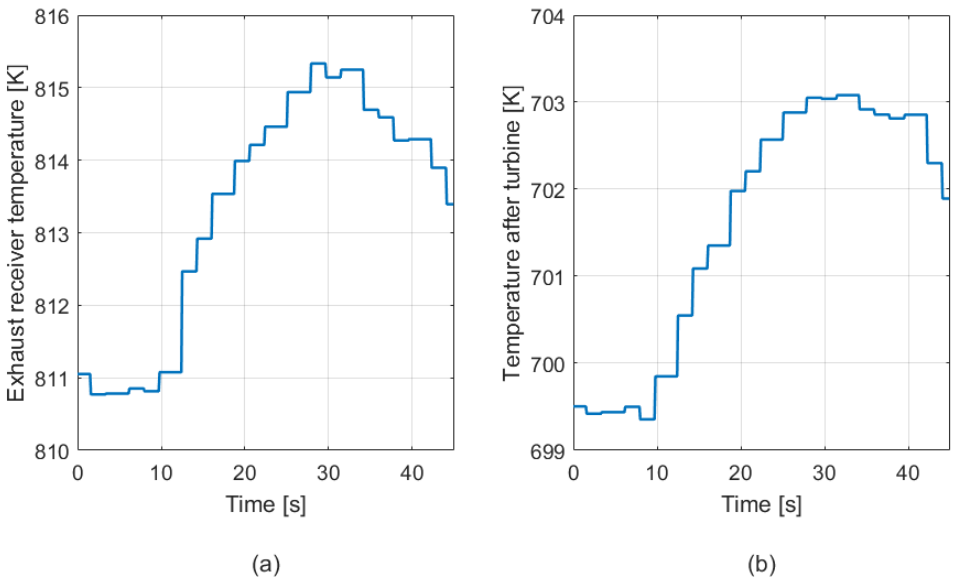

Figure 3.31: **Exhaust receiver temperature (a) and Temperature after turbine. (b) for BP - 45 mbar WP - 4s**

Increasing the wave period means the butterfly valve gets more time to partially shut down and fully re-open. This also means that the engine experience the maximum applied external back pressure for more time for higher wave periods back pressure wave. Due to this the exhaust side temperature changes with a larger value for higher wave period waves. This could only hold true up-to critical wave period. According to P. Hield [12], above critical wave period back pressure wave,

the changes in the parameters becomes constant [12]. He found during his research that, above 12 seconds, the change in parameters became constant. The test engine is subjected to maximum wave period of 8s in this research studies. The adopted verified model is used to simulate engine performances with higher wave periods and discussed in detail in section 5.2.

The back pressure waves with amplitude 45 mbar and wave period of 4s and 8s are tested on the engine at all the set points. The results are plotted in figure 3.32. For all the loads, the exhaust receiver temperature is always higher for 8s back pressure wave in comparison to 4s wave period back pressure wave.

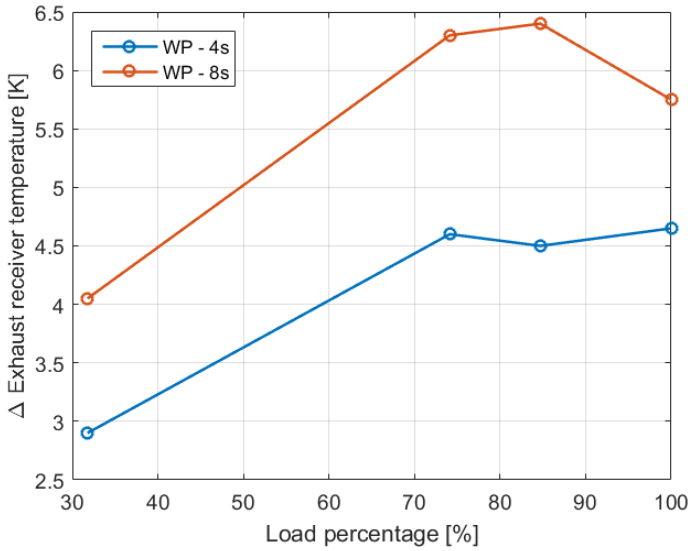

Figure 3.32: **Change in exhaust receiver temperature**

The change in parameters for multiple waves is higher than the single wave input of same amplitude and wave period. The increase in maximum temperature due to multiple back pressure waves of 4 seconds and 8 seconds wave period is approximately 5.7 K and 4.5 K, respectively. This trend was also seen in the case of amplitude change of back pressure waves as shown in figure 3.22.

Chapter 4

DE-B MODEL MATCHING

The measurements from the dynamic back pressure experiments is already discussed in the previous chapter. The experimental results are used to verify the adopted Diesel engine - B model. The Diesel engine model (DE-B) adopted for this research is a mean value estimated model (MVEM) developed at TU Delft, since 1998. The model is already matched to simulate the performance of the test engine by Sapra et. al. [3]. All the parameters specified in the adopted model can be divided into 3 sub division [39].

- The known parameters - These parameters are simply known and available from the engine manual. For example gas constant, compression ratio, stroke length etc.
- The set parameters - These parameters can be estimated as non-dimensional function of a known parameter. For example, the inlet and exhaust manifold diameters can be expressed as to a certain percentage of the bore diameter.
- The unknown parameters - These parameters are fundamental to the model. They are calibrated to the measured data. For example, mu-phi parameter which is a measure of the flow resistance of the cylinders during scavenging.

The various sub-systems of the model was already matched for the smooth functioning of the model before adopting it for this master thesis result. This matching of sub system is called system matching. Such matching is already performed for the MVEM model. The turbocharger model is also required to match with diesel engine model in order to validate the model. In this matching, first air swallow characteristics of the compressor is matched by matching compressor flow to the engine flow. This is followed by matching turbine flow to exhaust flow. At last, matching of turbine power to compressor power (Buchi balance). This is how the MVEM is calibrated and matched. The modeling of the various sub systems of the the Diesel Engine - B model is discussed in appendix C.

In this chapter, the adopted model is used to simulate the engine performance with the same back pressure waves measured during the experiment. The simulated results are compared with measurements. The quantitative and qualitative analysis of measurements and simulations gives the error between the measurements and simulations. This shows the extent to which the adopted model can accurately simulate the engine performance. The verified model provides the missing parameters which cannot be recorded at the time of experiments. For instance, air excess ratio,

governor response and fuel flow rate cannot be measured during the experiments. Furthermore, the can be used to simulate engine performances with higher sea states and wave periods which could not be tested on the diesel engine. The simulated results are used to develop the engine envelope to find the smoke and thermal overload limits/ The continuous lines of air excess ratio and exhaust valve temperature are plotted in the engine envelope. These smoke and thermal limits are further used to find the externally applied back pressure limits. This is discussed in detail in section 5.4.

4.1 STATIC MODEL MATCHING

The DE-B model adopted for the simulation purposes was already matched with MAN4L2027 diesel engine at The Netherlands Defence Academy by Sapra et al [3] as the experiments are performed on the same engine. The static experiments are performed at 30 mbar and 43 mbar steady state back pressure. The static model simulates the engine performance at the same static back pressure. The simulated results are compared with the static measurements from the experiment. Figure 4.1 shows the inlet receiver pressure and inlet receiver temperature from the experiments and simulations together.

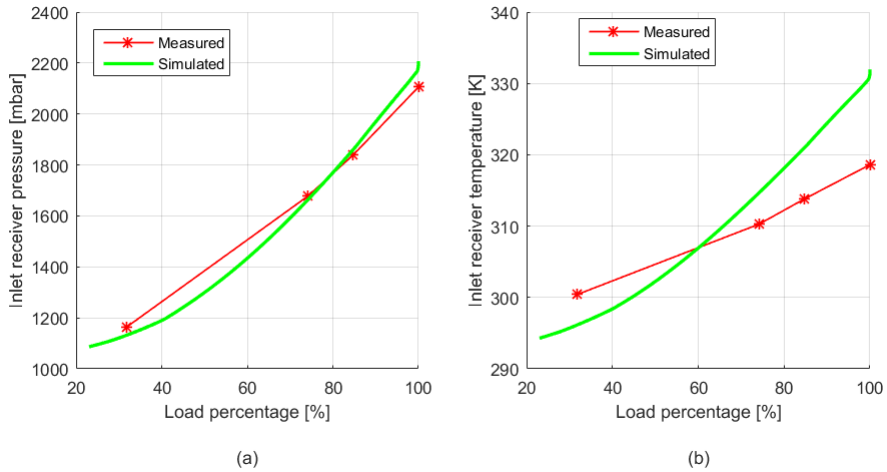

Figure 4.1: **Static matching - Inlet receiver temperature (a) and Inlet receiver pressure(b). BP - 43 mbar , Load - 340KW, RPM - 981**

The maximum error of 4.17% for inlet receiver pressure occur at maximum load of 340 KW. Similarly, the exhaust side temperature parameters are compared from the simulation and experiments. The figure 4.2 (a) shows the exhaust receiver temperature where as figure 4.2 (b) shows the temperature after turbine. The maximum error of 13.8% in temperature after turbine is at 108 KW where as exhaust receiver temperature's error is maximum (10.5%) at 108 KW. Despite, model is already matched with the test engine before, the error is more than 10% at 108 KW. This could be because the fuel injector for cylinder unit 1 is replaced after the model was matched to the engine. The fuel injector is replaced by a smaller injector on the test engine. Moreover, the test engine is equipped with pulse turbocharger. Changing the injector could have affected the turbocharger matching. It is also difficult to

model the pressure pulse produced by the pulse turbocharger. Sapra et. al. [3] have modelled this pulse turbocharger with zinner correction factors.

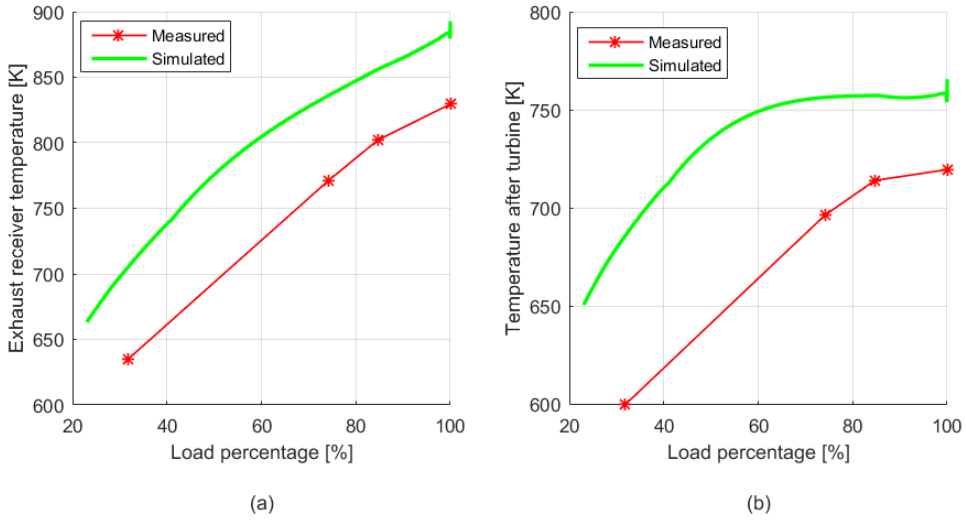

Figure 4.2: **Static matching - Exhaust receiver temperature (a) and Temperature after turbine(b). BP - 43 mbar**

This concludes the verification of the model with the static results obtained from the experiments performed on the diesel engine. The error percentage between simulated and measured parameters results for 43 mbar static back pressure at all load set points is shown in table 4.1. Since the error is more than 10%, it cannot be said that the model is ideally matching with the experiments.

Table 4.1: **Error percentage between measured and simulated results - Static BP - 43 mbar**

Load [KW]	Load percentage [%]	Temperature after turbine error [%]	Exhaust receiver temperature error [%]	Inlet receiver pressure error [%]
108	31.76	13.8	10.5	2.49
252	74.12	8.6	8.4	0.77
288	84.71	6.02	6.7	1.08
340	100	5.4	6.7	4.17

4.2 STEP CHANGE

The first step for verifying adopted DE-B model with the dynamic experiment results are performed in this section. The model is fed with the same input back pressure wave, replicated with butterfly valve and measured during the experiment. The adopted model had a bug in the programming. Therefore, simulated results shows an initial glitch in the recorded parameters. When the model is subjected to a step change of 43 mbar back pressure in 4s at 340KW, the results simulated by the model

with bug is shown in figure 4.3. The figure 4.3(a) and 4.3(b) shows simulated applied back pressure and the corresponding effect on the exhaust receiver temperature when the model is running with the active bug.

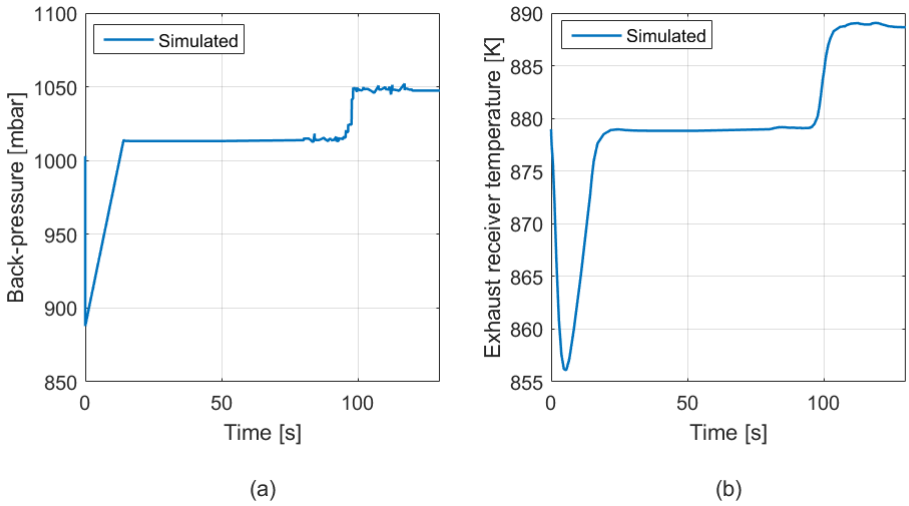

Figure 4.3: **Step up change with glitch. Simulated back pressure (a) and Simulated exhaust receiver temperature (b). BP -43 mbar Time - 4s**

In the above figure, the back pressure input is such given that the back pressure step up starts at time equal to 80s. But in figure 4.3 (a) an unknown peak can be seen at the starting of the simulated back pressure wave. Since the simulated back pressure is affected by the bug, the corresponding exhaust receiver temperature also shows the same glitch at the start. This bug is present because of an unnecessary MATLAB function in the Simulink model. The MATLAB function along with the model is shown in the appendix B. After removing that MATLAB function, the engine performance is again simulated with the same step up back pressure of 43 mbar in 4s. This is visible in figure 4.4 as simulated back pressure and exhaust receiver temperature can be seen without any glitch.

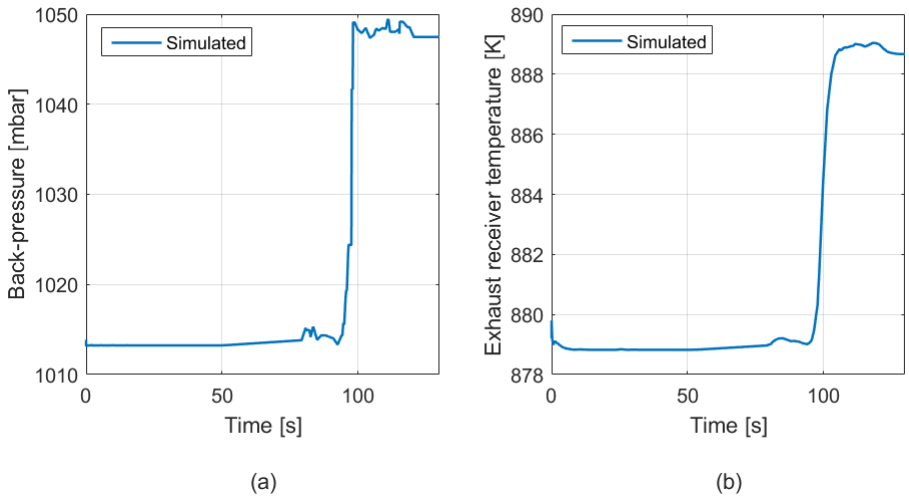

Figure 4.4: **Step up change without glitch. Simulated back pressure (a) and Simulated exhaust receiver temperature (b). BP -43 mbar Time - 4s**

After removing the bug from the DE-B model, the model can be verified by comparing the simulated parameters to the measured parameters from the experiments. First, the comparison is carried out between measured and simulated results for step up change of 43 mbar back pressure in 4s at maximum set point. The figure 4.5 (a) and (b) shows measured and simulated back pressure, respectively. Figure 4.5 (c) shows the normalized simulated and normalized measured back pressure perfectly superimposed on each other. Normalising the parameters rescales the values into a range of 0 -1. After rescaling, it is easy to compare and search for similar trends between simulated and measured results.

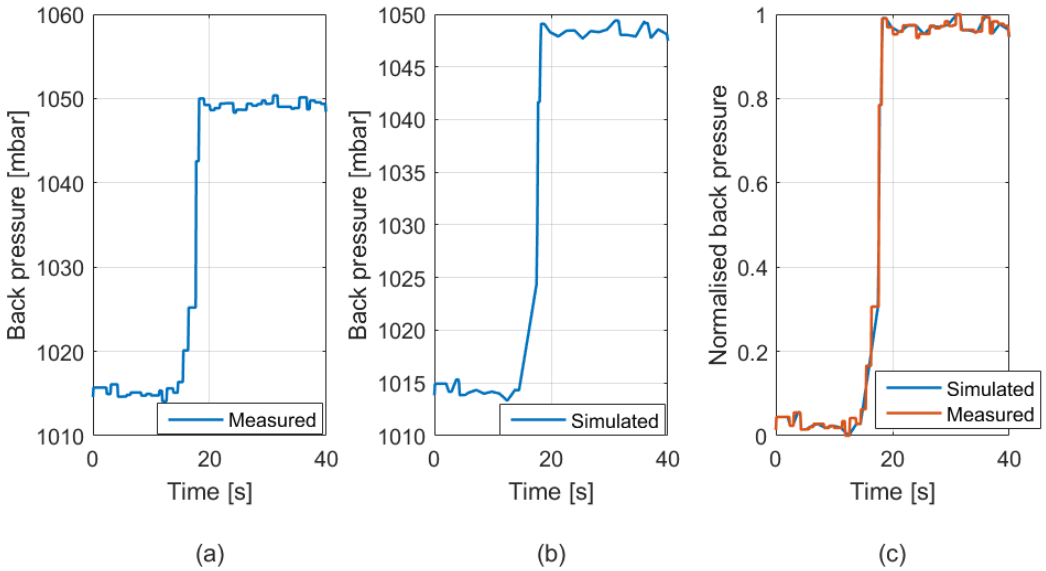

Figure 4.5: **Step up change in back pressure. Measured (a), simulated (b) and normalized (c). BP -43 mbar Time - 4s**

The normalization is carried out using the following formula -

$$z_i = \frac{x_i - x_{min}}{x_{max} - x_{min}} \tag{4.1}$$

where

- x_i - Data points (x_1, x_2, x_3 .....x_n).
- x_{max} - Maximum value of data point.
- x_{min} - minimum value of data point.

A step increase in back pressure reduces the pressure ratio across the turbine, slowing down the turbocharger. This leads to a reduction in compressor discharge pressure and inlet receiver pressure. The measured, simulated and normalized inlet receiver temperature is shown in figure 4.6. From figure 4.6(c), it can be stated that measured and simulated inlet receiver responds at the same time for the increase in back pressure. The drop in measured inlet receiver pressure is 45 mbar whereas the simulated inlet receiver pressure drops by 40 mbar.

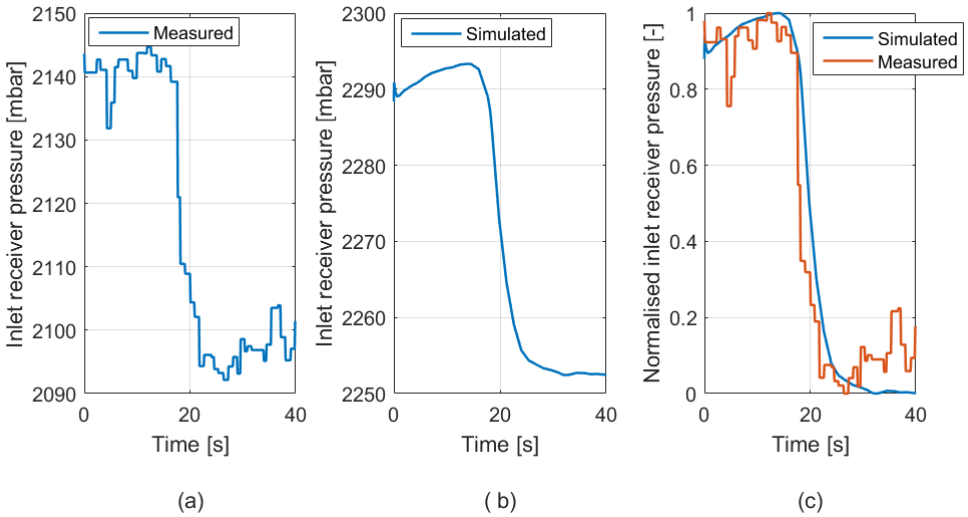

Figure 4.6: **Inlet receiver pressure. Measured (a), simulated (b) and normalized (c). Step up BP -43 mbar Time - 4s**

The air mass flow into the engine is reduced with decreasing compressor discharge pressure caused by increasing the back pressure. Due to the reduction of air intake, the air excess ratio also reduces as shown in figure 4.7(a). After increased back pressure, the engine needs to perform more work to pump out exhaust gasses from the cylinder, thus required more fuel. The governor responds to this by increasing the fuel rack which increases the fuel flow rate at the same time. The simulated governor response along with flow fuel rate is shown in figure 4.7(b) and 4.7(c).

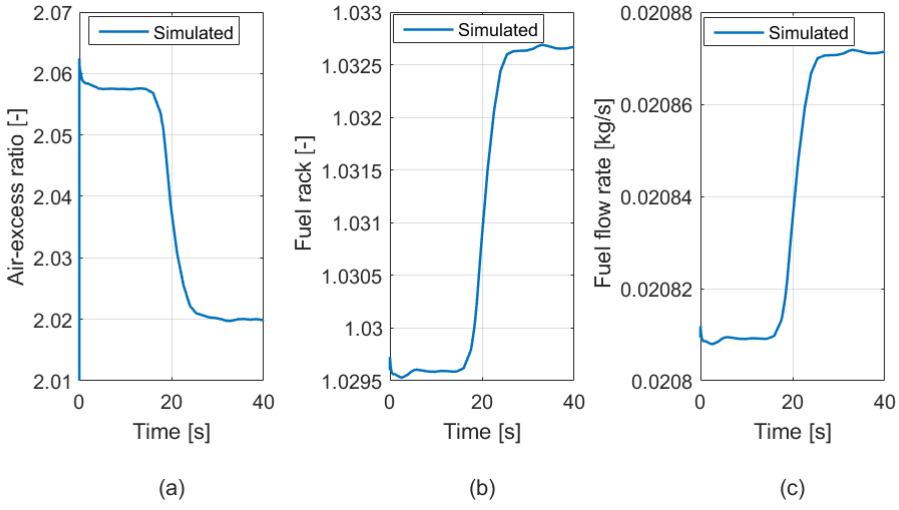

Figure 4.7: **Simulated air excess ratio (a), simulated governor response (b) and simulated fuel flow rate (c). Step up BP -43 mbar Time - 4s**

The increased fuel flow increase the temperature on the exhaust side of the engine. The measured, simulated and normalized exhaust receiver temperature for the 43 mbar back pressure is shown in figure 4.8. The increase in measured exhaust receiver temperature is 13 K whereas the simulation shows an increase of 10 K. The simulated temperature response (blue line) in figure 4.8(c) is fast compared to

the measured response (red line). This is mainly because of selected settings of the governor control. The governor block in the model consist of proportional - integral control where as the governor on test engine consist of proportional integral derivative (PID) controller. The simulated exhaust receiver temperature response can be delayed by changing the turbocharger settings. On changing the turbocharger settings, also delays the response of inlet receiver pressure which is currently matching as shown in figure 4.7(c).

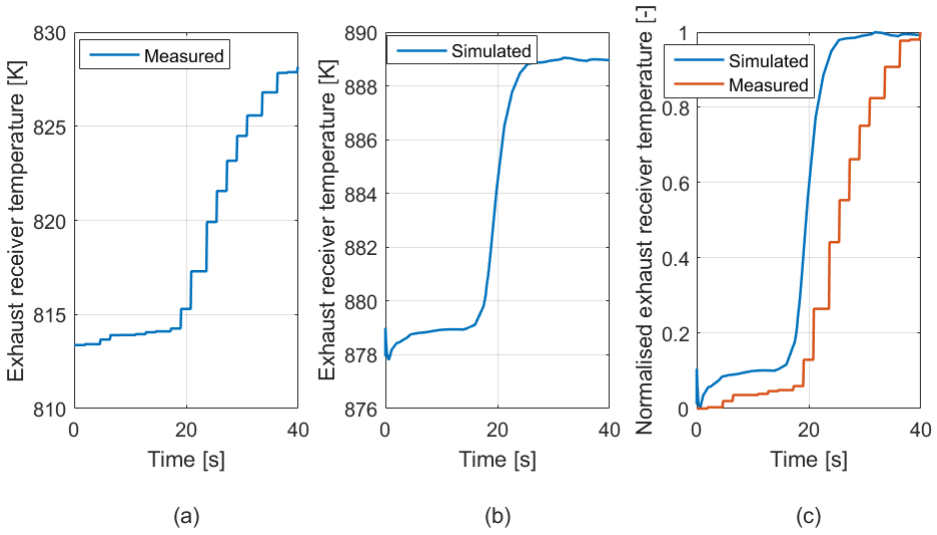

Figure 4.8: **Exhaust receiver temperature. Measured (a), simulated (b) and normalized (c). Step up BP -43 mbar Time - 4s**

This concludes the verification of the Diesel engine - B model. In next sections, the model is used to simulate the performance of diesel engine with the back pressure waves measured during the experiment.

4.3 AMPLITUDE CHANGE

The Diesel engine - B model is subjected to single and multiple back pressure waves. The amplitude and wave period of the input waves is exactly the same as the back pressure wave measured during the experiment. The major aim of these simulations is to analyze the parameters which cannot be measured during the experiments. For example air excess ratio, fuel flow rate etc. Similar to the previous chapter, the simulated results for single and multiple back pressure amplitude change are discussed in separate sections.

SINGLE WAVES

The model is simulated with a single back pressure wave of amplitude 25 mbar and 45 mabar with the same wave period of 6s at 340 KW. The obtained results are compared with the measured results from the experiment discussed in the previous chapter. The model is subjected to an input back pressure wave of 45 mbar and 6s wave period. This input wave is the same back pressure wave, measured during the experiment as shown in figure 3.13(a). Due to the same input as measurement,

a perfect match of the back pressure at the exhaust outlet can be seen in figure 4.9. Figure 4.9(a) shows the normalized measured and normalized simulated back pressure wave plotted on each other. Along with normalized back pressure, the simulated inlet receiver pressure (b) and normalized inlet receiver pressure (c) are also shown in the same figure.

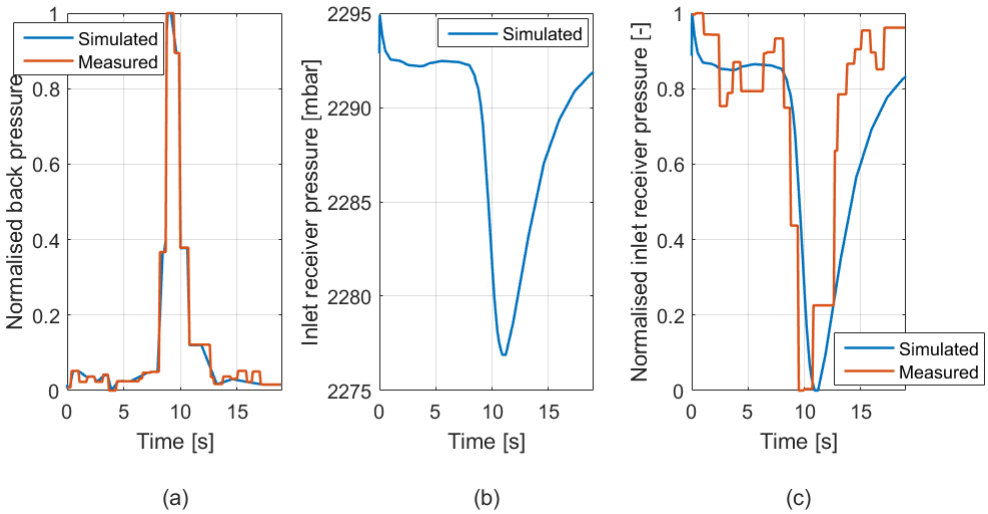

Figure 4.9: **Normalized back pressure (a), simulated inlet receiver pressure (b) and normalized inlet receiver pressure (c). BP -45 mbar Wave period - 6s**

The single fluctuation in the back pressure leads to the drop in the simulated inlet receiver pressure. The inlet receiver pressure drop for 25 mbar back pressure wave is shown in figure 4.10(b). On comparing with figure 4.9(b), it can be stated that like experiments, simulations also show that the inlet receiver pressure drop is also higher for the higher amplitude of back pressure. Moreover, the model predicts the drop without any lag compared to the experiment measurements. This can be seen from the simulated and measured normalized inlet receiver pressure for 45 mbar and 25 mbar in figures 4.10(c) and 4.9(c). Thus, it can be said that the model also follows the trend shown by the experiments for inlet receiver pressure.

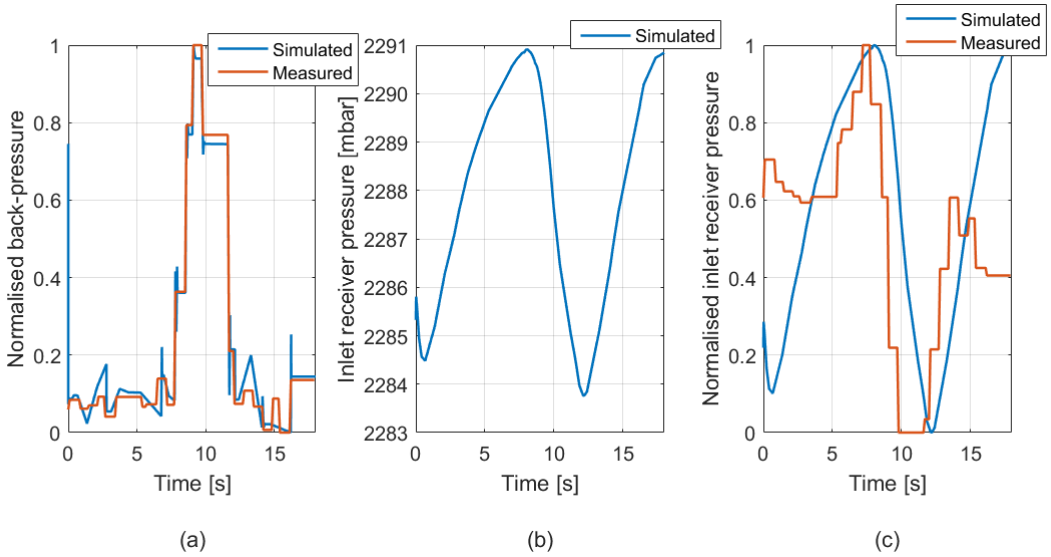

Figure 4.10: **Normalized back pressure (a), simulated inlet receiver pressure (b) and normalized inlet receiver pressure (c). BP -25 mbar Wave period - 6s**

The increase in back pressure decreases air intake as the compressor discharge pressure reduces. There is an increment in fuel flow rate to compensate for the extra pumping work by the engine. More fuel and less inlet air flow decreases the air-fuel ratio and thus, decreasing air excess ratio. The air excess ratio values tells us whether the engine is breathing properly or not. If the air-excess ratio falls below the engine manual's limit, black smoke can be seen in the exhaust. Black smoke in the exhaust signifies incomplete combustion. Therefore, air excess ratio can be used to define the smoke limits for the engine as discussed in detail in section 5.4.1. The air excess ratio along with fuel flow rate is shown for 45 mbar back pressure wave in figure 4.11. It is clear from the figure that the moment fuel flow increases, air excess ratio start dropping. On comparing the same parameters for 25 mbar and 6s back pressure wave (refer to figure 4.12) at same load. It displays that the air excess ratio drop is higher for the higher back pressure amplitude or wave with higher significant height.

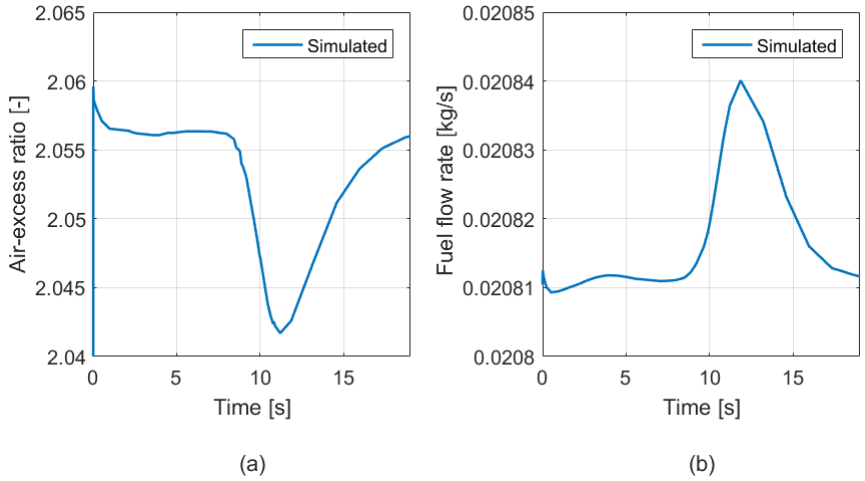

Figure 4.11: **Simulated air excess ratio (a), simulated fuel flow rate (b). BP -45 mbar Wave period - 6s**

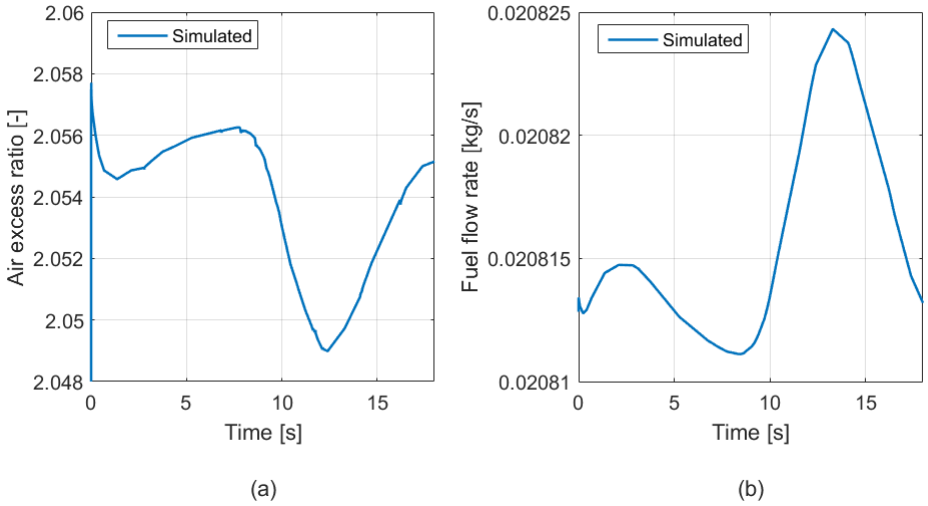

Figure 4.12: **Simulated air excess ratio (a), simulated fuel flow rate (b). BP -25 mbar Wave period - 6s**

To compensate for the extra pumping work to remove the exhaust gasses, the fuel flow rate increases the fuel into the system. This leads to an increase in the exhaust receiver temperature. Figure 4.13 and 4.14 shows the increase in exhaust receiver temperature due to 45 mbar and 25 mbar back pressure amplitude respectively. The increment in simulated exhaust receiver temperature is 2.7 K for 45 mbar, 6s back pressure wave. The 25 mbar back pressure wave demonstrates an increment of 1.7 K. Thus, it can be clearly said that the increase in simulated exhaust receiver temperature is also higher for higher back pressure amplitude. But on the other hand, it is clear from the figure 4.14(b) that the simulated exhaust receiver responding faster than the measurements. This is because of the selected controller settings of the governor and turbocharger.

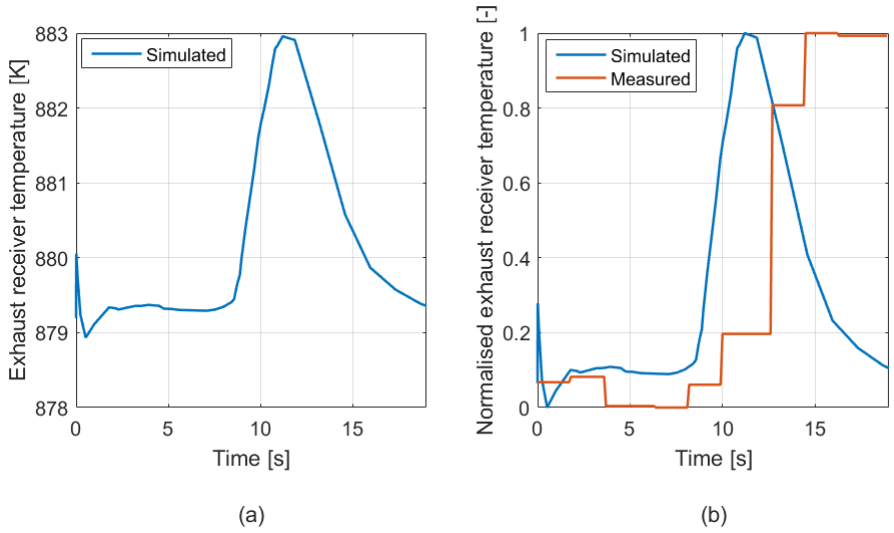

Figure 4.13: **Simulated exhaust receiver temperature (a), Normalized exhaust receiver temperature (b). BP -45 mbar Wave period - 6s**

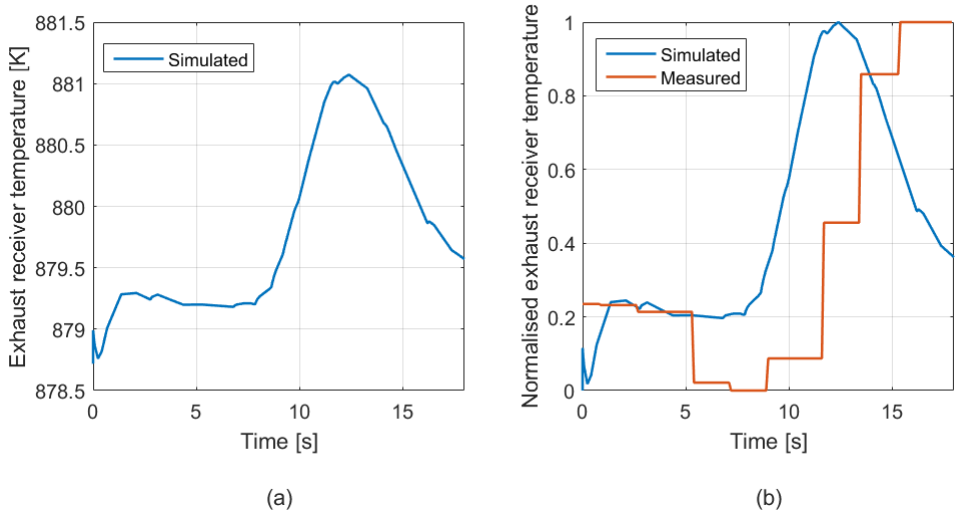

Figure 4.14: **Simulated exhaust receiver temperature (a), Normalized exhaust receiver temperature. BP -25 mbar Wave period - 6s**

After comparing the two simulated results to each other in the above figures, they are also compared with the experimental measurements. On analyzing the simulated results against the measurements quantitatively, it is found that the model is predicting higher increments in temperature than the experiments. This can be seen for any load in the figure 4.15 as increments are higher for simulated exhaust receiver temperatures. This shows that despite the adopted model following the trend shown in the experiment, it is not perfect matched to predict the exact performance of the diesel engine.

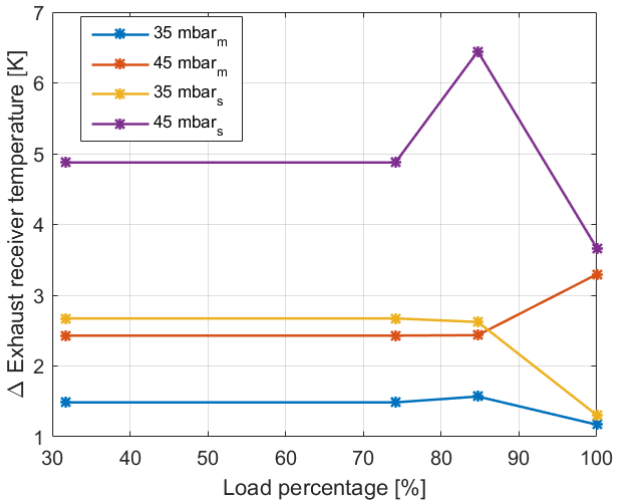

Figure 4.15: **Measured (m) and simulated (s) exhaust receiver temperature increment for single back pressure waves**

After the quantitative analysis, qualitative analysis carried out and the absolute values of the parameters for experiment and simulations are compared to each other. The error between the absolute values of inlet receiver pressure and exhaust receiver temperature is shown in figure 4.16. The error between measurement and simulations for inlet receiver pressure is maximum at 340 KW but always remain below 10% at all loads. The error in exhaust receiver temperature is more than 10% at 108 KW but remains less than 10% at higher set points. The error in exhaust receiver temperature is high at 108 KW because the static model is also showing the biggest error for 108 KW. The static model also shows maximum error in inlet receiver pressure at 340 KW. The same trend is shown by the dynamic model in which maximum error occurs at 340 KW.

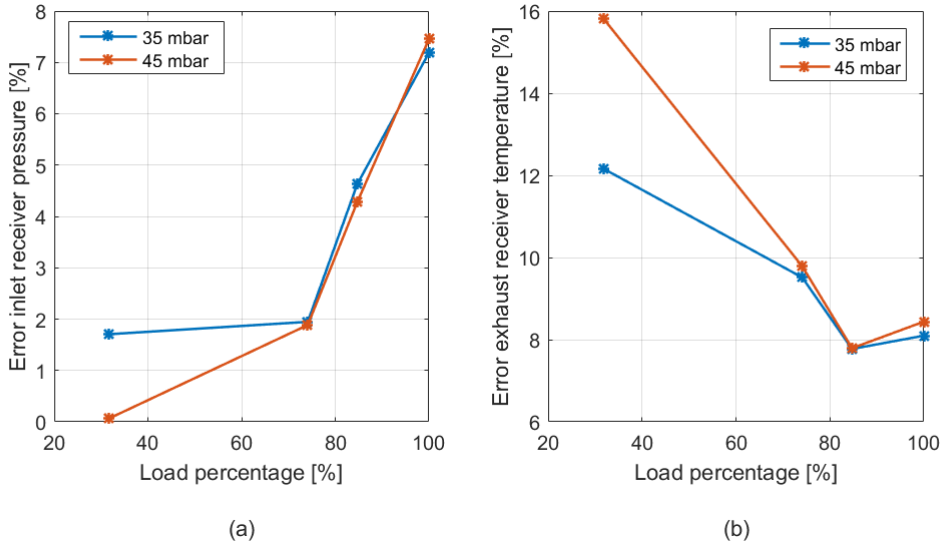

Figure 4.16: **Absolute error between measurement and simulations for inlet receiver pressure (a) and exhaust receiver temperature (b) for single back pressure wave.**

4.4 MULTIPLE WAVES

In this section, the model is used to simulate the effect of multiple waves on engine performance. The back pressure wave input is the same back pressure waves replicated by the butterfly valve and measured during experiments. The simulations are carried out for back pressure wave amplitude of 35 mbar and 45 mbar with the same wave period of 6 seconds at 340 KW. The simulated and measured back pressure at the turbine outlet is normalized and superimposed for 45 mbar multiple wave input. It is shown in figure 4.17.

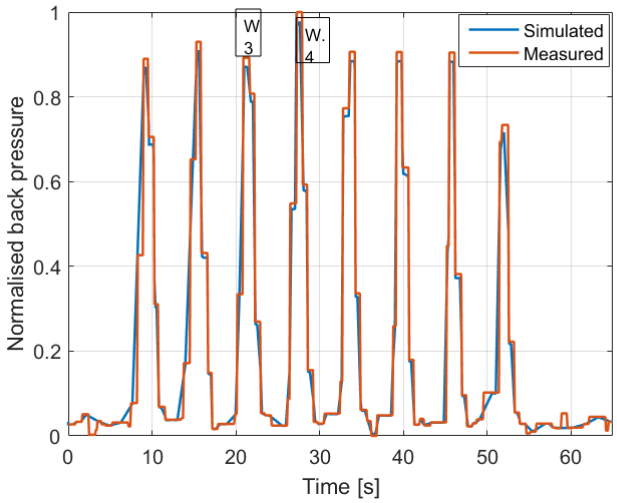

Figure 4.17: **Normalized back pressure. BP -45 mbar Wave period - 6s**

With multiple fluctuations in external applied back pressure, the inlet receiver pressure also fluctuates. The fluctuating inlet receiver pressure response for the 45 mbar back pressure wave is plotted in figure 4.18(a) which shows a maximum drop of inlet receiver pressure of 16 mbar. This pressure drop is half of the pressure drop measured when the same back pressure is applied during the experiments as shown in figure 3.18(b). On superimposing the normalized measured and simulated inlet receiver pressure for 45 mbar wave, the plot obtained is shown in figure 4.18(b). It can be seen that the simulated drop in pressure response is following the trend of the measured drop. Moreover, it is found out that the back pressure waves in which the engine experiences higher back pressure for more time near the peak of back pressure wave tend to show bigger change in the parameter. For instance, the number three back pressure wave (W3) in figure 4.17 is lower than number four wave (W4) but still, the maximum drop is the same for both the waves.

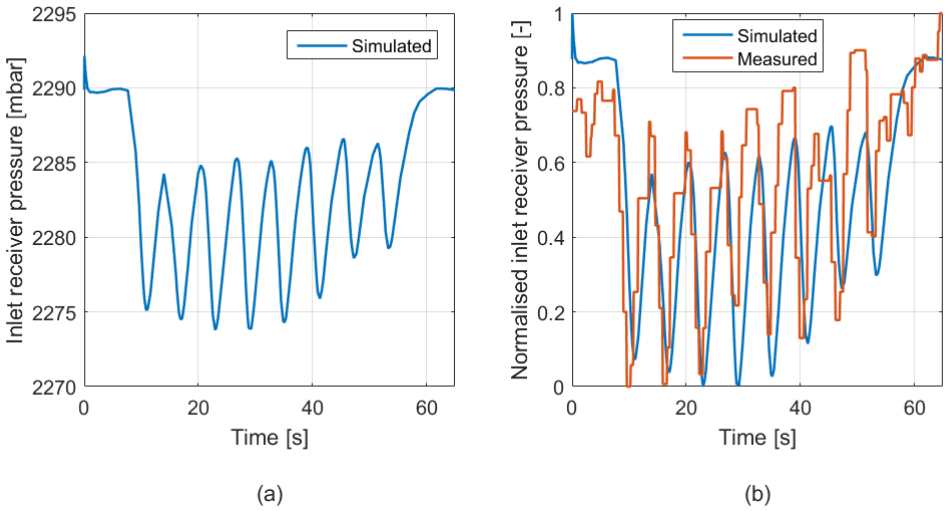

Figure 4.18: **Simulated inlet receiver pressure (a) and normalized inlet receiver pressure (b). BP -45 mbar Wave period - 6s**

The same model is also used to simulate the engine performance due to 35 mbar back pressure amplitude. The results are shown in figure 4.19. The simulation also provides evidence that the drop in inlet receiver pressure is higher for 45 mbar than 35 mbar.

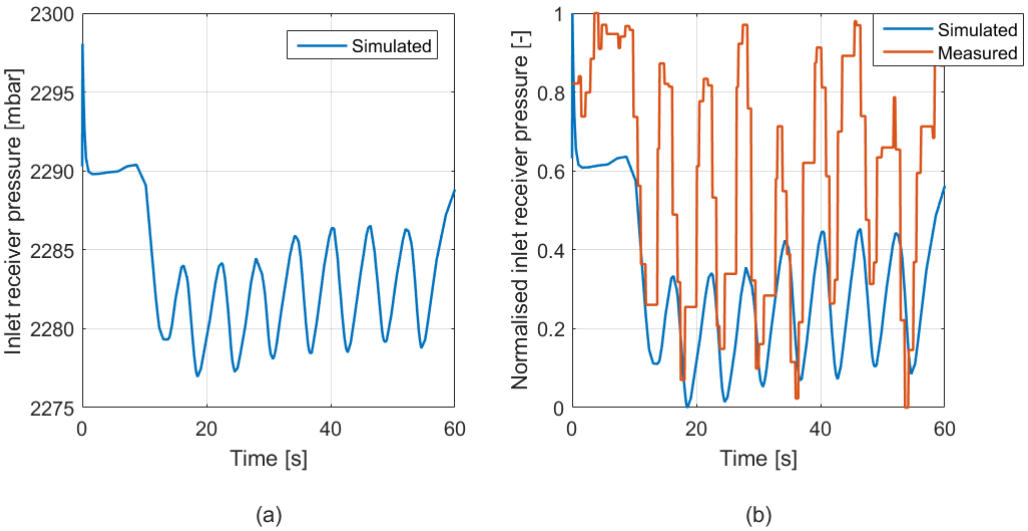

Figure 4.19: **Simulated inlet receiver pressure (a) and normalized inlet receiver pressure (b). BP -35 mbar Wave period - 6s**

The air excess ratio also dips and fuel flow rate increases with increasing back pressure. The change in air excess ratio and fuel flow rate is more for 45 mbar than 35 mbar dynamic back pressure wave. The figure 4.20 and 4.21 respectively, shows the drop in air excess ratio (a) and increase in fuel flow rate for 45 mbar and 35 mbar.

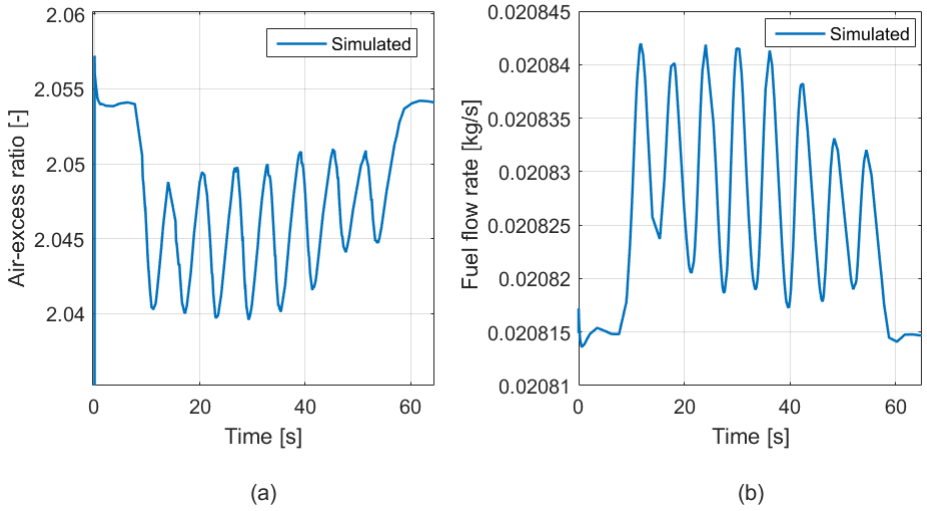

(a) (b)

Figure 4.20: **Simulated air excess ratio (a), simulated fuel flow rate (b). BP -45 mbar Wave period - 6s**

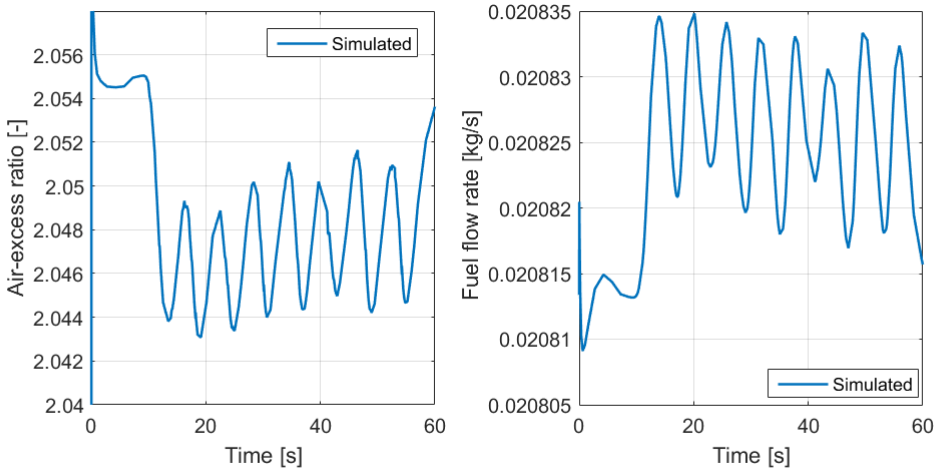

(a) (b)

Figure 4.21: **Simulated air excess ratio (a), simulated fuel flow rate (b). BP -35 mbar Wave period - 6s**

The pulsation in the fuel flow rate leads to the pulsation of exhaust receiver temperature. The simulated results also suggest that the high amplitude of external back pressure leads to a bigger change in fuel flow rate, thus higher change in exhaust receiver temperature. The exhaust receiver temperature increment for 45 mbar multiple back pressure wave is 3.5 K as shown in figure 4.22(a) whereas for 35 mbar wave the increment of 2.8 K as plotted in figure 4.23(a). The simulated normalized exhaust receiver temperature (figure 4.21(b)) shows that the temperature probe is having a low sampling frequency. Therefore, the measurements are not showing any troughs and crest as presented by the model results. Thus, the way simulations are reaching the peaks and then reducing but the same trend is missing in the measurements. The response of simulated exhaust receiver temperature is fast then measured temperature. This is because of the controller settings of the governor

in the model. Furthermore, the turbocharger control settings could also be used to match the simulation and measured temperature results but, it also affects the simulated inlet receiver pressure by slowing it down. In addition, the governor in the test engine consist of a PID controller where as the governor block in the model uses a PI controller. This could be another reason that the simulations are faster than the measured temperature. For measurements, it looks like that the temperature response from every single wave is adding up to reach the maximum exhaust receiver temperature .

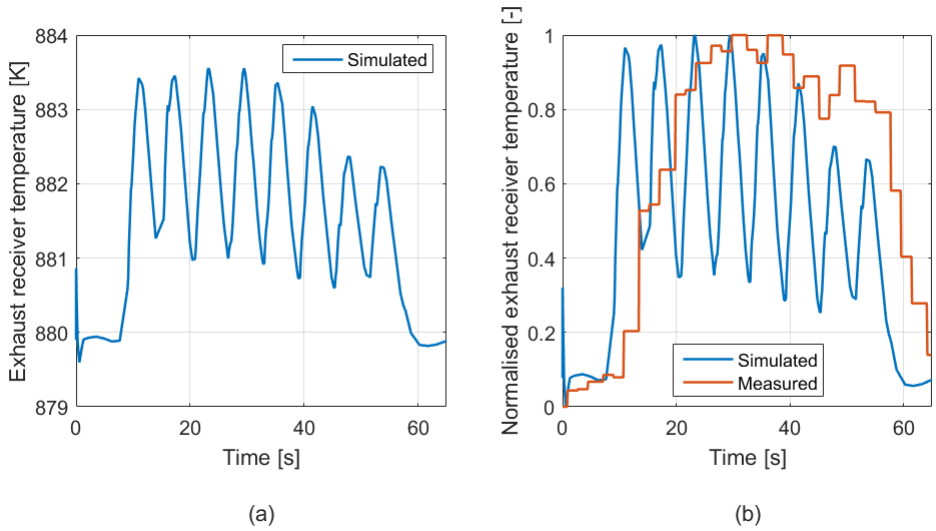

Figure 4.22: **Simulated exhaust receiver temperature (a), Normalized exhaust receiver temperature (b). BP -45 mbar Wave period - 6s**

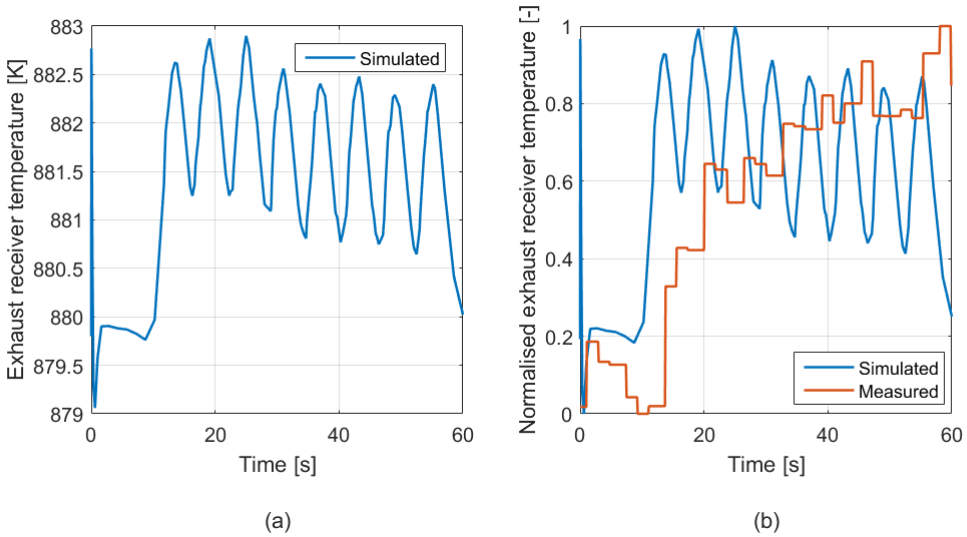

Figure 4.23: **Simulated exhaust receiver temperature (a), Normalized exhaust receiver temperature. BP -35 mbar Wave period - 6s**

On performing the quantitative analysis for amplitude change in multiple waves, it is found that for higher loads the increment in exhaust receiver temperature is very close to the simulation. This is evident from figure 4.24 where it can be seen

that the experimental and simulated temperature increments are very close to each other. The model shows a large difference between the experimental and simulated results at low load (108 KW) due to error in the static model. Moreover, the drop in inlet receiver pressure for simulation is less compared to the experiments as shown earlier.

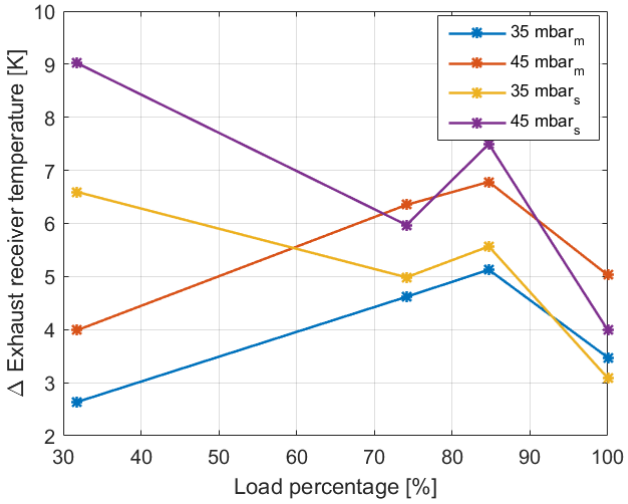

Figure 4.24: **Measured (m) and simulated (s) exhaust receiver temperature increment for multiple back pressure waves**

The qualitative analysis is performed at all loads and absolute error for inlet receiver pressure and exhaust receiver temperature is shown in figure 4.25. It shows that the absolute error in inlet receiver pressure is less than 10% at all loads. The error percentage must never increase above 10% as it is not considered good for matching. But, exhaust receiver temperature shows the highest error at low loads as the static model is showing. The absolute error in exhaust receiver temperature is less than 10% for higher loads. This is because the error present in the static back pressure model. On comparing the errors of static and dynamic back pressure results at all loads, shows that for both models the error in temperature is highest at 108 KW, where as, for inlet receiver pressure, both static and dynamic model shows the maximum error at 340 KW.

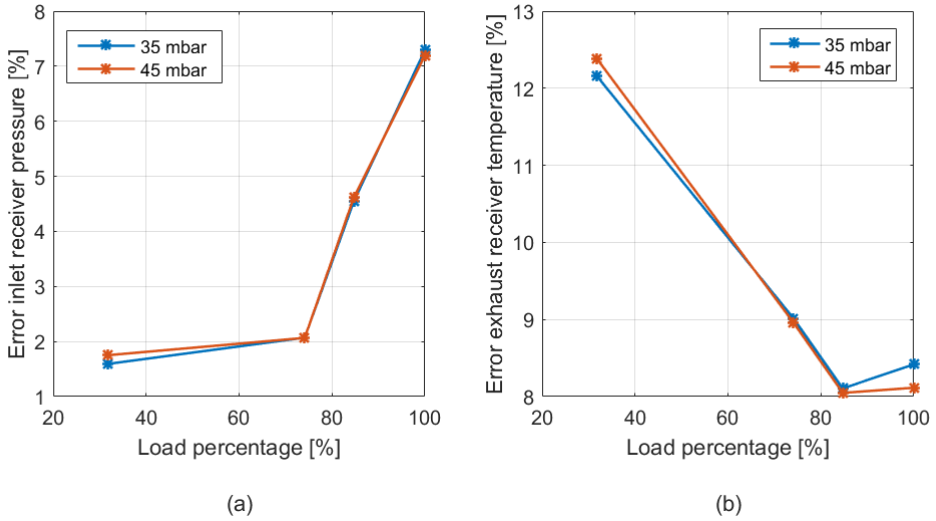

Figure 4.25: **Absolute error between measurement and simulations for inlet receiver pressure (a) and exhaust receiver temperature (b) for multiple back pressure waves.**

4.5 WAVE PERIOD CHANGE

In this section, the simulations are run with a back pressure of the same amplitude (45 mbar) with different wave period (4s and 8s). The effect of the wave period on the engine performance is analyzed in this section. The comparison is carried out between different wave period's simulated results. Moreover, the experimental results of performance and simulated results performance are compared with each other and analyzed. This is carried out for both single and multiple waves.

4.5.1 SINGLE WAVES

The engine performance is replicated for single back pressure wave of wave period 4s, 8s with maximum amplitude of 45 mbar at 340 KW and 981 rpm. The normalized back pressure, simulated inlet receiver pressure and normalized inlet receiver pressure for 8s back pressure wave is shown in figure 4.26. The drop in simulated inlet receiver pressure (figure 4.26(b)) is nearly half of the drop in the measured inlet receiver pressure shown in figure **??**(b).

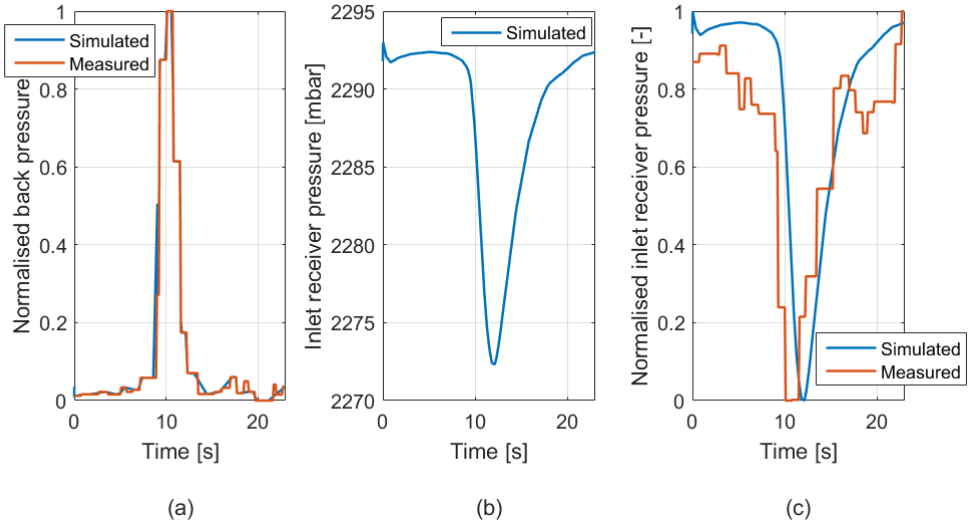

Figure 4.26: **Normalized back pressure (a), simulated inlet receiver pressure (b) and normalized inlet receiver pressure (c). BP -45 mbar Wave period - 8s**

The above simulated 45 mbar, 8s back pressure waves effect on the diesel engine can be compared with the 45 mbar. 4s back pressure wave effect at 340Kw as shown in figure 4.27. On comparing the two simulated results, it can be stated simulations also shows that inlet receiver pressure drop is also higher for higher wave period back pressure. The drop in inlet receiver pressure for 8s is 20 mbar whereas, for 4s it is 13 mbar. This is because with increase in wave period, the engine experiences higher back pressure for more time compared to lower wave period. Thus, it can be stated that the wave period also shows the same trend as observed during the experiment.

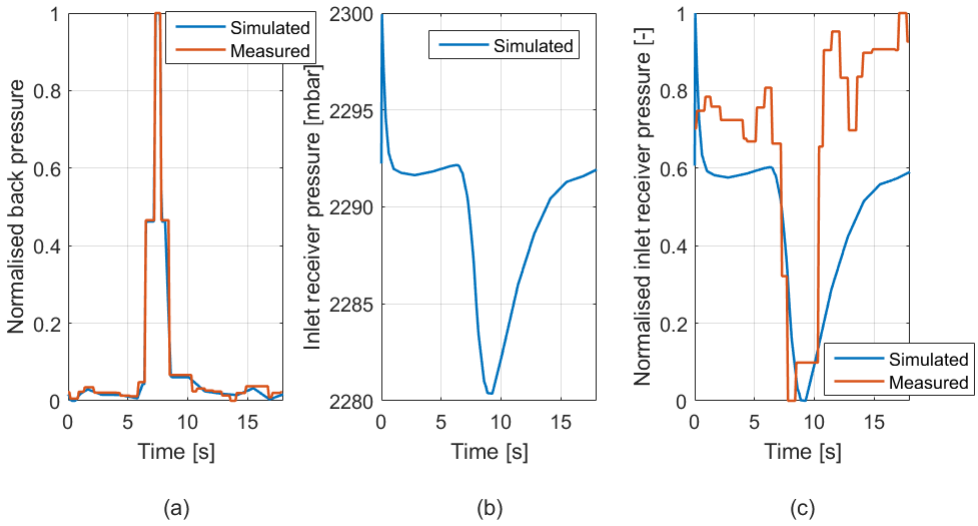

Figure 4.27: **Normalized back pressure (a), simulated inlet receiver pressure (b) and normalized inlet receiver pressure (c). BP -45 mbar Wave period - 4s**

The increase in back pressure decreases air intake and increases the fuel flow.

More fuel and less air, decreases the air fuel ratio and thus, decreasing air excess ratio. The air excess ratio along with fuel flow rate is shown for 8s back pressure wave in figure 4.28. On comparing the same parameters for 45 mbar and 4s back pressure wave presented in figure 4.29 at same load displays that the air excess ratio drop is higher for the higher wave period wave input.

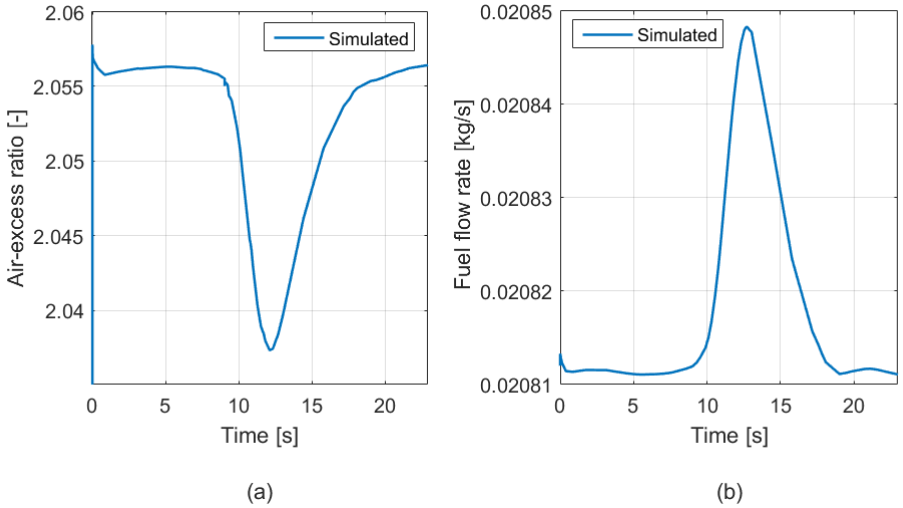

Figure 4.28: **Simulated air excess ratio (a), simulated fuel flow rate (b). BP -45 mbar Wave period - 8s**

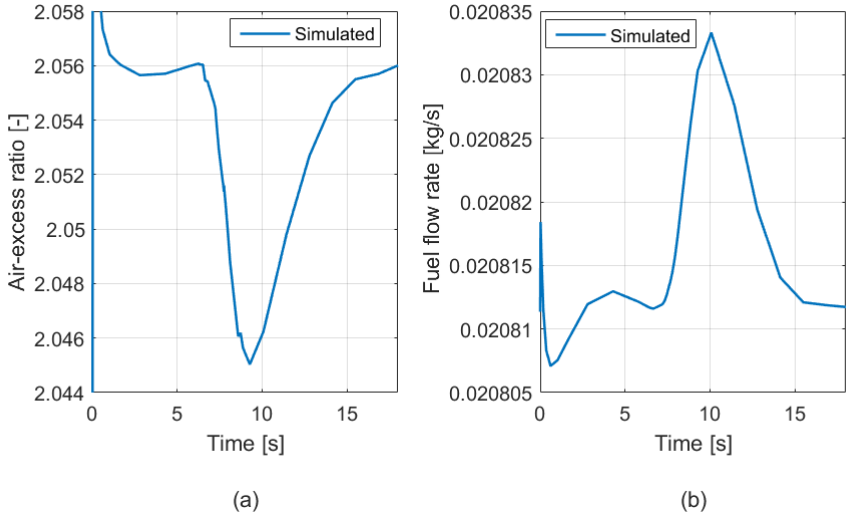

Figure 4.29: **Simulated air excess ratio (a), simulated fuel flow rate (b). BP -45 mbar Wave period - 4s**

The change in the fuel flow rate increases the fuel into the system. This leads to an increase in the exhaust receiver temperature. Figure 4.30 and 4.31 shows the increase in exhaust receiver temperature due to 8s and 4s back pressure wave respectively. On comparing them with each other, it is evident that the increase in simulated exhaust receiver temperature is also higher for higher wave period. The fluctuation in exhaust receiver temperature for 8s wave is around 4.5 K which

is higher than 2.5 K increase for 4s wave. The lag in measured temperature is also shown in figure 4.30 by normalizing the temperature and superimposing on the simulated result. The measured temperature measurement is slow as temperature probe sampling frequency is low. Therefore, the measured temperature is slow in rising to the maximum temperature and tends to take more time further to come back to the initial value which is missing in the figure as the measurement was stopped at 23 seconds. On the other hand, simulations are fast compared to measurement.

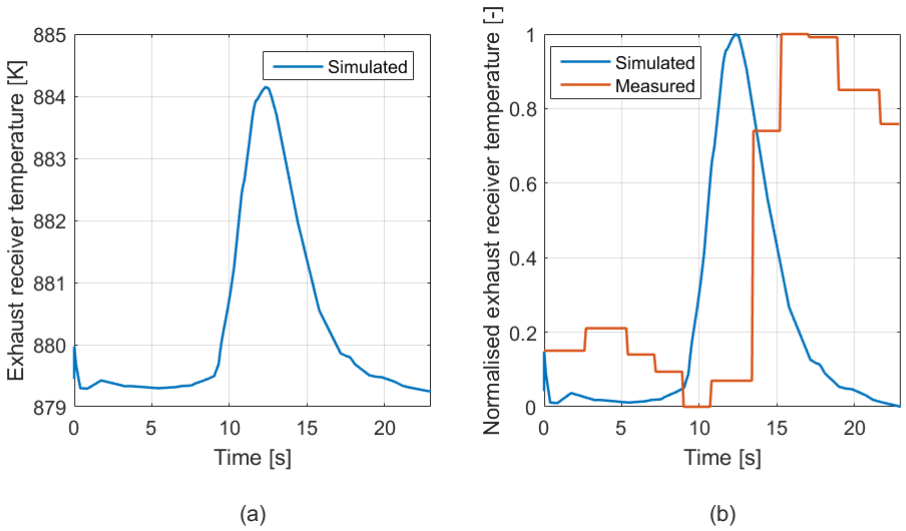

Figure 4.30: **Simulated exhaust receiver temperature (a), Normalized exhaust receiver temperature (b). BP -45 mbar Wave period - 8s**

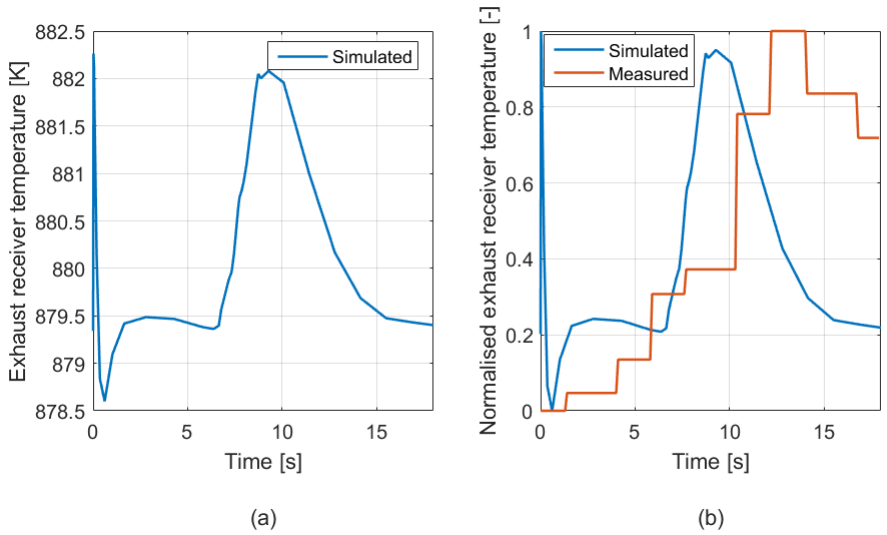

Figure 4.31: **Simulated exhaust receiver temperature (a), Normalized exhaust receiver temperature. BP -45 mbar Wave period - 4s**

Moreover, on analyzing the simulated results against the measurements, it can be stated that the increase in exhaust receiver temperature for measurements in 3.25(a) is larger than the results from the simulation as shown in figure 4.30. The

experimental and simulated increment in the exhaust receiver temperature for 8s and 4s wave input is plotted in figure 4.24. Similar to the single wave amplitude change, the increments are more for the model results at all loads. But it also showed that increment is higher for higher wave period which is valid for both experiments and simulations. Since error is more at low loads, the difference is also higher at 108 KW.

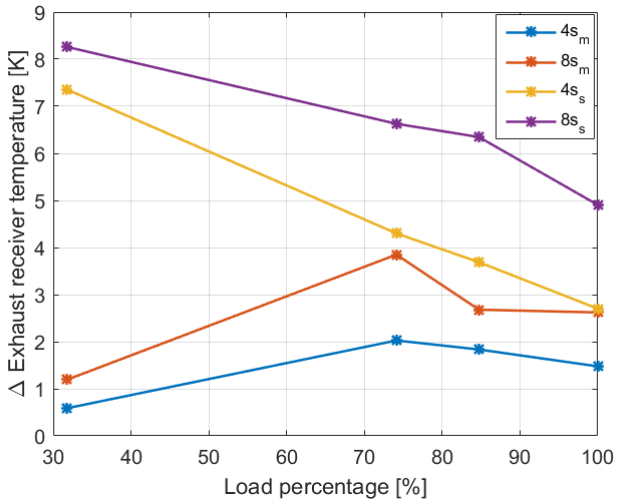

Figure 4.32: **Measured (m) and simulated (s) exhaust receiver temperature increment for single back pressure waves**

The absolute error also shows the similar trend observed for the single wave amplitude change. The error in inlet receiver pressure is highest at maximum load as shown in figure 4.33(a) but remains below 10% at all loads. The error in exhaust receiver pressure is shown in figure 4.33(b) which is highest at 30% load and reduces below 10% at higher loads.

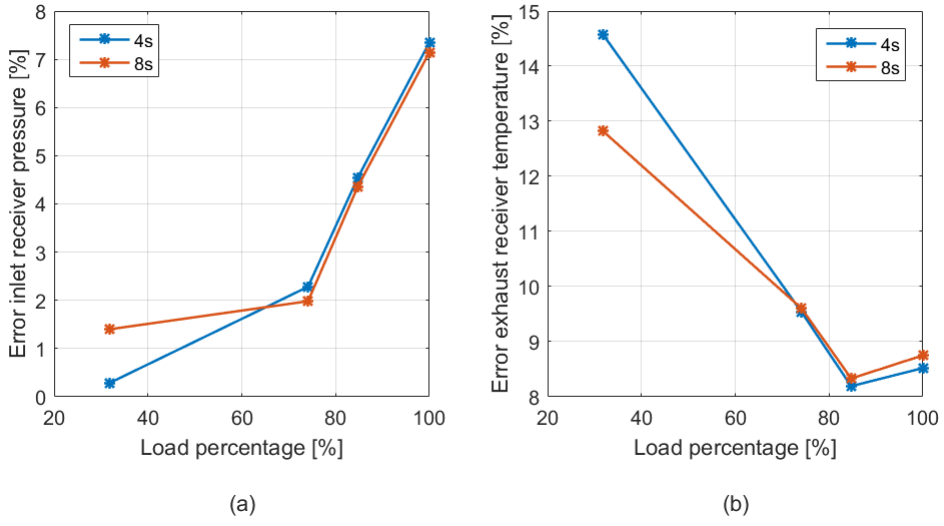

Figure 4.33: **Absolute error between measurement and simulations for inlet receiver pressure (a) and exhaust receiver temperature (b) for single back pressure waves.**

4.5.2 MULTIPLE WAVES

In this section, the model is used to simulate the effect of multiple waves on engine performance with multiple back pressure waves of wave periods 4s and 8s. The back pressure wave input is the same back pressure waves replicated by the butterfly valve as shown in the same subsection of chapter 4. The simulations are carried out for both back pressure multiple waves with same back pressure amplitude at 340 KW. The effect of wave period on the engine performance is analyzed in this section. For the starting, the simulated and measured back pressure wave at the turbine outlet is normalized and superimposed for 8s wave as shown in figure 4.34.

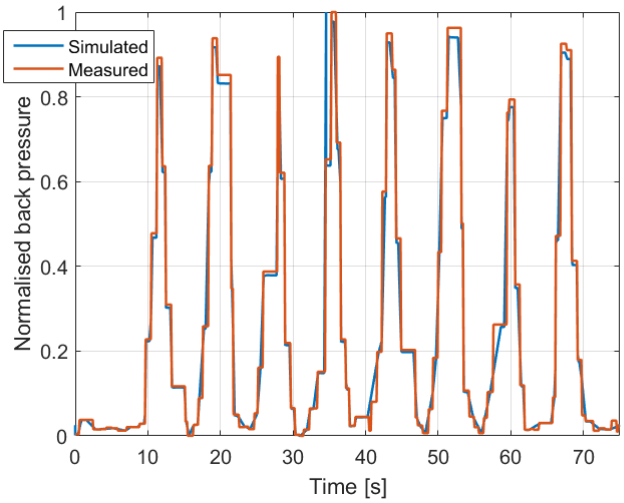

Figure 4.34: **Normalized back pressure. BP -45 mbar Wave period - 8s**

With multiple fluctuations in external applied back pressure, the inlet receiver pressure also fluctuates. The fluctuating inlet receiver pressure response for the 8s back pressure wave is shown in figure 4.35(a). On superimposing the normalized measured and simulated inlet receiver pressure for 8s wave, the plot obtained is shown in figure 4.35(b). It can be seen that the drop in simulated inlet receiver pressure response is following the measured drop. It is also noted that the back pressure waves in which the engine experiences higher back pressure for more time or more step change at higher back pressure tend to show more change in parameter. For instance, the number 2 wave in figure 4.34 reaches to less back pressure compared to number 4 wave. The change in inlet receiver pressure in figure 4.35 (a) is larger for the wave number 2 compared to wave number 4. This shows that wider the width of the back pressure peaks, larger is the change in the parameters.

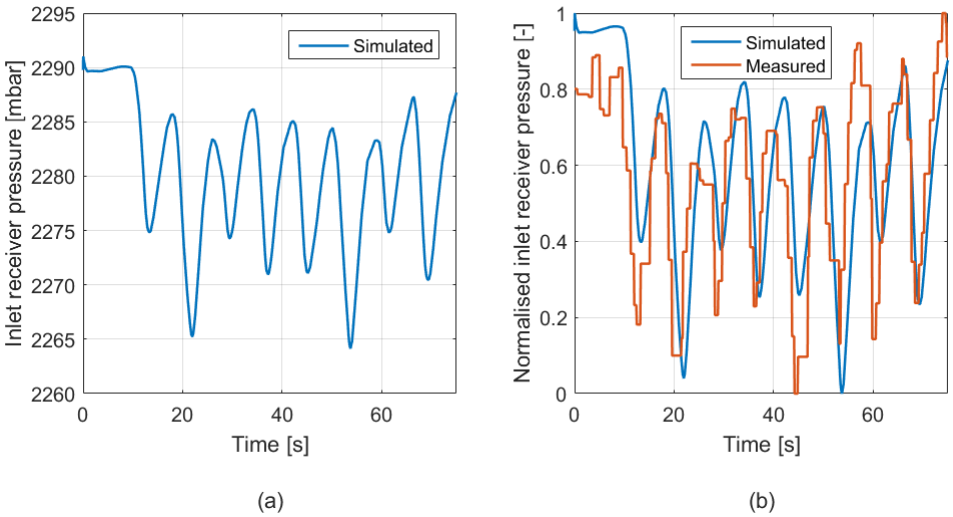

Figure 4.35: **Simulated inlet receiver pressure (a) and normalized inlet receiver pressure (b). BP -45 mbar Wave period - 8s**

The same model is also used to simulate the engine performance due to 4s back pressure wave. The back pressure wave measured and simulated is also plotted in figure 4.36. It can be seen that not all the back pressure waves are reaching the 45 mbar back pressure value. The effect of this can also be seen on the air excess ratio and exhaust receiver temperature.

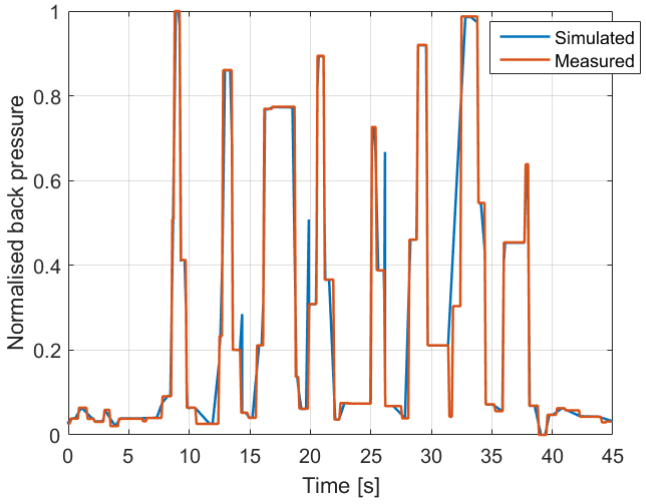

Figure 4.36: **Simulated inlet receiver pressure (a) and normalized inlet receiver pressure (b). BP -45 mbar Wave period - 4s**

The inlet receiver pressure results are shown in figure 4.37. The simulation also provide the evidence that the drop in inlet receiver pressure is higher for 8s wave (refer figure 4.35(a)) than 4s in figure 4.37(a).

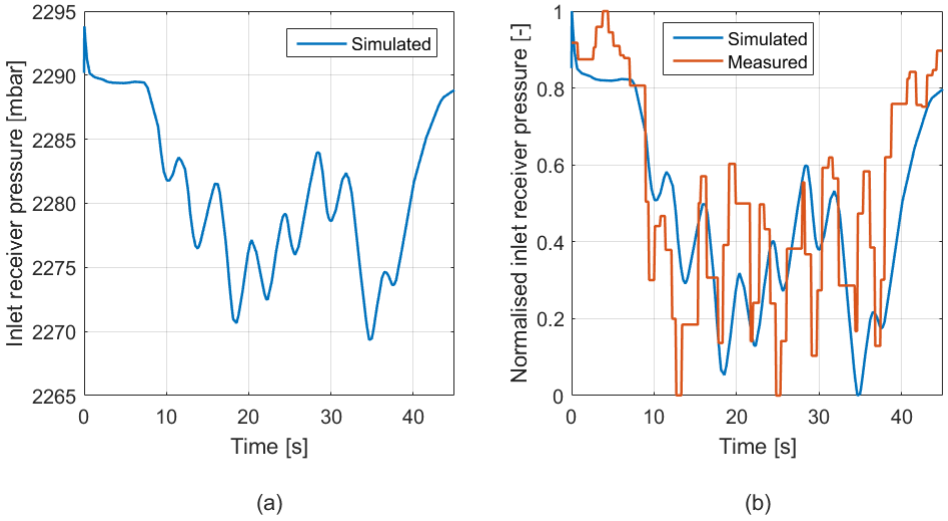

Figure 4.37: **Simulated inlet receiver pressure (a) and normalized inlet receiver pressure (b). BP -35 mbar Wave period - 4s**

The air excess ratio also dips and fuel flow rate increases with increasing back pressure. The change in air excess ratio and fuel flow rate is more for 8s than 4s. The figure 4.38 and 4.39 respectively, shows the drop in air excess ratio (a) and increase in fuel flow rate for 8s and 4s. In figure 4.37, the air excess ratio suddenly increases before 30 seconds. This is because the back pressure waves 3,4 and 5 in figure 4.36 were not able to reach the 45 mbar value where as wave 1 reaches to it. Thus the air excess ratio drops responding to the first back pressure wave. The back pressure reduces in wave 2 and it further reduces in third wave. The model responds to these waves and an increase in air excess ratio can be seen in the middle. The same trend is shown in figure 4.39(a) for simulated exhaust receiver temperature.

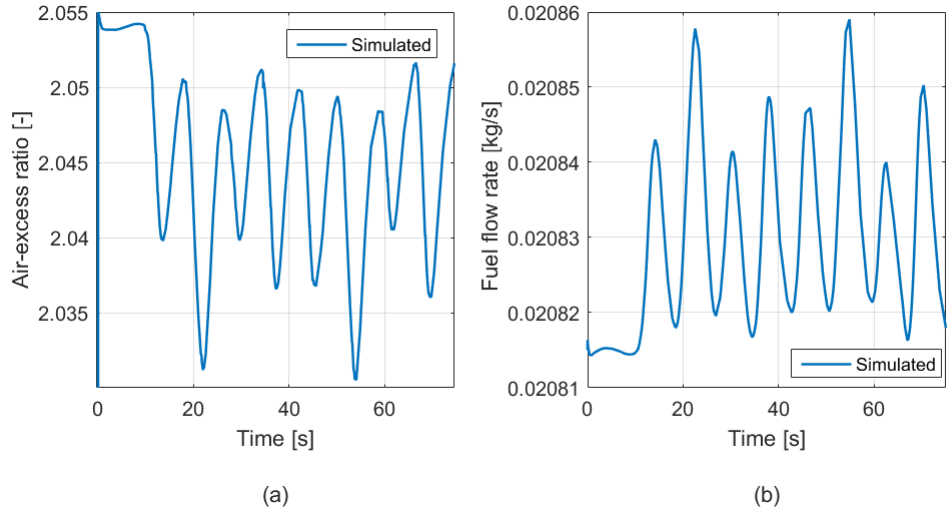

Figure 4.38: **Simulated air excess ratio (a), simulated fuel flow rate (b). BP -45 mbar Wave period - 8s**

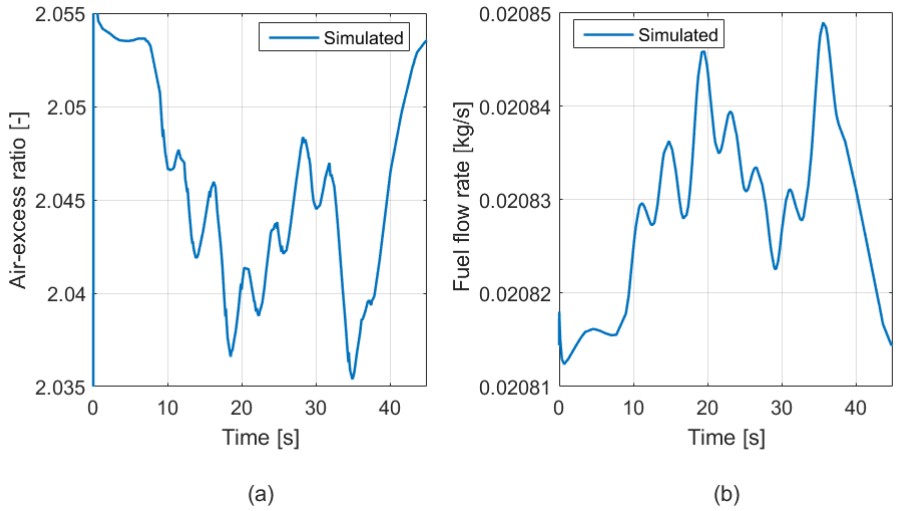

Figure 4.39: **Simulated air excess ratio (a), simulated fuel flow rate (b). BP -45 mbar Wave period - 4s**

The variations in the fuel flow rate leads to the change in exhaust receiver temperature.The effect of wave period on exhaust receiver temperature can be found out by comparing figure 4.40 and 4.41. For 8s multiple wave input, the increment in temperature is 5.9K whereas 4s wave gives an increment of 4.5K. Thus, simulated results also suggest that the high wave period of external back pressure leads to bigger change in fuel flow rate, thus higher change in exhaust receiver temperature. Similar to the previous sections, the lag in the measured temperature can be seen in the figures below.

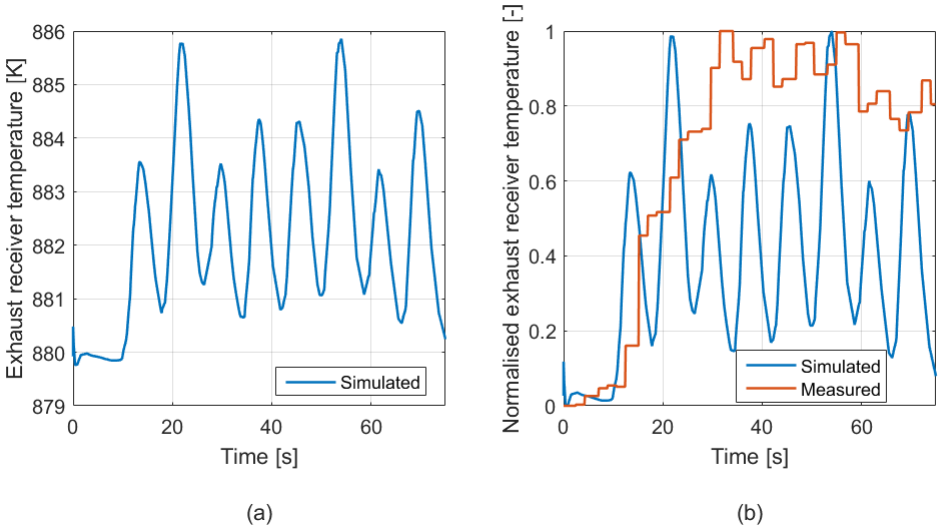

Figure 4.40: **Simulated exhaust receiver temperature (a), Normalized exhaust receiver temperature (b). BP -45 mbar Wave period - 8s**

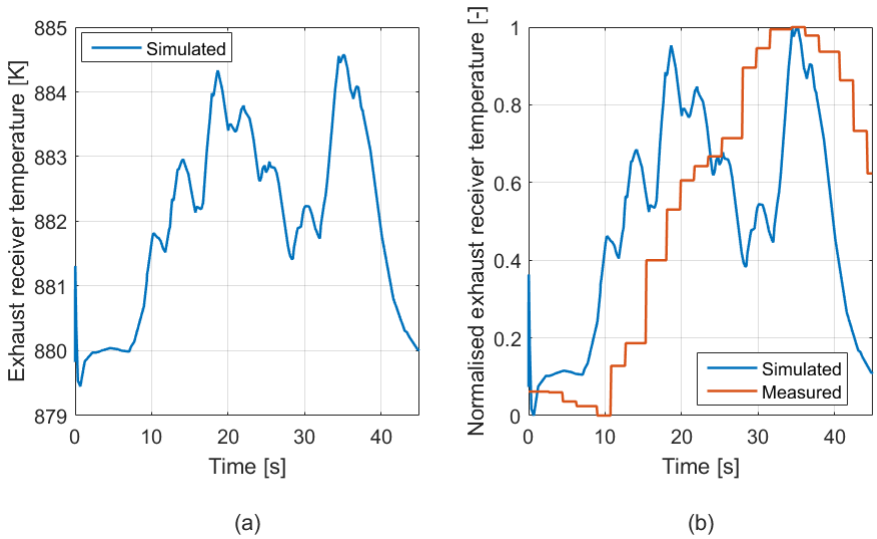

Figure 4.41: **Simulated exhaust receiver temperature (a), Normalized exhaust receiver temperature. BP -45 mbar Wave period - 4s**

After the quantitative analysis of measured and simulated inlet receiver temperature, it is noted that the increment in exhaust receiver temperature is higher at low loads i.e. 30.3% load as shown in figure 4.42. But at higher loads, the measured and simulated increment in temperature is very close to each other.

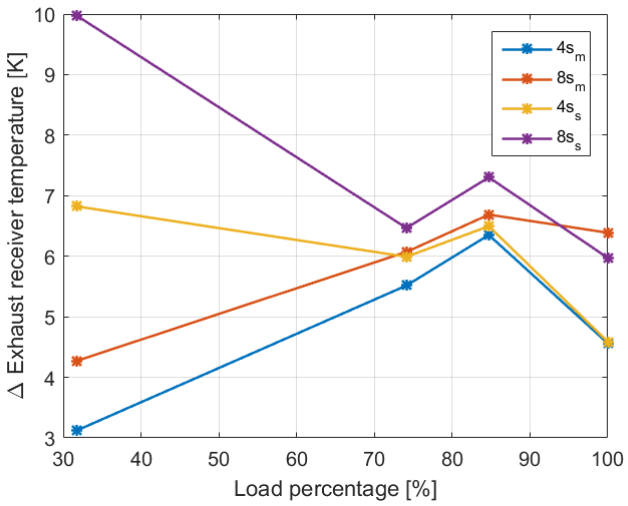

Figure 4.42: **Measured (m) and simulated (s) exhaust receiver temperature increment for multiple back pressure waves**

The absolute error between measured and simulated inlet receiver pressure and exhaust receiver temperature is also shown in figure 4.43. Similar to the multiple amplitude change effect, the inlet receiver pressure error remains below 10% at all loads. The exhaust receiver temperature shows an error of nearly 12 % at 108 KW. The static model also shows the maximum error in exhaust receiver temperature at 108 KW. For the rest of the load points, the absolute error is below 10%. The inlet receiver pressure shows maximum error at 340 KW. The error is maximum in both static and dynamic model. Since both model uses the same files, the error in static

model is visible in the dynamic model results.

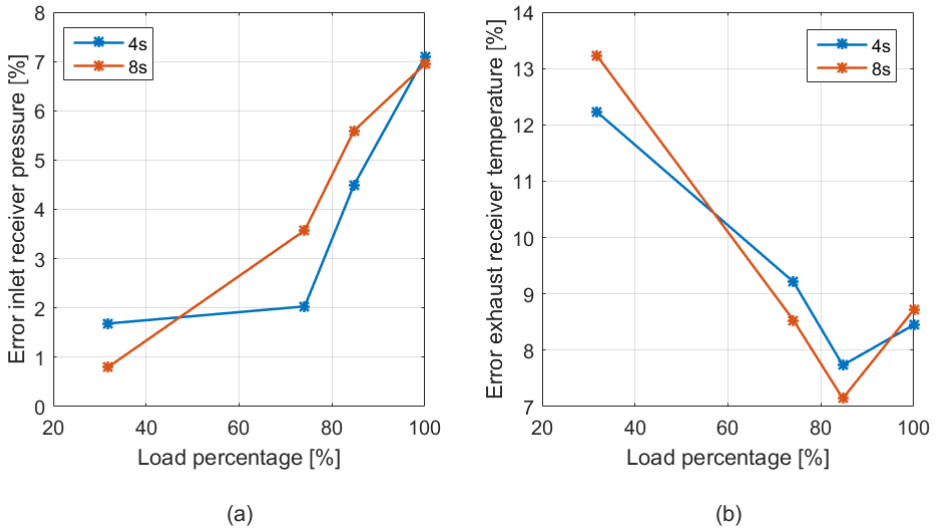

Figure 4.43: **Absolute error between measurement and simulations for inlet receiver pressure (a) and exhaust receiver temperature (b) for multiple back pressure waves.**

This concludes the comparison between the experimental and simulated results. The model is now used to simulate higher sea states which will be discussed in the next chapter.

Chapter 5

DISCUSSION

5.1 WAVE PERIOD 2S

Peter Hield [12], concluded in his research that below 4s wave period, fuel flow rate fluctuation amplitude is reduced due to the finite response time of the speed governor. To check this statement, the diesel engine model is subjected to an external back pressure wave with amplitude 45 mbar and wave period 2s. The 2s back pressure wave from the measurements is used as input for the model is shown in figure 5.1 (a). It is clear from the figure that none of the 8 waves can reach the required back pressure (1059 mbar) marked with the dotted red line. This is because of the fast movement of the electronically controlled butterfly valve and a large diameter of the exhaust line. Therefore, there is not enough time to build the exhaust back pressure of the required amplitude for 2-second wave. The simulated governor response to the 2s back pressure wave is also shown in figure 5.1(b).

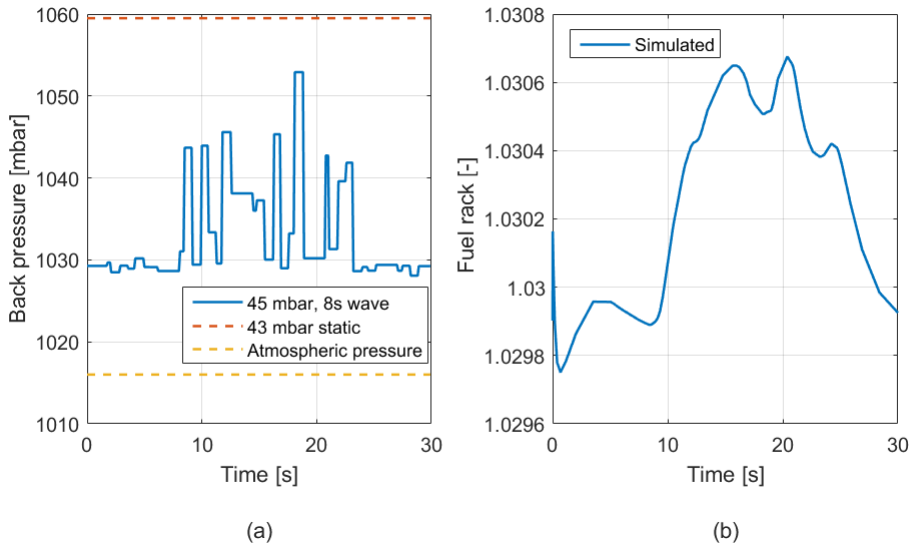

Figure 5.1: **Input BP - 45 mbar, WP - 2s (a) and simulated governor response (b). Load - 340 KW, speed - 981 rpm**

From the last chapter and above figure, it is clear that when the back pressure increases, the governor also increases the rack position to tackle the power reduction. The power is reduced due to extra pumping work performed by the engine to remove

exhaust gasses against the externally applied back pressure wave. This increases the fuel flow rate to the engine. On the other side, air excess ratio also reduces due to less air flow after the reduction in compressor discharge pressure. For 4s and 8s wave, the air excess ratio and fuel flow rate is shown in figure 4.39 and figure 4.38. Fuel flow rate increases with the increase in back pressure and decreases again with a decrease in back pressure for 4s and 8s. It can be said, that fuel flow rate follows the back pressure. In the case of a 2-second wave, the air excess ratio and fuel flow rate is shown in figure 5.2. The figure shows that the fuel flow rate fluctuations and air excess fluctuations are not there for all the 8 waves as we have seen for 4s and 8s. This is because of the finite response time of the governor to such fast change in back pressure. In other words, the governor is slow to respond to such fast changes in the back pressure and thus the fluctuations are missing for 2-second wave. P. Hield also stated the same results from his research. He said that below 4 s the fuel flow fluctuation amplitude reduced, most likely due to the finite response time of the speed governor [12].

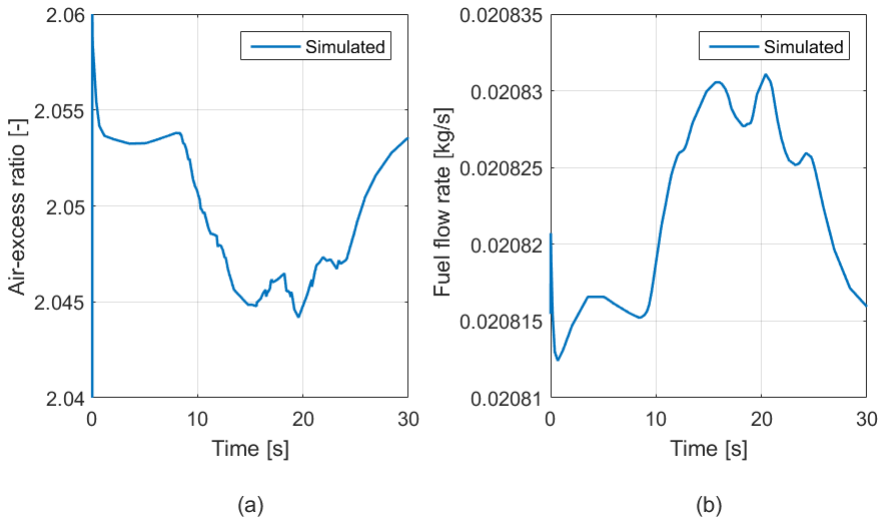

Figure 5.2: **Simulated air excess ratio (a) and simulated fuel flow rate (b). BP - 45 mbar, WP - 2s, load - 340 KW, speed - 981 rpm**

5.2 CRITICAL WAVE PERIOD

Peter Hield performed engine performance simulation on Ricardo Wave engine model. He stated that above 4 seconds wave period, there is an increment in parameters with an increase in the wave period. This is already proved experimentally in chapter third. But, he also stated that on increasing the wave period above a critical value, the change in the parameter or increment in the parameters remains the same. P. Hield found 12 seconds as the critical value of wave period for his model. In our research, the DE - B model is fed up with eight continuous wave of 45 mbar and a wave period of 8s, 16s, 24s, 32s, 40s, and 44s. With the increase in wave period, the model shows that the increment in the exhaust receiver temperature reduces such that it became constant near 44 seconds. The figure 5.3 (a) shows the change in exhaust receiver temperature for various wave periods.

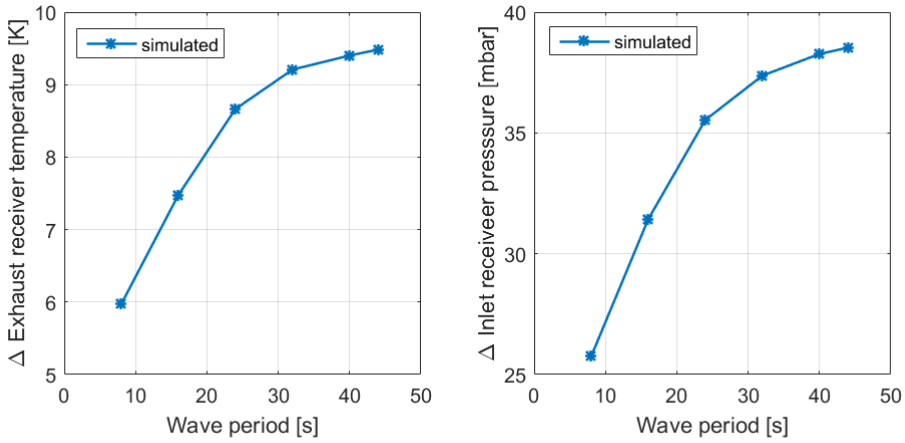

(a) (b)

Figure 5.3: **Change in simulated exhaust receiver temperature for BP - 45 mbar and various WP, load - 340 KW, speed - 981 rpm**

The change in inlet receiver pressure also follows the same trend as it remains same after 44 seconds. This is because on increasing the wave period, the wave crest tends to become flatter and maximum back pressure is applied for a longer time. Thus, at the peak of the waves constant static back pressure is acting. Once the peak behaves like a static back pressure input, the parameters does not change with increase in wave period. The figure below also shows that, critical wave period value of 44s, the change in air excess ratio and change in fuel flow rate also becomes constant.

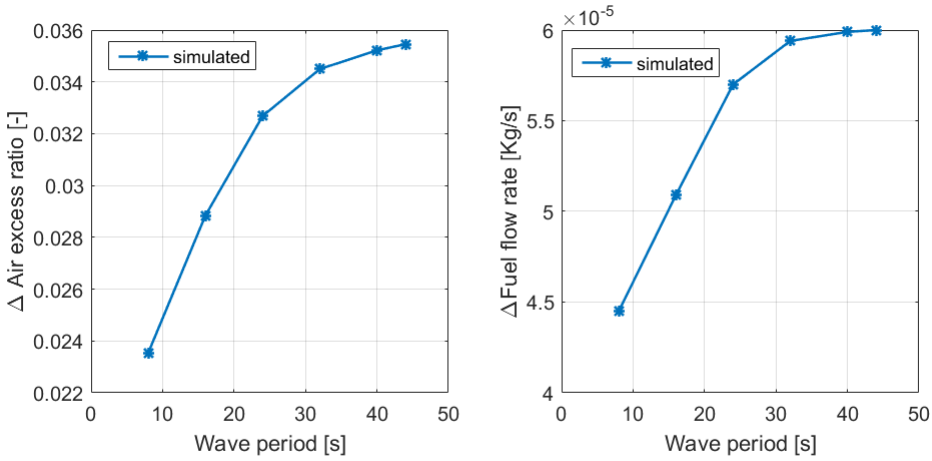

(a) (b)

Figure 5.4: **Change in simulated air excess ratio (a) and change in simulated fuel flow rate (b) for BP - 45 mbar and various WP, load - 340 KW, speed - 981 rpm**

The critical value for an engine or model depends on the type of governor, turbocharger settings, governor settings and controls. It is different for different diesel engines depending on their settings. Tauzia et.al [21] showed that the exhaust receiver temperatures (turbine inlet temperatures) found using engine model simu-

lations peaked to the same values for different wave periods (7.2s, 9.3s, 14.3s, and 16.4s). Thus, the effect of wave period of back pressure wave is insignificant. However, a discussion specifically on the effects of governor control and settings on engine performance against dynamic back pressure was not presented. This needs further investigation for the future works in which, the engine can be tested with higher wave periods to check the conclusion given in this section and find the critical wave period experimentally.

5.3 STATIC VS DYNAMIC

While performing the experiments, it was noted that the increase in parameters or change in parameters is higher for higher amplitude and higher wave period. It was also found that the change in parameters is higher for static back pressure change than for continuous waves of the same amplitude. Figure 5.5 shows the measured and simulated externally applied back pressure waves normalized and superimposed over each other. The red line in the same figure represents the steady-state back pressure of 43 mbar.

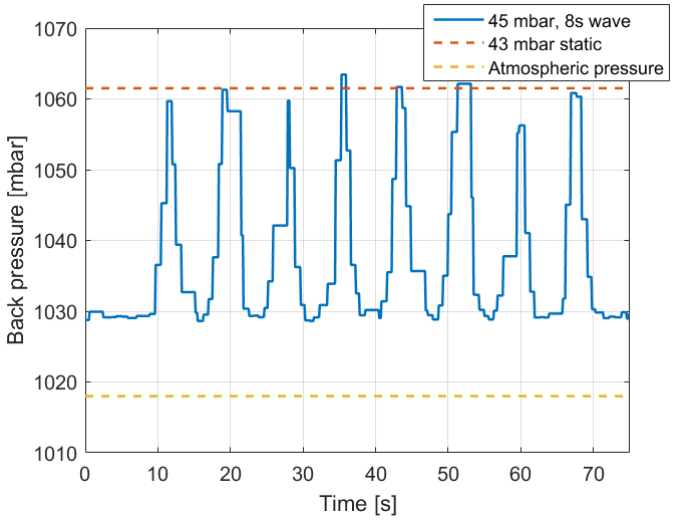

Figure 5.5: **Input multiple BP - 45 mbar, 8s and 43 mbar static, load - 340 KW, speed - 981 rpm**

The simulated exhaust receiver temperature for the back pressure wave input of 45 mbar, 8s is plotted along with the simulated exhaust receiver temperature for steady-state 43 mbar back pressure in figure 5.6. The exhaust receiver temperature for static 43 mbar back pressure input is higher than the back pressure wave of amplitude 45 mbar and wave period 8s.

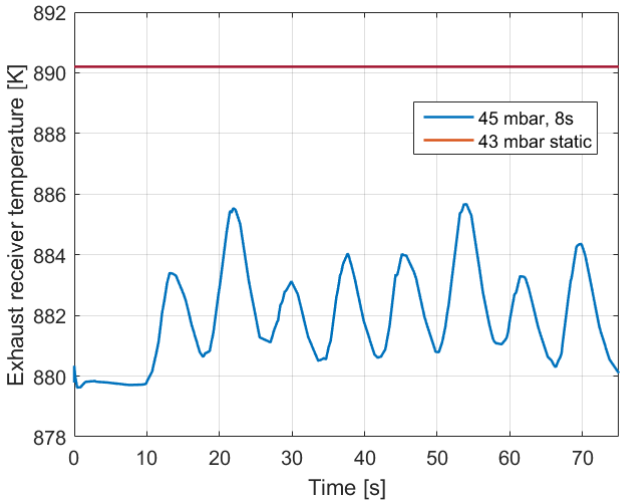

Figure 5.6: **Input multiple 45 mbar, 8s BP wave and 43 mbar static, load - 340 KW, speed - 981 rpm**

The exhaust receiver temperature increment depends on the fuel flow rate change which is governed by the governor response to the applied back pressure. The simulated governor response and simulated fuel flow rate for dynamic back pressure wave (45 mbar, 8s) and steady state back pressure (43 mbar) are plotted in figure 5.7. It can be seen that as the back pressure is increased, the governor changes the rack position such that fuel flow rate is increased. When the first back pressure wave reaches its peak, the governor still increases the fuel flow but remains below the simulated steady state fuel rate flow at all times. The back pressure remains at peak for a very small moment and starts reducing, the governor shuts the fuel rack reducing the flow rate in response to a decrease in back pressure. The fuel flow rate reduces till the second back pressure wave starts and governor repeats the procedure.

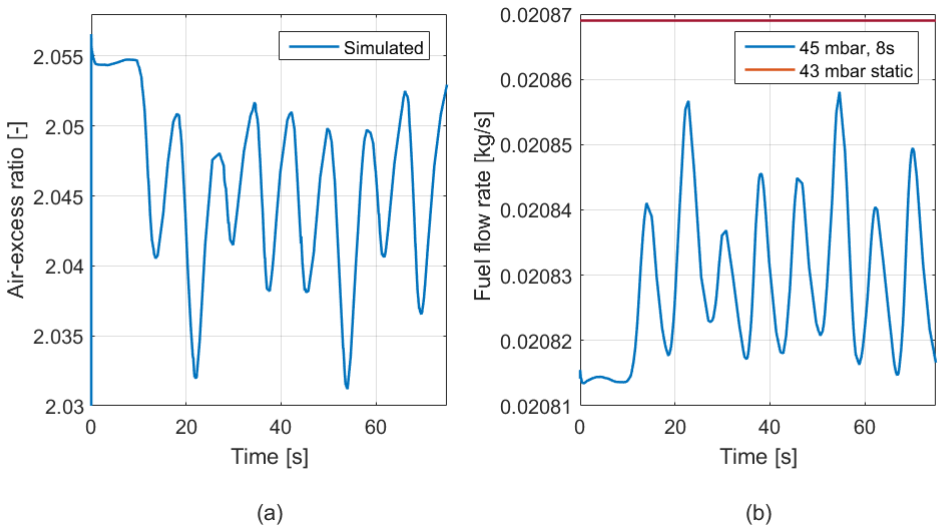

Figure 5.7: **Simulated governor response (a) and simulated fuel flow rate (b) for multiple 45 mbar, 8s BP wave and 43 mbar static at load - 340 KW, speed - 981 rpm**

The governor continuously and quickly responds to control the fuel flow rate against any fluctuations in back pressure. This fuel flow control by the governor helps limit the maximum fuel flow to tackle dynamic back pressure below the fuel flow value simulated for the static back pressure of 43 mbar. Thus, the lower values of fuel flow reached during dynamic back pressure indicate a lower fuel penalty compared to that found during static back pressure. The fast control of fuel flow by the governor and of the air-intake by the turbocharger in response to the fluctuating back pressure help keep the exhaust receiver temperatures during dynamic back pressure below the exhaust receiver temperature for a static back pressure of 43 mbar. This explains the smaller increments in exhaust receiver temperatures during dynamic back pressure and not able to reach the exhaust receiver temperature for static back pressure. This finding and explanation of lower maximum exhaust receiver temperatures during dynamic back pressure compared to static back pressure are contradictory to the results presented by Tauzia et. al. [21]. The author showed that the exhaust receiver temperatures (turbine inlet temperatures) found using engine model simulations peaked to the same values as those found during static back pressure of same amplitude. The author simulated the performances with wave period 7.2s, 9.3s, 13.1s and 16.4s. However, this could hold if the author is simulating performances near the critical wave period for the engine model. A discussion specifically on the effects of governor control and settings on engine performance against dynamic back pressure was not presented by Tauzia.

5.4 DEFINING BACK PRESSURE LIMITS

The experimental results in chapter 3 proved that exhaust receiver temperature is a critical parameter while increasing the back pressure. In addition to this, the simulation showed that air excess ratio and exhaust valve temperature can also exceed their critical limits. Therefore, exhaust receiver temperature, exhaust valve temperature and air excess ratio can be used as an indicator of thermal overloading and smoke limits of the diesel engine. This can be further used to find applied back pressure ceiling that is acceptable for the engine [40] [41]. This is further explained in detail in the next sub-sections.

5.4.1 SMOKE AND THERMAL OVERLOAD LIMIT

The combustion takes place in diesel engine's cylinder where fresh air is entered through the inlet side and fuel is injected through the fuel pump via fuel injector. Fuel is combust with an excess of air or oxygen to ensure complete combustion and prevent the formation of soot. The excess of air is characterized by the air excess ratio [42]. It is defined as the ratio between total fresh air mass in the cylinder to the minimum amount of air required for combustion [6]. Sapra et. al [3] used air excess ratio as an indicator to define the smoke limit of the engine by drawing the lines of constant air excess ratio in a static engine map. The same concept is used in this research thesis to define the smoke limits. For this, the engine is run at various speed and loads to cover the operating limits of the static map. The static map is prescribed by the engine manufacturer. The engine map along with points of simulations are shown in figure 5.8.

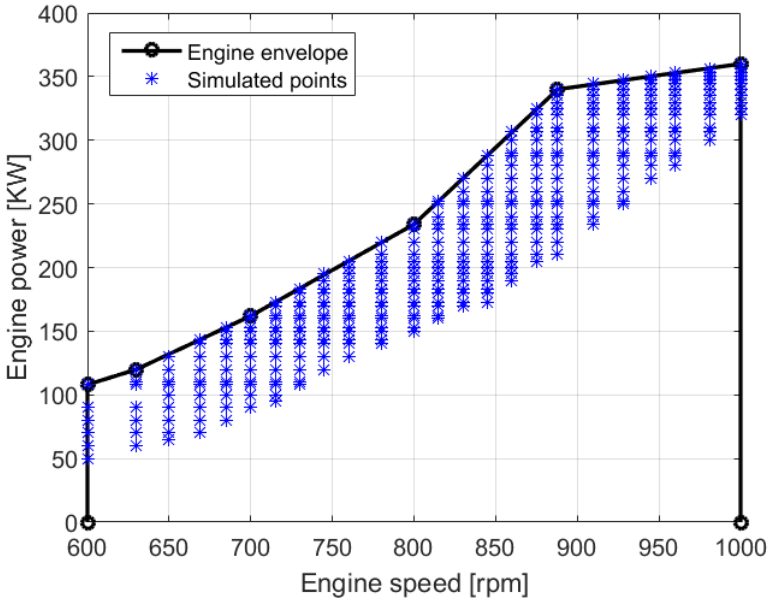

Figure 5.8: **Engine envelope (black line) along with simulated engine and rpm points (Blue points)**

The performance at all the points shown in the above figure is simulated and the values of the parameters are plotted on the map to capture the constant lines of air excess ratio, exhaust receiver temperature, exhaust valve temperature and inlet receiver pressure in the envelope. The simulations are carried out for pulse turbocharged diesel engine with 100 degree valve overlap. Figure 5.9 (a) captures the line of constant air excess ratio within the engine envelope whereas figure 5.9 (b) shows lines of constant inlet receiver pressure.

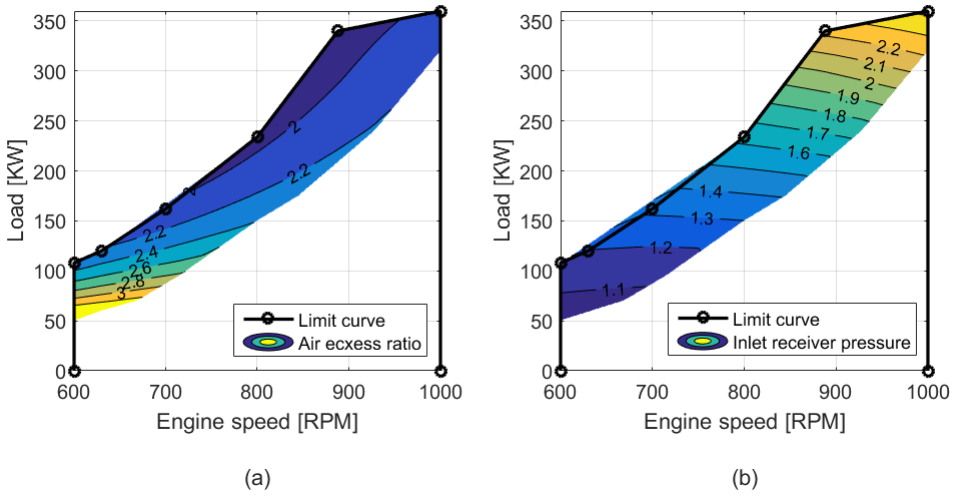

Figure 5.9: **Static engine envelope along with the constant line of air excess ratio (a) and constant lines of inlet receiver pressure for pulse turbocharged engine.**

The air excess ratio cannot be measured directly therefore, constant inlet receiver pressure lines can also be used for defining limits. Inlet receiver pressure can be used

to measure the air charged into the engine which divided by the fuel rack gives an approximate air excess ratio. But, figure 5.9 clearly shows that constant lines of inlet receiver pressure are not following the trend as continuous lines of air excess ratio. Therefore, the smoke limits can be represented in terms of air excess ratio. After defining the smoke limits, the thermal limits are defined with the help of simulated exhaust receiver temperature and simulated exhaust valve temperature with in the envelope. The exhaust valve temperature is estimated by the exhaust valve temperature estimator model in the MVEMr. The lines of constant exhaust valve temperature are shown in figure 5.10. It is very difficult to directly measure the exhaust valve temperature therefore, exhaust receiver temperature lines are also shown in figure 5.10 (b). On comparing these temperature envelopes with the envelopes produced by Sapra et. al. [3], it is clear that that the continuous lines of exhaust valve temperature and exhaust receiver temperature plotted in 5.10 does not follow the trend as it can be seen in his research. This could be because the author developed the temperature envelopes for the diesel engine equipped with constant turbocharger where as the envelope plotted for thermal limits in this research is for pulse turbocharged engine. In a pulse turbocharging system, the flow through the turbine reduces compared to that in case of a constant pressure system. Also, a pulse system turbine delivers more work than a constant pressure system. The pulse turbocharger model was already implemented in the MVEM.

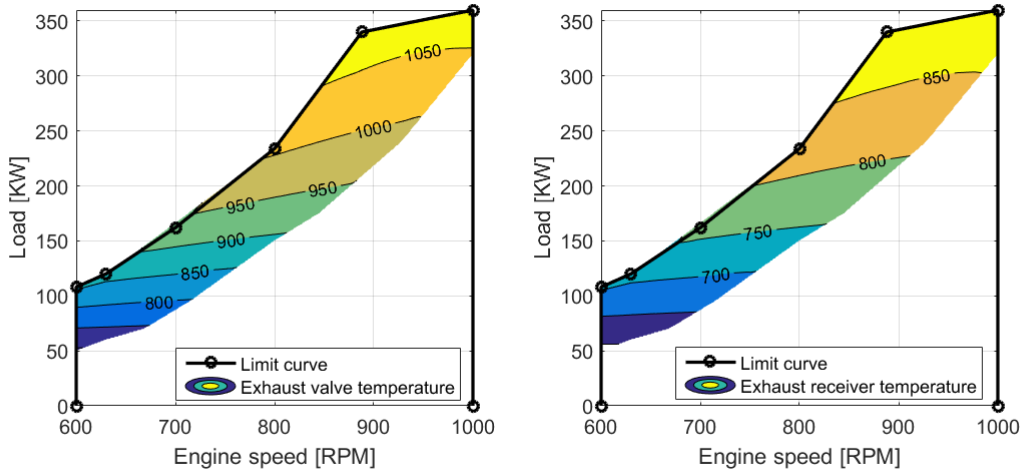

Figure 5.10: **Static engine envelope along with the constant lines of exhaust valve temperature (a) and constant lines of exhaust receiver temperature for pulse turbocharged engine.**

Both, exhaust receiver temperature and exhaust valve temperature show the same trend along the contours. This shows that both parameters can be used to define the thermal limit of the diesel engine.

5.4.2 ACCEPTABLE BACK PRESSURE LIMITS

The ceiling for acceptable back pressure is defined in the figures 5.11 and 5.12. In these plots, the y - axis in figures 5.9 and 5.10 is exchanged with the contour values

of the parameter. On exchanging the y-axis with air excess ratio values, figure 5.11 is obtained. It shows the constant engine power lines along with the air excess ratio envelope. The applied back pressure ceiling limits are also shown in the same figure. The engine is simulated with multiple back pressure wave of sea state 3 (75 mbar) and sea state 5 (2.75 mbar) and the wave period is kept the same at 8 seconds. For reference, the performance with no external back pressure is also plotted in the same figure. The air excess ratio for high back pressure values may fall below alarming values and can lead to black smoke which means incomplete combustion. The effects are larger at lower engine speed. The air excess ratio for sea state 3 is falling below the critical limit at maximum rpm (1000 rpm) where as sea state 5 is always below the critical air excess ratio limit at all loads. When the performance line for sea state 3 is below and out of the shaded region, it shows that the engine is running with less fresh air. In other words, it means that the diesel engine may emit black smoke due to incomplete combustion.

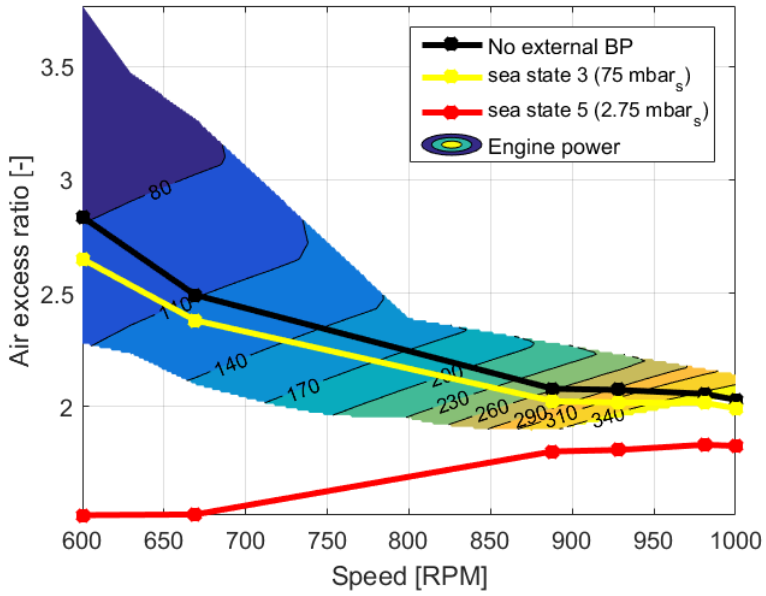

Figure 5.11: **Back pressure effect on air excess ratio of pulse turbocharged engine.**

Figure 5.12 shows the power contour lines for the exhaust valve temperature. From the plot and contour lines, it can be said that diesel engine cannot handle sea state 5 at any load. If subjected to the sea state 5, the diesel engine is thermally overloaded which can damage the diesel engine including turbocharger seals. For sea state 3, the exhaust valve temperature is above the critical limit below the rpm of 670. Thus, the diesel engine submerged exhaust can be by-passed from water to the atmosphere below 670 rpm. At maximum load, the exhaust valve temperature for sea state 3 is also above the limit. To counter this, the diesel engine load can be reduced at the maximum set point. By changing the load and rpm or by reducing the back pressure by bypassing the exhaust directly to the atmosphere are the two methods which can be used to keep the engine performance in the shaded region when external back pressure is applied.

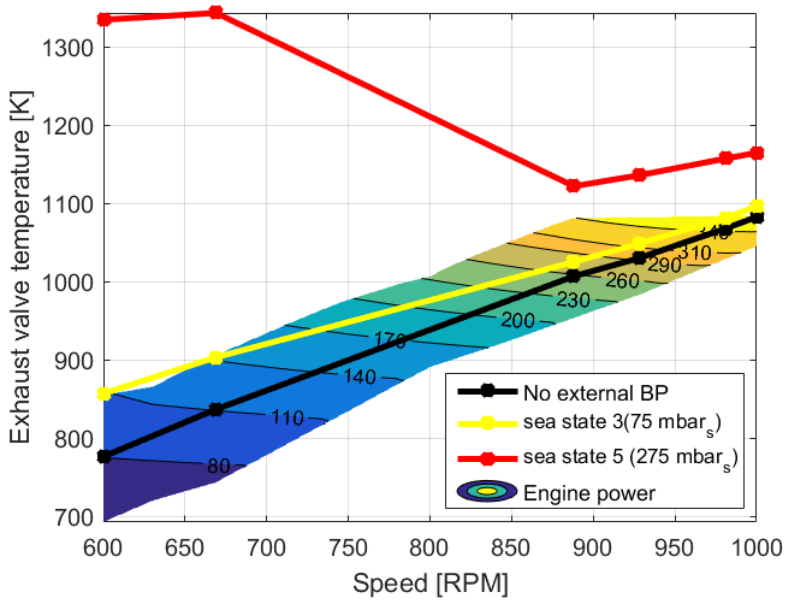

Figure 5.12: **Back pressure effect on exhaust valve temperature of pulse turbocharged engine.**

In this manner, the MVEM model can be used to define back pressure limits at any engine speed by applying the concept of smoke limit and thermal overloading.

Chapter 6

EMISSIONS

The emissions are measured with the help of Horriba emission analyzer for all the measurements. The sampling pipe is connected to the diesel engine after the electronically controlled butterfly valve. The other end of the sampling pipe enters the emission analyzer. The emission analyzer comes with calibration bottles which are used to calibrate the analyzer every day before start taking emission measurements. There is a big lag (more than 10 seconds) in the emission measurements to the increase of the back pressure. This is because the exhaust sampling pipe to the analyzer is very long. Therefore, the exhaust requires additional time to reach the analyzer increasing the delay. The equipment measures the following emissions in the exhaust of the diesel engine.

- Carbon monoxide (CO) in ppm.
- Sulphur dioxide (SO_2) in ppm.
- Nitric oxide (NO) in ppm.
- Oxygen (O_2) in percentage volume.
- Carbon dioxide (CO_2) in percentage volume.

The increase in back pressure reduces the pressure ratio across the turbine, slowing down the turbine, thus slowing down the compressor. This reduces the compressor discharge pressure and reduces the air intake to the engine. Sice, the emission analyzer was faulty at the time when engine was tested with static and step up back pressure at highest set point (340 KW, 981 rpm). Therefore, the results presented for step up change in this section is limited to 288 KW load at 928 rpm. For continuous waves, the emission data is availaible at 340 KW, 981 rpm. While discussing about emission measurements with back pressure waves of different amplitudes, the results are presented at 340 KW, 981 rpm. At 288 KW, the engine is subjected to 43 mbar step up back pressure input shown in figure 6.1 (a). To compensate for the additional pumping work to remove exhaust gasses from the engine, the governor increases the fuel. More air is required for complete combustion of the fuel. This decreases the oxygen percentage in the exhaust as more oxygen is used to combust the added fuel. The figure 6.1 (b) shows the drop in the oxygen volume percentage with step up of 43 mbar back pressure. The response of the oxygen percentage volume graph reduces after a big lag. The final value of oxygen percentage is lower than shown in the figure as the measurements stopped at 35 seconds.

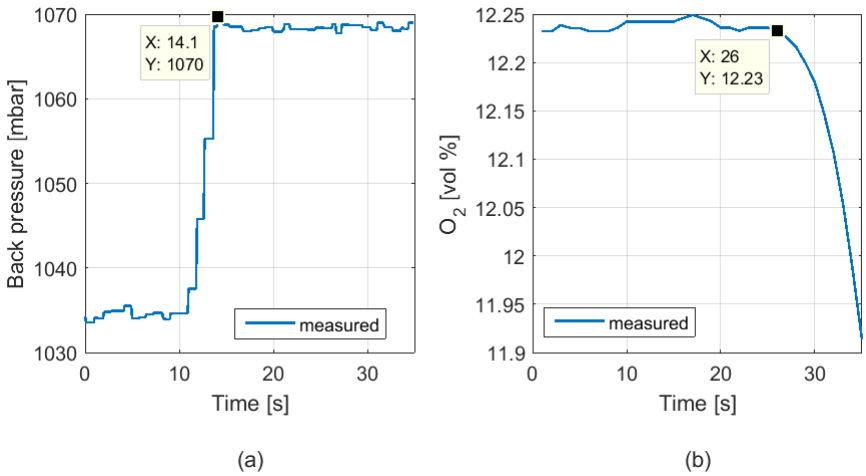

Figure 6.1: **Step up BP-43 mbar, Time - 4s (a) and Oxygen (% volume) measurement (b). Load - 288 KW, Speed - 928 rpm**

Combustion of more fuel with reduced fresh air intake increases the emission of carbon monoxide showing the increase in incomplete combustion. Moreover, the production of carbon dioxide also increases with an increase in fuel flow. It can be seen in figure 6.2.

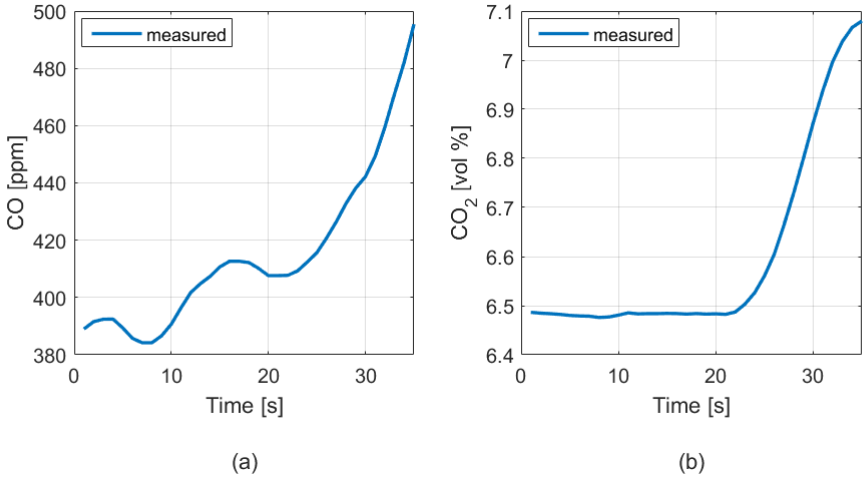

Figure 6.2: **Carbon monoxide (CO) (a) and Carbon di-oxide (CO_2) (b) for dynamic step up BP-43 mbar, Time - 4s, load - 288 KW, speed - 928 rpm**

Combustion of more fuel at higher back pressure, increases the temperature on the exhaust side [43]. Higher temperature favors the production of Nitric oxide by oxidizing the nitrogen in the air which can be seen in figure 6.3 (a). The back pressure increases the fuel input to the engine which increases the production of Sulphur di-oxide [44]. The emission of sulphur oxides is from the oxidizing the sulphur present in the fuel.

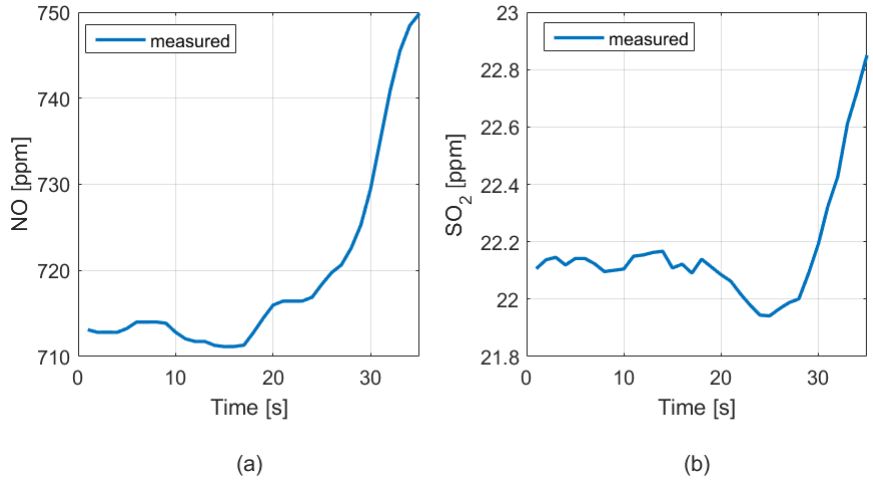

Figure 6.3: **Nitric oxide (NO) (a) and Sulphur di-oxide (SO_2) (b) for dynamic step up BP-43 mbar, Time - 4s, load - 288 KW, speed - 928 rpm**

This trend for the emissions found for all the measurements at any load. On depth analysis of the results, it is found that the increment or change in the exhaust emissions is more for high amplitude of back pressure with constant wave period. Figure 6.4 and 6.5 shows the back pressure wave along with oxygen percentage for 35 mbar, 6s and 45 mbar, 6s back pressure wave. The maximum drop in oxygen percentage for 45 mbar back pressure is 0.41 % by volume where as for 35 mbar back pressure wave is 0.34vol % at 340 KW, 981 rpm. This is because more fuel is consumed for higher back pressure, thus, more oxygen is consumed from the air reducing oxygen percentage in the exhaust.

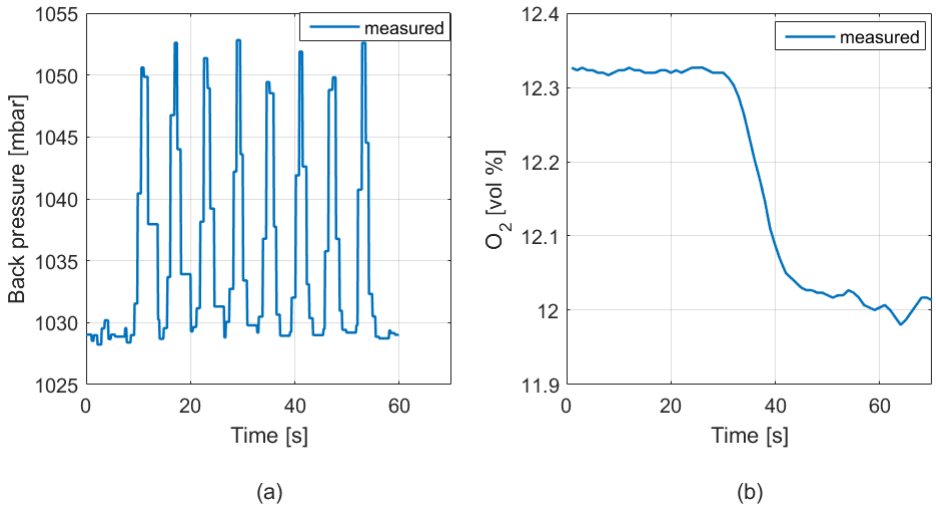

Figure 6.4: **BP - 35 mbar, WP - 6s (a) and Oxygen (% volume) measurement (b). Load - 340 KW, Speed - 981 rpm**

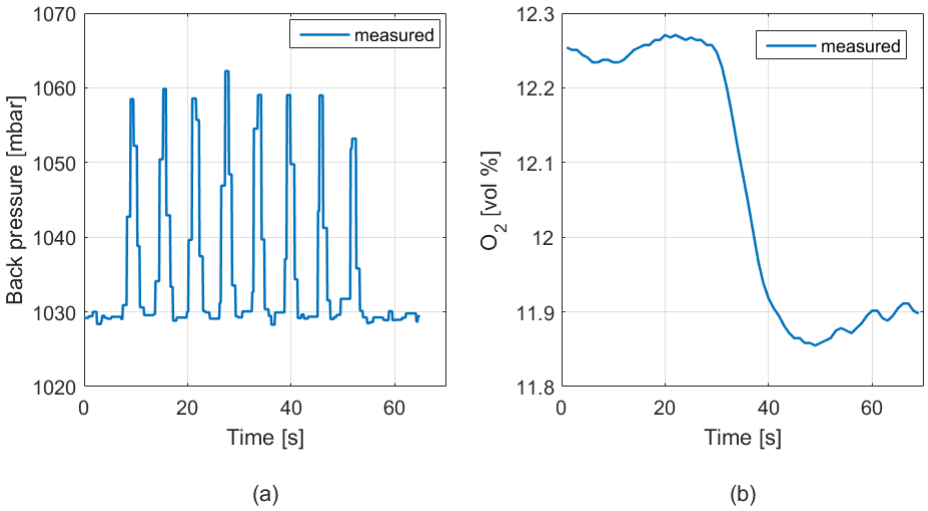

Figure 6.5: **BP - 45 mbar, WP - 6s (a) and Oxygen (% volume) measurement (b). Load - 340 KW, Speed - 981 rpm**

The oxygen percentage is measured at all loads for the same 35 mbar and 45 mbar back pressure waves. The results are shown in 6.6. The red line for 45 mbar is always above 25 mbar blue line. It means that the drop in oxygen percentage in the exhaust is higher for higher back pressure at all loads.

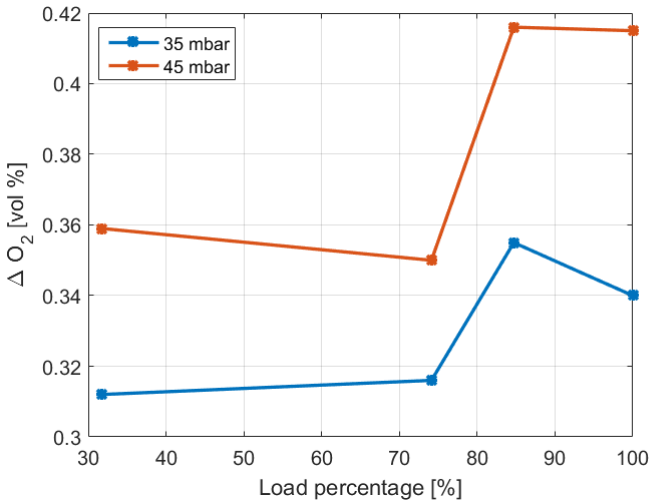

Figure 6.6: **Oxygen (% volume) measurement at all loads**

The carbon monoxide and carbon dioxide for the 35 mbar dynamic back pressure and 45 mbar dynamic back pressure wave are shown in figures 6.7 and 6.8. The increment in carbon monoxide and carbon dioxide is more for for higher amplitude of back pressure. The carbon di oxide volume percentage increases by 0.27 vol% for 35 mbar back pressure where as, for 45 mbar the increment is 0.32 vol %. The carbon monoxide increment is 63.9 ppm for 35 mbar back pressure wave and 76.6 ppm for 45 mbar back pressure wave at 340 KW. More fuel is used in the engine, thus more carbon dioxide and carbon monoxide is produced.

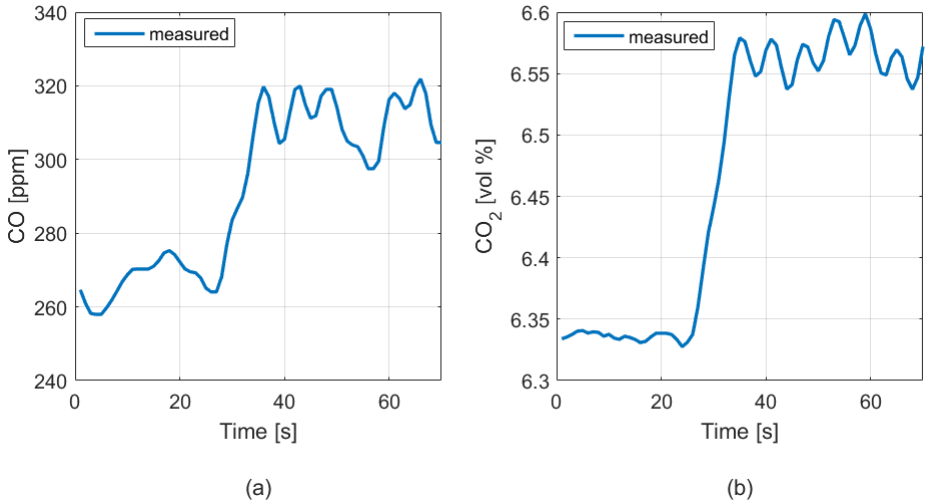

Figure 6.7: **Carbon monoxide (CO) (a) and Carbon di-oxide (CO_2) (b) for dynamic BP- 35 mbar, Time - 6s, load - 340 KW, speed - 981 rpm**

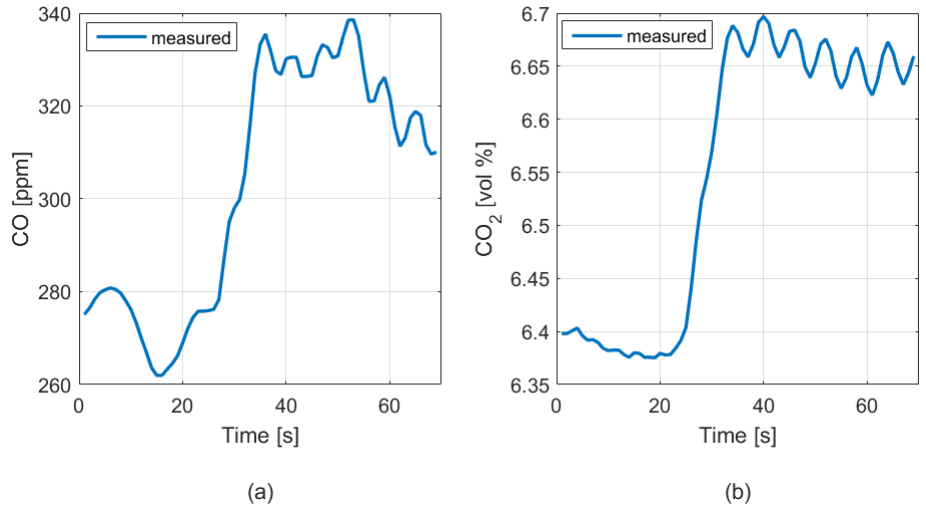

Figure 6.8: **Carbon monoxide (CO) (a) and Carbon di-oxide (CO_2) (b) for dynamic BP- 45 mbar, Time - 6s, load - 340 KW, speed - 981 rpm**

The figure 6.9 shows the carbon monoxide and carbon dioxide measurements from the engine exhaust at various loads are shown. The increment in CO and CO_2 measurements are higher for 45 mbar back pressure, stating that the increment is higher for higher back pressure. Moreover, the increment is higher for higher loads compared to the increments of both emission parameter at lower loads.

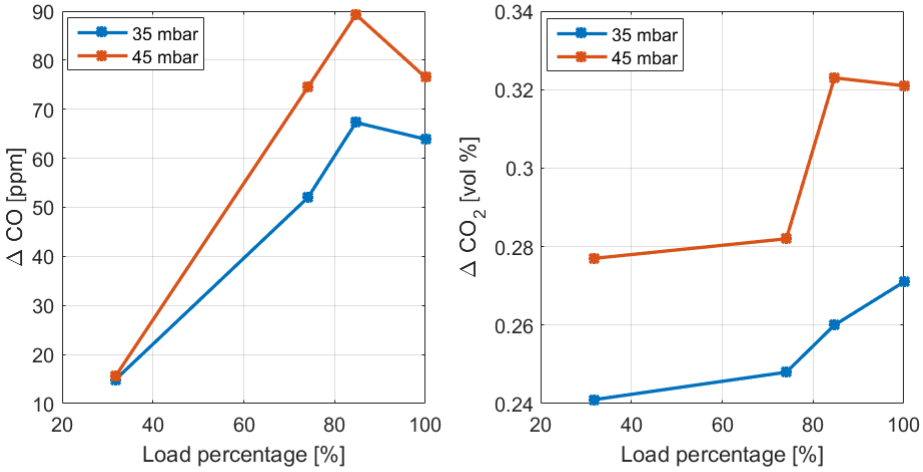

Figure 6.9: **Carbon monoxide (ppm) (a) and carbon dioxide (% volume) (b) measurement at all loads**

The nitrous oxide and sulphur dioxide increment in the exhaust emission are also measured higher for higher back pressure. Figure 6.10 and figure 6.11 can be compared to prove the statement. The increase in nitrous oxide and sulphur di oxide for 35 mbar back pressure wave is 24.2 ppm and 0.7 ppm. For 45 mbar back pressure wave the increment in nitrous oxide and sulphur dioxide is 25.9 ppm and 0.98 ppm. The theory says that there should be a decrease in the nitrous oxide with an increase in back pressure at higher loads. But, the experimental measurements show the opposite trend. Therefore, there is a need for further investigation on this.

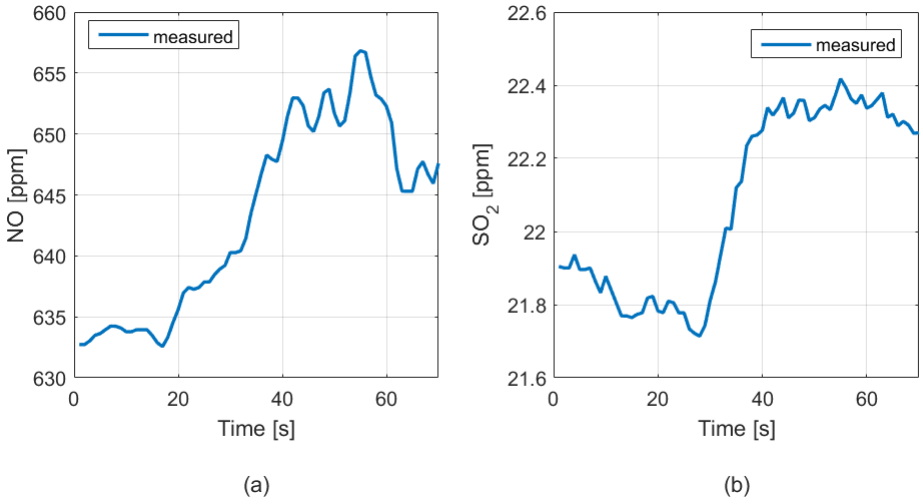

Figure 6.10: **Carbon monoxide (CO) (a) and Carbon dioxide (CO_2) (b) for dynamic BP- 35 mbar, Time - 6s, load - 340 KW, speed - 981 rpm**

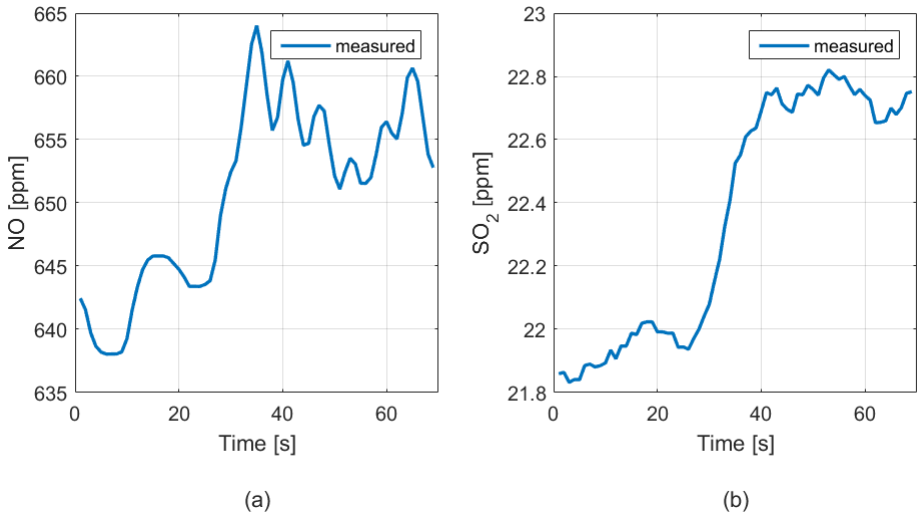

Figure 6.11: **Nitric oxide (NO) (a) and Sulphur di-oxide (SO_2) (b) for dynamic BP-45 mbar, Time - 6s, load - 340 KW, speed - 981 rpm**

The figure 6.12 shows that the increment in NO and SO_2 is higher for higher back pressure. The measured nitrous oxide and sulphur dioxide is plotted at load points for 35 mbar and 45 mbar back pressure waves. The NO decreases with load but the difference between NO measurements for 45 mbar and 35 mbar back pressure wave is very close to each other. Therefore, it can be said that the NO increases with a small value with increment of back pressure.

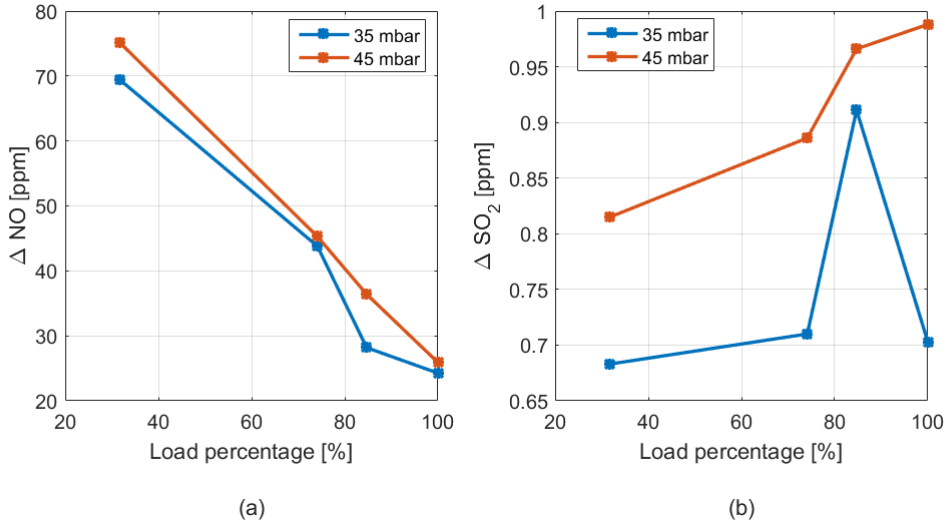

Figure 6.12: **Nitrous oxide (ppm) (a) and Sulphur dioxide (% volume) (b) measurement at all loads**

The similar trend is missing when the emission measurements were compared for the different wave periods back pressure wave. The table 6.1 shows the change in emission for different wave periods back pressure wave. It is clear from the table below that the emission trend observed for higher amplitude of back pressure wave is not found for higher wave period back pressure wave with constant amplitude.

Table 6.1: **Change (Δ) in emission parameter for wave periods 4s, 6s and 8s back pressure wave.**

Load [KW]	BP [mbar]	WP [s]	NO [ppm]	O_2 [vol %]	CO_2 [vol %]	CO [ppm]	SO_2 ppm
108	45	4	73.1	0.34	0.26	16.04	0.77
108	45	6	75.1	0.35	0.277	16.60	0.81
108	45	8	66.8	0.32	0.262	17.32	0.787
252	45	4	35.2	0.37	0.294	71.6	0.913
252	45	6	45.38	0.35	0.28	74.58	0.89
252	45	8	45.20	0.39	0.32	94.99	0.97
288	45	4	42.31	0.44	0.32	59.79	1.01
288	45	6	36.46	0.41	0.32	63.93	1.01
288	45	8	40.06	0.44	0.36	74.91	1.16
340	45	4	13.40	0.41	0.30	80.08	0.86
340	45	6	25.97	0.42	0.32	76.60	0.99
340	45	8	26.38	0.46	0.36	92.78	1.15

Chapter 7

CONCLUSION AND RECOMMENDATIONS

7.1 CONCLUSIONS

In this master thesis research, the experimental and simulated study was carried out to investigate the effect of dynamic back pressure in varying sea on the performance of the pulse turbocharger 4 stroke marine diesel engine due to underwater exhaust. The test engine is subjected to static, step up, single and multiple back pressure waves (for amplitude change and wave period change) to understand the effect of dynamic back pressure (amplitude and wave period) on diesel engine's parameters. The adopted model is used to simulate and measure engine parameters cannot be measured on the test engine. Moreover, the performances are simulated for extreme back pressure and wave periods which could not be tested experimentally. The main conclusions from the master thesis results are stated below -

- Increasing wave amplitude of single and multiple back pressure waves increases the thermal loading of the engine. Therefore, higher the sea state higher will be the increase in exhaust receiver temperature thus, higher thermal loading.
- Increasing the wave period of the back pressure wave also increases the exhaust receiver temperature.
- The increments in maximum exhaust receiver temperature were higher against multiple back pressure waves compared to those found against a single back pressure wave of same wave amplitude and wave period.
- The effect of dynamic back pressure on the performance of the diesel engine was not severe when compared to the steady state (static) back pressure measurements. Therefore, a marine engine designed for one value of steady state back pressure could handle higher amplitude of dynamic back pressure.
- Engine model simulations showed that fuel flow controlled by governor and turbocharger's air intake controls helps in keeping the fuel penalty and exhaust receiver temperature below the value for a static back pressure of similar pressure amplitude. However, at a certain critical value of the dynamic wave period the governor and turbocharger response may be unable to dampen the adverse effects of dynamic back pressure. Above the critical wave period, the

fuel flow rate and exhaust receiver temperature for dynamic back pressure could reach the static fuel flow rate and exhaust receiver temperature of static back pressure of the same amplitude.

- The recorded emission shows an increase in measured NO, CO, SO_2 and CO_2 with an increase in static or dynamic back pressure at all loads. On the other hand, O_2 decreases with an increase in static or dynamic back pressure at all loads.

7.2 RECOMMENDATIONS

The following recommendations for the future works -

- The critical value of wave period above which the change in parameters remains the same should be tested experimentally. In this research, the test engine is subjected to the maximum wave period of 8s. By experimenting with higher wave period and same back pressure amplitude, the critical value of wave period for an engine can be found experimentally.

- The governor and turbocharger settings can be tuned finally to reduce the error between the simulated and measured results. This can be done by introducing PID controller inside the governor model. In this research, the governor block consists of a PI controller whereas the test engine governor used PID control.

- The measured emission shows an increase in the measured NO at higher back pressure at all loads. Since no publicly available research found which supports the measured results. Therefore, it is recommended to investigate the emissions further with dynamic back pressure.

- The research is carried out with an assumption that the exhaust outlet is placed such that the back pressure reduces to zero at the trough of the back pressure waves. In the real scenario, this is not possible due to the relative motion of exhaust outlet, sea waves, waves produced by the ship's motion and swells.

- The butterfly valve produces square back pressure waves measured during the experiments. It should be checked whether the engine experiences square wave when real sea waves act on the exhaust outlet.

- The simulations prove that the governor is mainly responsible for handling the back pressure. By playing with governor settings, the back pressure can be tackled effectively. This should be checked experimentally.

Appendix A

HISTORICAL WAVE DATA

The historical wave data is obtained from The National Data Bouy Center (NDBC). NDBC maintains a network of data collecting bouys and coastal stations, around the globe measuring the waves and storing the historical data. The data used in this research is taken from NDBC. The data is recorded by bouy number 44066 on the eastern coast of the United States of America. Table A.1 shows the details of the bouy 44066.

Table A.1: **Details of station 44066**

Type of bouy	3-meter foam buoy
payload	SCOOP payload
GPS coordinates	39.618 N 72.644 W (39°37'5" N 72°38'37" W)
Site elevation	sea level
Air temp height	4 m above site elevation
Anemometer height	5 m above site elevation
Barometer elevation	sea level
Sea temp depth	0.6 m below water line
Water depth	78 m
Watch circle radius	155 yards

The real time data for bouy 44066 is shown in the figure A.1. The diesel engine cannot be subjected to back pressure above 0.5 mWC (50 mbar gauge), therefore, only the applicable data is shown in the table below. The data shown in the figures is recorded for various months in 2018 by the bouy and processed by the NDBC.

#YY	MM	DD	hh	mm	WDIR	WSPD	GST	WVHT	DPD	APD	MWD	PRES	ATMP	WTMP	DEWP	VIS	TIDE
#yr	mo	dy	hr	mn	degT	m/s	m/s	m	sec	sec	degT	hPa	degC	degC	degC	mi	ft
2018	01	03	22	50	77	5.4	7.0	0.47	4.17	4.00	280	1020.7	3.9	11.2	-1.1	99.0	99.00
2018	01	03	23	50	85	5.8	7.2	0.45	10.00	3.55	132	1020.0	4.9	11.2	0.3	99.0	99.00
2018	01	04	00	50	90	7.2	9.2	0.49	2.86	3.30	91	1018.7	6.0	11.2	1.7	99.0	99.00
2018	01	10	20	50	143	1.9	2.7	0.47	9.09	4.79	166	1031.0	7.0	11.9	1.2	99.0	99.00
2018	01	10	21	50	182	3.5	5.1	0.48	10.00	5.21	138	1031.2	7.3	11.9	1.6	99.0	99.00
2018	01	10	22	50	170	3.4	4.7	0.45	10.00	5.01	155	1031.3	7.7	11.8	2.4	99.0	99.00
2018	01	10	23	50	157	3.9	5.5	0.49	10.00	5.42	154	1031.5	8.0	11.8	2.6	99.0	99.00
2018	01	11	01	50	152	5.5	6.7	0.46	10.00	4.71	161	1031.2	8.7	11.7	4.1	99.0	99.00
2018	01	22	10	50	159	4.4	5.1	0.49	6.25	4.95	191	1021.8	10.8	9.7	9.5	99.0	99.00
2018	01	27	01	50	188	3.9	5.3	0.45	14.81	4.35	116	1038.8	3.9	8.4	-2.9	99.0	99.00
2018	01	27	02	50	190	5.5	6.8	0.44	14.81	3.98	202	1038.3	4.9	8.6	-1.9	99.0	99.00
2018	01	27	03	50	199	6.6	8.0	0.48	2.60	3.42	196	1037.9	5.7	8.7	-0.8	99.0	99.00
2018	03	12	04	50	7	1.7	2.2	0.46	8.33	4.44	175	1017.8	4.9	6.8	-1.2	99.0	99.00
2018	03	12	05	50	30	3.4	4.2	0.46	12.12	5.17	62	1017.3	5.2	6.9	-1.7	99.0	99.00
2018	03	12	06	50	36	5.5	6.5	0.43	12.90	4.91	104	1016.5	5.1	6.8	-1.0	99.0	99.00
2018	03	12	07	50	54	6.1	7.4	0.47	7.14	4.10	173	1015.6	5.1	6.8	0.0	99.0	99.00
2018	04	06	13	50	129	5.7	6.4	0.46	16.00	4.16	208	1019.8	7.2	7.5	1.0	99.0	99.00
2018	04	06	14	50	162	8.8	10.2	0.45	13.79	3.46	66	1018.6	8.3	7.6	2.7	99.0	99.00
2018	04	22	17	50	334	2.3	2.6	0.47	4.17	3.91	235	1029.6	7.9	8.0	3.9	99.0	99.00
2018	04	22	18	50	326	1.3	2.0	0.44	16.00	4.19	133	1029.4	8.1	8.1	4.0	99.0	99.00
2018	04	22	19	50	319	1.0	1.3	0.44	9.09	4.42	165	1028.9	8.6	8.5	4.5	99.0	99.00
2018	04	22	20	50	106	0.9	1.4	0.42	16.00	4.45	104	1028.6	8.5	8.9	3.8	99.0	99.00
2018	04	22	21	50	207	1.9	2.4	0.41	9.09	4.73	143	1028.6	8.8	8.6	5.0	99.0	99.00
2018	04	22	22	50	209	3.8	4.6	0.40	14.81	4.88	52	1028.5	8.3	8.1	5.8	99.0	99.00
2018	04	22	23	50	210	3.0	3.5	0.37	12.90	4.73	128	1028.5	8.0	7.9	5.4	99.0	99.00
2018	04	23	00	50	217	3.7	4.2	0.37	14.81	5.16	52	1028.9	8.0	7.6	5.0	99.0	99.00
2018	04	23	01	50	229	4.1	4.5	0.36	13.79	5.39	164	1029.3	8.1	7.4	4.4	99.0	99.00
2018	04	23	02	50	227	4.2	5.2	0.32	12.12	5.26	65	1029.3	8.2	7.4	4.5	99.0	99.00
2018	04	23	03	50	232	4.1	4.7	0.33	13.79	5.44	82	1029.3	8.2	7.4	4.4	99.0	99.00
2018	04	23	04	50	245	3.5	4.1	0.34	14.81	5.40	89	1029.5	7.9	7.3	5.8	99.0	99.00
2018	04	23	06	50	236	2.6	3.0	0.33	14.81	5.48	181	1029.6	7.9	7.2	5.4	99.0	99.00
2018	04	23	07	50	249	3.4	4.5	0.32	14.81	5.41	116	1029.6	8.0	7.3	5.2	99.0	99.00
2018	04	23	08	50	259	3.3	3.7	0.35	14.81	5.32	82	1030.2	8.0	7.3	5.3	99.0	99.00
2018	04	23	09	50	267	2.1	2.5	0.34	13.79	4.77	68	1030.7	7.9	7.3	5.5	99.0	99.00
2018	04	23	10	50	235	2.0	2.6	0.39	14.81	6.07	126	1031.3	8.6	7.2	4.8	99.0	99.00
2018	04	23	11	50	138	1.8	2.3	0.35	14.81	5.87	62	1031.8	8.2	7.3	6.2	99.0	99.00
2018	04	23	12	50	170	1.5	2.1	0.35	14.81	6.06	70	1032.1	8.0	7.6	6.9	99.0	99.00
2018	04	23	13	50	176	2.1	2.6	0.35	13.79	6.16	75	1032.3	8.4	8.0	6.9	99.0	99.00
2018	04	23	14	50	160	1.9	2.3	0.37	13.79	6.92	276	1032.4	8.9	8.2	6.5	99.0	99.00
2018	04	23	15	50	181	1.0	1.3	0.33	12.12	6.53	302	1032.0	9.3	8.8	6.6	99.0	99.00

Figure A.1: **Standard meteorological data**

```
2018 04 23 15 50 181  1.0  1.3  0.33 12.12  6.53 302 1032.0   9.3   8.8   6.6 99.0 99.00
2018 04 23 16 50 358  0.5  0.8  0.35 13.79  6.67 108 1031.8   9.9   9.2   6.0 99.0 99.00
2018 04 23 17 50 167  0.1  0.4  0.31 14.81  6.51  95 1031.8  11.4   8.8   4.6 99.0 99.00
2018 04 23 18 50 161  0.2  0.5  0.32 14.81  6.60  94 1031.8  12.0   8.9   4.5 99.0 99.00
2018 04 23 19 50 204  1.6  1.9  0.33  8.33  6.56 162 1031.4  12.2  10.7   5.1 99.0 99.00
2018 04 23 20 50 182  1.6  1.9  0.35 14.81  7.23 135 1031.3  12.1  11.7   6.3 99.0 99.00
2018 04 23 21 50 174  1.7  2.0  0.37 14.81  7.20 329 1031.1  11.7  10.8   7.8 99.0 99.00
2018 04 23 22 50 140  1.9  2.1  0.37  7.69  7.12 154 1030.8  10.9  10.3   9.0 99.0 99.00
2018 04 23 23 50 155  1.7  1.8  0.34  8.33  7.08 164 1031.1  10.3  10.3   9.3 99.0 99.00
2018 04 24 00 50 121  2.7  2.9  0.37 13.79  6.51 357 1031.2  10.4   9.5   8.9 99.0 99.00
2018 04 24 01 50 125  2.4  2.7  0.36 14.81  7.04  55 1031.6   9.8   8.3   8.8 99.0 99.00
2018 04 24 02 50 120  2.5  3.0  0.38  9.09  7.27 151 1031.2   9.5   8.4   8.5 99.0 99.00
2018 04 24 03 50 114  2.5  2.7  0.38 12.90  7.31 102 1030.8   9.5   8.2   8.4 99.0 99.00
2018 04 24 04 50 123  2.8  3.0  0.36 12.90  6.80 108 1030.4   9.6   8.0   8.2 99.0 99.00
2018 04 24 05 50 142  2.8  3.0  0.35 14.81  6.37 164 1030.2   9.7   8.1   7.9 99.0 99.00
2018 04 24 06 50 125  2.8  3.0  0.36  7.69  6.21 145 1029.8   9.7   8.1   7.7 99.0 99.00
2018 04 24 07 50 136  3.2  3.6  0.37 14.81  6.21   6 1029.6   9.8   8.0   7.8 99.0 99.00
2018 04 24 08 50 129  3.8  4.6  0.40 14.81  5.62 311 1029.4   9.7   7.7   7.7 99.0 99.00
2018 04 24 09 50 117  4.2  4.7  0.38  9.09  6.09 141 1029.2   9.7   7.8   7.8 99.0 99.00
2018 04 24 10 50 114  3.3  3.7  0.40 13.79  5.68 113 1029.5   9.8   7.7   7.4 99.0 99.00
2018 04 24 11 50 116  2.6  2.8  0.41  9.09  5.50 171 1029.9   9.8   7.8   7.4 99.0 99.00
2018 04 24 12 50 119  3.5  3.9  0.43  9.09  5.32 153 1029.5  10.0   8.3   7.3 99.0 99.00
2018 05 25 00 50 186  4.6  5.3  0.47  7.69  5.58 153 1019.8  14.4  12.9  13.4 99.0 99.00
2018 06 10 00 50 184  2.8  3.1  0.46  8.33  5.16 140 1017.2  17.2  16.1  17.2 99.0 99.00
2018 06 10 01 50 203  4.1  4.6  0.46  9.09  5.24 117 1017.6  16.9  15.7  16.9 99.0 99.00
2018 06 10 02 50 244  2.8  3.2  0.46  8.33  5.38 164 1017.7  16.7  15.4  16.7 99.0 99.00
2018 06 10 03 50 256  1.2  1.6  0.47 12.12  5.27 102 1017.4  16.9  15.6  16.9 99.0 99.00
2018 06 10 04 50 253  2.6  2.9  0.47  8.33  5.17 130 1016.9  16.7  15.4  16.7 99.0 99.00
2018 06 10 09 50  42  4.0  4.4  0.47  8.33  5.08 147 1016.0  16.6  16.0  16.6 99.0 99.00
2018 06 10 11 50  47  2.7  3.0  0.47  4.55  5.23 217 1016.6  16.8  16.0  16.6 99.0 99.00
2018 06 10 13 50  44  5.9  6.6  0.46  7.69  5.68 135 1016.9  17.1  15.8  14.7 99.0 99.00
2018 06 10 14 50  50  5.0  5.6  0.46  9.09  5.76 126 1017.0  16.8  15.5  14.4 99.0 99.00
2018 06 10 20 50  71  4.1  4.7  0.49  7.69  3.93 158 1014.9  16.9  15.4  13.2 99.0 99.00
2018 06 10 21 50  63  4.3  5.3  0.47  9.09  4.36 120 1014.8  16.4  15.4  13.8 99.0 99.00
2018 06 10 22 50  66  5.0  5.9  0.47  9.09  4.15 143 1014.2  16.2  15.3  14.1 99.0 99.00
2018 06 10 23 50  64  5.5  6.5  0.48 10.00  3.93 135 1014.6  16.1  15.3  14.1 99.0 99.00
2018 06 11 01 50  50  8.7 10.3  0.49  8.33  3.66 122 1015.0  15.7  15.1  11.2 99.0 99.00
2018 06 16 06 50 237  2.6  3.1  0.49  9.09  5.17 124 1016.1  16.2  15.7  15.3 99.0 99.00
2018 06 16 08 50 267  3.4  3.9  0.47  9.09  5.12 149 1016.4  16.6  15.7  15.1 99.0 99.00
2018 06 16 10 50 261  2.1  2.5  0.46  8.33  5.37 130 1016.9  16.9  15.7  15.5 99.0 99.00
2018 06 16 11 50 260  2.1  2.2  0.45  9.09  5.00 144 1016.9  16.8  15.8  15.9 99.0 99.00
2018 06 16 12 50 274  4.0  4.6  0.46  8.33  5.34 130 1017.2  16.9  15.9  16.3 99.0 99.00
2018 06 16 13 50 279  3.1  3.6  0.49  9.09  5.79 146 1017.0  17.2  16.0  16.2 99.0 99.00
2018 06 16 14 50 267  2.7  3.1  0.46  9.09  5.63 143 1017.0  17.4  16.3  16.4 99.0 99.00
2018 06 16 15 50 253  3.1  3.6  0.44  8.33  5.73 143 1017.0  17.6  16.7  16.4 99.0 99.00
```

Figure A.2: **Standard meteorological data**

```
2018 06 16 17 50 257  4.2  4.8  0.42  9.09  5.67 143 1016.1  17.9  16.8  16.6 99.0 99.00
2018 06 16 18 50 261  4.7  5.4  0.48  9.09  5.13 179 1016.4  18.1  16.7  16.8 99.0 99.00
2018 06 16 19 50 259  3.0  3.5  0.47  8.33  5.18 137 1016.1  18.2  16.8  17.0 99.0 99.00
2018 06 16 20 50 247  3.5  4.1  0.43  9.09  4.79 151 1016.2  18.4  16.9  16.8 99.0 99.00
2018 06 16 21 50 222  3.6  4.2  0.41  8.33  5.17 139 1016.1  18.5  16.9  16.4 99.0 99.00
2018 06 16 22 50 222  4.2  4.7  0.43  8.33  5.04 146 1016.2  18.5  17.1  16.4 99.0 99.00
2018 06 16 23 50 220  4.9  5.7  0.39  8.33  4.73 128 1015.8  18.1  17.0  16.7 99.0 99.00
2018 06 17 00 50 220  4.0  4.4  0.40  7.69  4.50 150 1016.2  18.0  16.9  16.8 99.0 99.00
2018 06 17 01 50 223  3.9  4.4  0.39  8.33  4.48 140 1016.7  18.1  16.8  16.8 99.0 99.00
2018 06 17 02 50 230  4.3  4.9  0.39  9.09  4.62 113 1017.1  18.1  16.8  16.3 99.0 99.00
2018 06 17 03 50 236  4.0  4.5  0.41  8.33  4.60 151 1017.2  18.1  16.7  16.3 99.0 99.00
2018 06 17 04 50 237  4.8  5.4  0.41  8.33  4.23 137 1017.3  18.4  16.7  15.8 99.0 99.00
2018 06 17 05 50 225  3.9  4.4  0.43  8.33  4.56 179 1017.6  18.3  16.6  15.3 99.0 99.00
2018 06 17 06 50 213  4.2  4.9  0.39  8.33  4.38 165 1017.1  18.3  16.5  15.7 99.0 99.00
2018 06 17 07 50 217  4.4  5.1  0.41  8.33  4.22 171 1016.6  18.2  16.5  15.6 99.0 99.00
2018 06 17 08 50 232  3.8  4.4  0.44  8.33  4.41 144 1017.0  18.0  16.4  15.8 99.0 99.00
2018 06 17 09 50 230  3.3  3.8  0.43  9.09  4.34 148 1017.4  18.0  16.4  16.3 99.0 99.00
2018 06 17 10 50 222  2.9  3.2  0.41  8.33  4.52 135 1017.5  18.0  16.4  16.6 99.0 99.00
2018 06 17 11 50 238  2.6  3.1  0.44  8.33  4.85 180 1018.1  18.2  16.4  16.7 99.0 99.00
2018 06 17 12 50 252  2.9  3.1  0.43  8.33  4.63 127 1018.6  18.4  16.6  16.6 99.0 99.00
2018 06 17 13 50 240  3.2  3.5  0.42  8.33  4.77 165 1018.4  18.4  16.8  17.0 99.0 99.00
2018 06 17 14 50 239  2.9  3.4  0.44  9.09  4.83 133 1018.7  18.6  17.1  16.7 99.0 99.00
2018 06 17 15 50 251  3.1  3.5  0.42  9.09  4.71 135 1019.2  18.9  17.4  16.9 99.0 99.00
2018 06 17 16 50 216  2.0  2.4  0.41  9.09  4.72 140 1019.1  19.0  17.8  17.1 99.0 99.00
2018 06 17 17 50 208  2.6  3.0  0.38  8.33  4.65 103 1018.5  19.2  18.2  17.6 99.0 99.00
2018 06 17 18 50 224  2.7  3.1  0.44  9.09  5.29 137 1018.5  19.4  18.2  17.8 99.0 99.00
2018 06 17 19 50 206  3.5  3.9  0.40  9.09  5.11 114 1018.5  19.5  18.4  18.0 99.0 99.00
2018 06 17 20 50 201  3.8  4.3  0.41  8.33  5.36 161 1018.5  19.6  18.3  17.9 99.0 99.00
2018 06 17 21 50 197  2.8  3.3  0.38  8.33  4.98 153 1018.6  19.8  18.5  17.9 99.0 99.00
2018 06 17 22 50 184  3.8  4.3  0.43  9.09  5.23 155 1018.7  19.7  18.4  17.7 99.0 99.00
2018 06 17 23 50 183  3.6  3.9  0.37  8.33  5.40 165 1018.6  19.4  18.4  18.1 99.0 99.00
2018 06 18 00 50 179  3.4  3.9  0.44  8.33  5.84 161 1018.5  19.3  18.2  18.8 99.0 99.00
2018 06 18 01 50 187  2.8  3.3  0.41  8.33  5.38 161 1018.8  19.4  18.1  19.2 99.0 99.00
2018 06 18 02 50 179  4.3  4.9  0.39  8.33  5.21 152 1018.7  19.4  18.1  19.2 99.0 99.00
2018 06 18 03 50 187  4.2  4.6  0.39  9.09  5.09 161 1018.5  19.5  17.8  18.4 99.0 99.00
2018 06 18 04 50 173  3.7  4.3  0.40  8.33  4.84 169 1018.3  19.0  17.8  18.4 99.0 99.00
2018 06 18 05 50 196  3.6  4.3  0.44  8.33  5.03 145 1018.1  19.2  17.6  18.5 99.0 99.00
2018 06 18 06 50 207  2.7  3.2  0.39  8.33  4.67 165 1018.2  19.0  17.4  18.0 99.0 99.00
2018 06 18 07 50 215  1.2  1.6  0.41  9.09  4.48 158 1018.2  18.8  17.2  17.4 99.0 99.00
2018 06 18 08 50 168  1.8  2.1  0.39  9.09  4.31 127 1018.2  18.5  17.0  17.1 99.0 99.00
2018 06 18 09 50 161  2.9  3.3  0.42  8.33  4.81 165 1018.2  18.7  17.0  17.4 99.0 99.00
2018 06 18 10 50 166  3.3  3.7  0.40  9.09  4.99 156 1018.5  19.0  17.1  17.7 99.0 99.00
2018 06 18 11 50 175  3.5  4.0  0.42  9.09  5.19 149 1018.2  19.2  17.2  17.8 99.0 99.00
2018 06 18 12 50 169  4.2  4.7  0.44  9.09  5.34 166 1017.4  19.1  17.2  17.9 99.0 99.00
2018 06 18 13 50 176  4.2  5.0  0.42  8.33  5.39 146 1017.1  19.3  17.5  18.5 99.0 99.00
```

Figure A.3: **Standard meteorological data**

where-

- WDIR - Wind direction (the direction the wind is coming from in degrees clockwise from true N) during the same period used for WSPD.
- WSPD - Wind speed (m/s) averaged over an eight-minute period for buoys and a two-minute period for land stations. Reported Hourly.
- GST - Peak 5 or 8 second gust speed (m/s) measured during the eight-minute or two-minute period. The 5 or 8 second period can be determined by payload.
- WVHT - Significant wave height (meters) is calculated as the average of the highest one-third of all of the wave heights during the 20-minute sampling period.
- DPD - Dominant wave period (seconds) is the period with the maximum wave energy.

- APD - Average wave period (seconds) of all waves during the 20-minute period.
- MWD - The direction from which the waves at the dominant period (DPD) are coming. The units are degrees from true North, increasing clockwise, with North as 0 (zero) degrees and East as 90 degrees.
- PRES - Sea level pressure (hPa).
- ATMP - Air temperature (Celsius).
- WTMP - Sea surface temperature (Celsius).
- DEWP - Dewpoint temperature taken at the same height as the air temperature measurement.
- VIS - Station visibility (nautical miles).
- PTDY - Pressure Tendency is the direction (plus or minus) and the amount of pressure change (hPa)for a three hour period ending at the time of observation.
- TIDE - The water level in feet above or below Mean Lower Low Water (MLLW).

Appendix B

DE-B MODEL GLITCH

The following shows the image of the simulink DE-B model. The box in the centre shows the MATLAB condition responsible for the glitch in the dynamic model. Removing that MATLAB function removes the bug from the model.

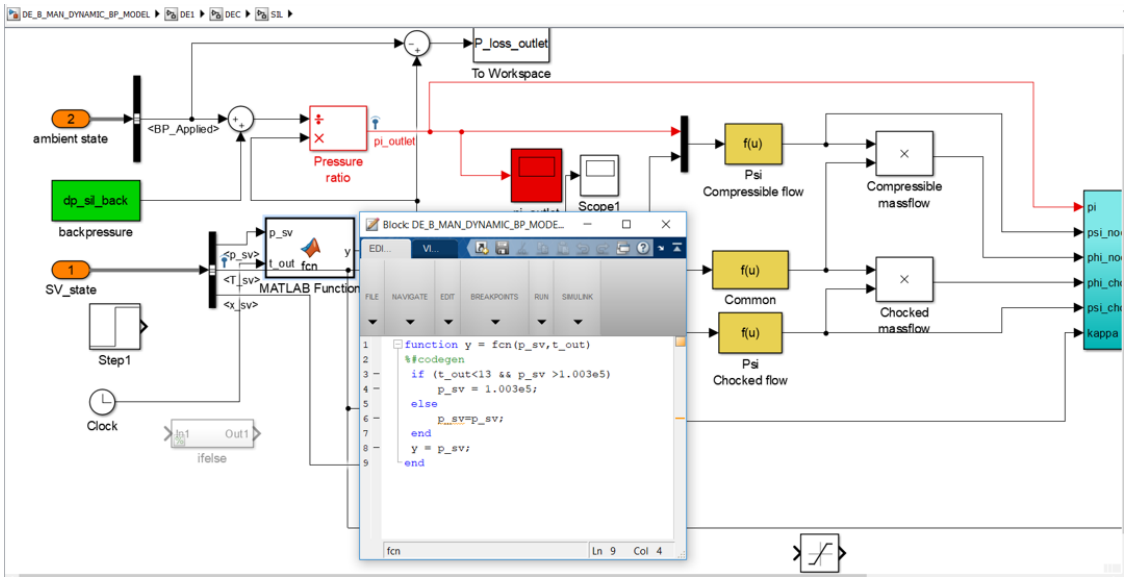

Appendix C

MODELING

The various parts of the diesel engine is modelled and explained in detail as follows.

C.0.1 AIR FILTER

The air filter is modeled as a resistance element. The mass flows are calculated from the pressure differences using the momentum equation. The analytical derivation is obtained from the 'Diesel Engine Volume '2'- Turbocharging by Prof. D. Stapersma [5]. A flow through the resistance is considered which is in-compressible. Moreover, velocity downstream volume is considered zero and the pressure in the downstream volume element is the same as the pressure in the throat. The mass flow through the resistance is calculated by

$$\dot{m} = \rho \cdot A_{eff} \cdot v \tag{C.1}$$

The pressure in the throat and after is assumed same. After integrating the momentum equation the mass flow through the resistance with pressure loss can be written as

$$\begin{aligned} \dot{m} &= A_{eff} \cdot \sqrt{\frac{2}{(1+\zeta_{in})} \cdot \frac{p_{in}}{R \cdot T_{in}} \cdot (p_{in} - p_{out})} \\ &= \frac{A_{eff}}{\sqrt{(1+\zeta_{in})}} \cdot \frac{p_{in}}{\sqrt{R \cdot T_{in}}} \cdot \sqrt{2} \cdot \sqrt{1 - \frac{p_{out}}{p_{in}}} \end{aligned} \tag{C.2}$$

The loss factor can be replaced by the resistance factor (ϕ). The effective area can be written in terms of geometric area multiplied by the contraction factor ($A_{eff} = \mu \cdot A$).

$$\dot{m} = (\mu \cdot \phi) \cdot A \cdot \frac{p_{in}}{\sqrt{R \cdot T_{in}}} \cdot \sqrt{2} \cdot \sqrt{1 - \frac{p_{out}}{p_{in}}} \tag{C.3}$$

For ease of understanding, the mass flow through the resistance can be summarized by :

$$\dot{m} = (\mu \cdot \phi) \cdot A \cdot \frac{p_{in}}{\sqrt{R \cdot T_{in}}} \cdot \psi \tag{C.4}$$

where Ψ is function of the pressure ratio (π).

$$\psi = \sqrt{2} \cdot \sqrt{1 - \frac{1}{\pi}} \quad forin - compressibleflow \tag{C.5}$$

$$\psi = \sqrt{\frac{2\gamma}{\gamma - 1}} \cdot \sqrt{\frac{1}{\pi}^{\frac{2}{\gamma}} - \frac{1}{pi}^{\frac{\gamma+1}{\gamma}}} \quad forcompressibleflow, nonchocking \tag{C.6}$$

$$\psi = \sqrt{\gamma \cdot \frac{2}{\gamma + 1}^{\frac{\gamma+1}{\gamma-1}}} \quad forcompressibleflow, choking \tag{C.7}$$

C.0.2 INLET VOLUME AND AIR COVER

Inlet volume and air cover are modeled as control volumes. The principle of conservation of mass and conservation of energy are used to calculate instantaneous mass and instantaneous temperatures. The instantaneous temperatures are derived from incoming and outgoing mass flows. The instantaneous pressures are calculated from the ideal gas equation. The analytical derivation is obtained from the 'Diesel Engine Volume '2'- Turbocharging by Prof. D. Stapersma [5].

Mass balance

$$\frac{dm}{dt} = \dot{m_{in}} - \dot{m_{out}} \tag{C.8}$$

Density:

$$\rho = \frac{m}{V} \tag{C.9}$$

Gas law :

$$p = \rho \cdot R \cdot T \tag{C.10}$$

Temperature is constant or taken from energy balance.

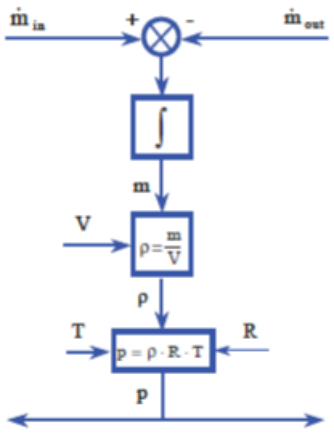

Figure C.1: Block diagram volume element (mass balance) [5]

The energy balance of a volume:

$$\frac{d(m \cdot u}{dt} = h_{in} \cdot \dot{m_{in}} - hout \cdot \dot{m_{out}} \dot{Q} - \dot{W} \tag{C.11}$$

Differentiate the internal energy and assuming perfect mixing

$$h_{net} = h \tag{C.12}$$

For the basic volume shown in figure C.2 heat transfer and work are zero:

$$p = \rho \cdot R \cdot T \tag{C.13}$$

Temperature is constant or taken from energy balance.

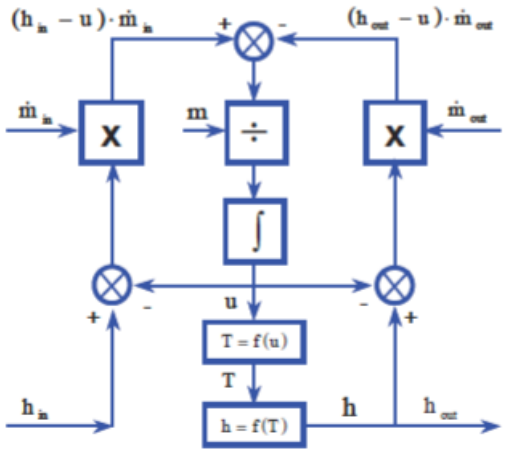

Figure C.2: Block diagram volume element (energy balance). [5]

$$du = c_v \cdot dT \quad \Longrightarrow \quad u = c_v \cdot T \tag{C.14}$$

$$dh = c_p \cdot dT \quad \Longrightarrow \quad h = c_p \cdot T \tag{C.15}$$

Insert in energy balance

$$c_v \cdot \frac{dT}{dt} = \frac{(c_p \cdot T_{in} - c_v \cdot t) \cdot \dot{m_{in}} - (c_p \cdot T_{out} - c_v \cdot T) \cdot \dot{m_{out}}}{m} \tag{C.16}$$

Assume perfect mixing i.e. homogeneous volume:

$$T_{out} = T \tag{C.17}$$

Then:

$$m \cdot_v \cdot \frac{dT}{dt} = (c_p \cdot T_{in} - c_v \cdot T) \cdot \dot{m_{in}} - R \cdot T \cdot \dot{m_{out}} \tag{C.18}$$

This is a differential equation for the temperature that is coupled to the mass balance.

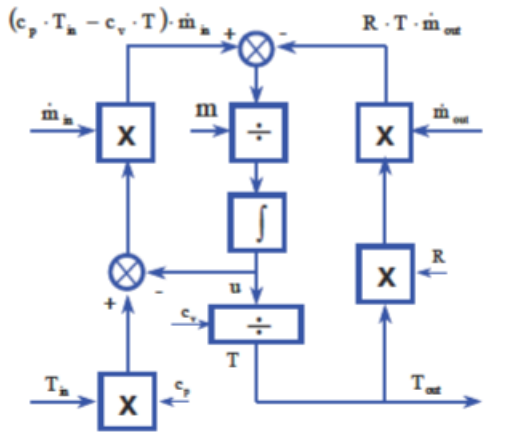

Figure C.3: Energy balance transformed into temperature balance. [5]

heat transfer is taken to be zero for simplicity but, the volume elements have a heat loss which is modelled using the following equation:

$$\dot{Q} = -\alpha \cdot A \cdot (T_{wall} - T_g) \tag{C.19}$$

where,

- α : heat transfer coefficient
- A : Area
- T_{wall} : Wall temperature
- T_g : Gas temperature

Once the temperature is known, the pressure p can be calculated:

$$p = \frac{m \cdot R \cdot T}{V} \tag{C.20}$$

C.0.3 COMPRESSOR AND TURBINE

Compressor and turbine model is an empirical model uses normalized non-dimensional properties originally developed by Baan [45].

C.0.4 CHARGE AIR COOLER

Charge air cooler is also a heat exchanger and the model for the purpose is adopted from C.Dijkstra [46]. It is modeled as the temperature change of the steel lump with heat flow on gas side and water side. This modeling description is taken from the research of C. Dijkstra who modeled air cooler as a heat ex-changer [46]. The air cooler consist of two stages, a high temperature heat ex-changer and a low temperature heat ex-changer, both these models are identical apart from their input. The heat ex-changer is modeled as a lump of steel with a heat flow on the gas side and a heat flow on the cooling water side.

$$dT = \frac{\dot{Q}}{m \cdot c} \tag{C.21}$$

The temperature of the steel lump follows from thr net heat input :

Where as the mass 'm' is the mass of the cooling water pipes inside the air cooler and 'c' is the specific heat used material. And the wall temperature is now calculated by integrating dT:

$$T_{wall} = \int \frac{\dot{Q}}{m \cdot c} dt \tag{C.22}$$

The heat flow on the waterside and air side equals :

$$\dot{Q} = c_p \cdot \dot{m} \cdot (T_{in} - T_{out}) \tag{C.23}$$

The temperature 'T_{in}' is the temperature of the flow when entering the heat ex-changer, the temperature of the flow at the heat ex-changer outlet equals:

$$T_{out} = T_{wall} - (T_{wall} - T_{in}) \cdot e^{\frac{-\alpha \cdot A}{c_p \cdot \dot{m}}} \tag{C.24}$$

In which 'A' is the heat exchanging surface which is smaller on the waterside than on the gas side. The heat exchange coefficient α is calculated by means of the Nusselt number.

$$\alpha = Nu \cdot \frac{\lambda}{d} \tag{C.25}$$

Where λ is the heat conduction coefficient and d is the hydraulic diameter of one tube. Nusselt is a function of the Prandtl number and Reynolds number.

$$Nu = 0.0023 \cdot Re^{0.8} \cdot Pr^{0.3} \tag{C.26}$$

C.0.5 CYLINDER

The in-cylinder process in diesel engines is divided into two parts. They are

1. Seiliger cycle
2. Gas exchange process

They can be further divided into discrete processes as shown in figure C.4 in which cylinder pressure is shown with respect to the crank angle for one complete cycle. The Seiliger cycle ends at point 6 which also marks the starting of the gas exchange process. They are explained briefly in the upcoming sections.

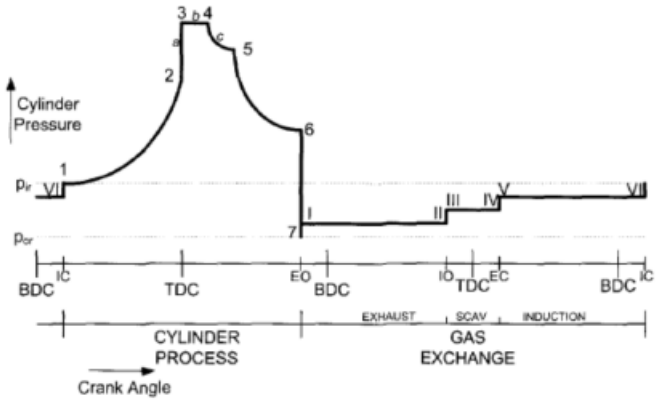

Figure C.4: In-cylinder processes w.r.t crank angle [5]

Seiliger Cycle

Seiliger cycle is an exceptional way to model the in-cylinder process. It uses the pressure ratio, volume ratio and temperature ratio of various stages to define the whole cycle. The Seiliger cycle consisted of 6 defined thermodynamic stages [6]. The station points between these stages are designated 1 to 6. The stages are as follows -

- 1-2 polytropic compression
- 2-3 iso-volumetric combustion, i.e. at constant volume,

- 3-4 isobaric combustion and expansion, i.e. at constant pressure
- 4-5 isothermal combustion and expansion, i.e. at constant temperature
- 5-6 polytropic expansion
- 6-1 iso-volumetric heat rejection to the environment, i.e. at constant volume

The process can be depicted in a p-V diagram as shown in figure C.5

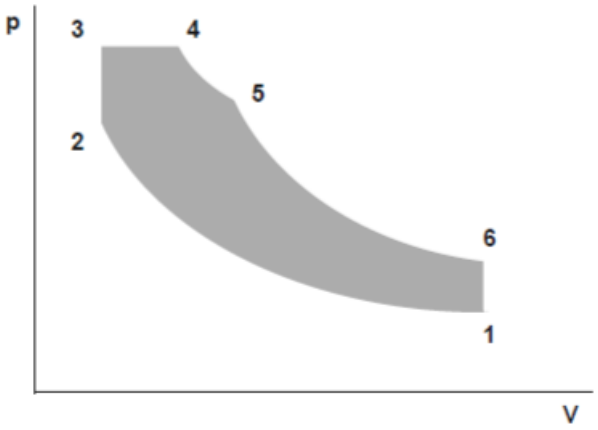

Figure C.5: Seiliger cycle P-V diagram [6]

The Seilinger cycle can analytically be defined as shown in table **??**. The parameters r_c and r_e is effective compression and effective expansion ratio whereas 'a', 'b' and 'c' are the combustion shape parameters. In stage 2-3 the iso-volumetric combustion takes place, therefore pressure increases at the same volume. Similarly, in stage 3-4 the pressure and stage 4-5 temperature remain constant. The extensive literature on the topic can be found in 'Diesel Engines Volume 1 - Performance Analysis' by D. Stapersma.

Stage	Volume ratio φ	Pressure ratio π	Temperature ratio τ
1-2	$\frac{V_1}{V_2} = r_c$	$\frac{p_2}{p_1} = {r_c}^{n_c}$	$\frac{T_2}{T_1} = {r_c}^{n_c-1}$
2-3	$\frac{V_3}{V_2} = 1$	$\frac{p_3}{p_2} = \mathrm{a}$	$\frac{T_3}{T_2} = \mathrm{a}$
3-4	$\frac{V_4}{V_3} = \mathrm{b}$	$\frac{p_2}{p_1} = {r_c}^{n_c}$	$\frac{T_2}{T_1} = {r_c}^{n_c-1}$
4-5	$\frac{V_5}{V_4} = \mathrm{c}$	$\frac{p_2}{p_1} = {r_c}^{n_c}$	$\frac{T_2}{T_1} = {r_c}^{n_c-1}$
5-6	$\frac{V_6}{V_5} = r_e$	$\frac{p_2}{p_1} = {r_c}^{n_c}$	$\frac{T_2}{T_1} = {r_c}^{n_c-1}$
6-1	$\frac{V_1}{V_2} = \frac{r_e \cdot c \cdot b}{r_c}$	$\frac{p_2}{p_1} = {r_c}^{n_c}$	$\frac{T_2}{T_1} = {r_c}^{n_c-1}$

Table C.1: **Seilinger cycle defined anaytically**

GAS EXCHANGE PROCESS

Gas exchange process consists of discrete processes like induction, exhaust and scavenging. During these processes, various mass flows involved enter and/or exit the system (cylinder). The gas exchange process in which the different mass flows enter the cylinder is shown in figure C.6.

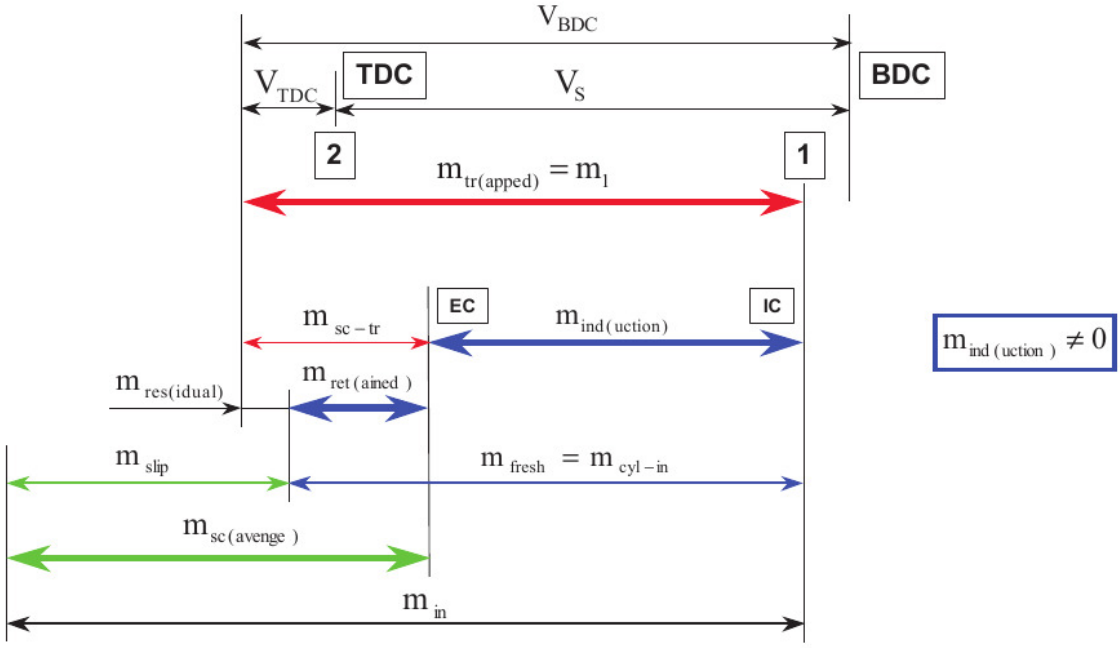

Figure C.6: Partition of mass flows at the inlet of a 4 stroke engine [5]

The mechanisms by which the air is swallowed into the engine, i.e. the air supply to the engine, that consists of three parts- namely induction mass($\dot{m_{ind}}$ during induction, pressurizing.

$$\dot{m_{in}} = \dot{m_{ind}} + \dot{m_{pr}} + \dot{m_{sc}} \tag{C.27}$$

- $\dot{m_{ind}}$ - Induction mass is the mass drawn into diesel engine by the movement of the piston during inlet stroke.
- $\dot{m_{pr}}$ - Pressurizing is the filling of the cylinder with fresh air from inlet receiver by opening the inlet valve. This equalizes the pressure between inlet receiver and cylinder.
- $\dot{m_{sc}}$ - When both inlet and exhaust valves are open, there is a pressure difference across the engine. The mass flow due to this is called scavenging mass. During scavenging, part of the mass is slipped ($\dot{m_{slip}}$ through the cylinder till the closing of the inlet or exhaust valve. The mass remained in the cylinder after closing both the valves is the retained mass ($\dot{m_{ret}}$. Now,

$$\dot{m_{sc}} = \dot{m_{slip}} + \dot{m_{ret}} \tag{C.28}$$

From equation C.27 and C.28 -

$$\dot{m_{in}} = \dot{m_{ind}} + \dot{m_{pr}} + \dot{m_{ret}} + \dot{m_{slip}} \tag{C.29}$$

The total trapped air inside the cylinder is the sum of fresh mass ($\dot{m_{fresh}}$) and a residual mass ($\dot{m_{ind}}$) leftover from the previous cycle. The fresh mass comes from induction, pressurizing and the retained mass. The retained mass together with residual mass constitutes the trapped mass ($\dot{m_{sc-tr}}$) in the cylinder after the scavenging. Therefore,

$$\dot{m_1} = \dot{m_{fresh}} + \dot{m_{res}} \tag{C.30}$$

$$\dot{m_1} = \dot{m_{ind}} + \dot{m_{pr}} + \dot{m_{ret}} + \dot{m_{res}} \tag{C.31}$$

$$\dot{m_{sc-tr}} = \dot{m_{ret}} + \dot{m_{res}} \tag{C.32}$$

During inlet stroke mass flows into the cylinder is the combination of discrete flows explained in the figure C.6. Similarly, the mass flows out of the cylinder to the exhaust receiver during exhaust stroke can also be divided into various discrete flows. In figure C.7 the partitions of the exhaust flow are shown.

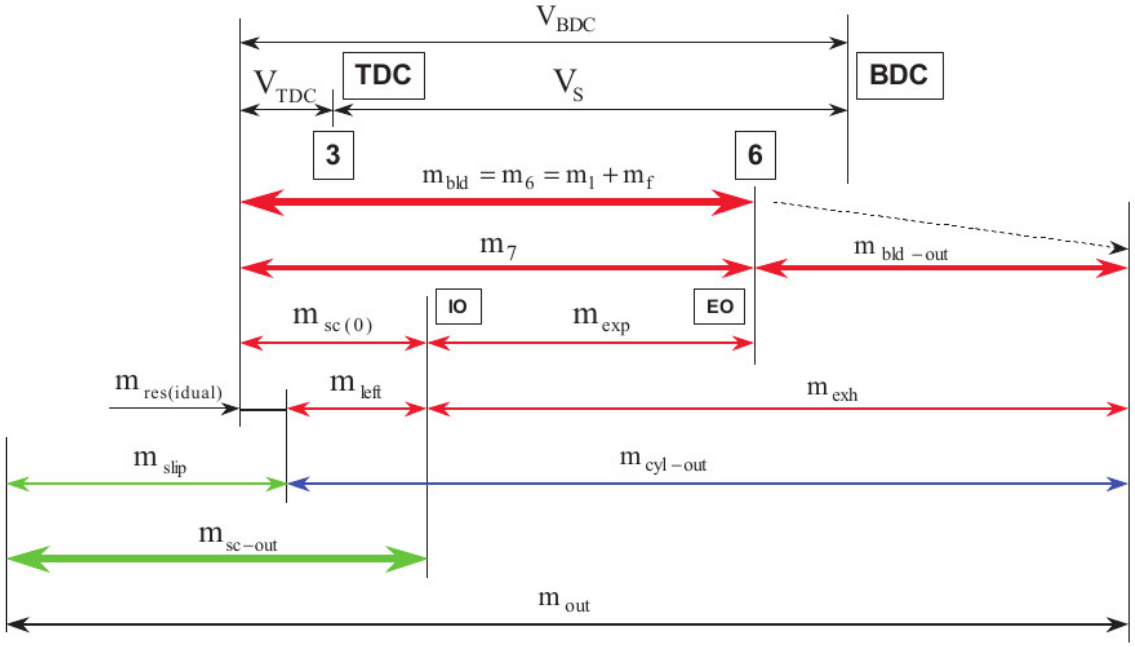

Figure C.7: Partition of mass flows at the outlet of a 4 stroke engine [5]

At Seiliger point '6', exhaust valve opens and blow down starts. A mass of blowdown flow ($\dot{m_{bld}}$) remains in the cylinder as residual foul mass ($\dot{m_{res}}$) and rest mass goes out of cylinder ($\dot{m_{cyl-out}}$). In other words,it can also be said that part of the flow is blown out ($\dot{m_{bld-out}}$) of cylinder and rest expands in the cylinder ($\dot{m_7}$). It can be said that,

$$\begin{aligned} \dot{m_6} &= \dot{m_{bld}} = \dot{m_1} + \dot{m_f} \\ \dot{m_{bld}} &= \dot{m_{cyl-out}} + \dot{m_{res}} \\ \dot{m_{bld}} &= \dot{m_7} + \dot{m_{bld-out}} \end{aligned} \tag{C.33}$$

The expanded mass is than exhausted out during exhaust stroke until inlet valve opens when scavenging begins such that

$$\dot{m_7} = \dot{m_{sc(0)}} + \dot{m_{exp}} \tag{C.34}$$

The total mass flow exhausted out of the cylinder is the sum of expelled mass ($\dot{m_{wxp}}$) and blown out mass ($\dot{m_{bld-out}}$). During scavenging part of the initial mass flows out of cylinder and rest remains as residual foul air. The flow coming out of the cylinder along with the slip mass from equation C.28 can be written as -

$$\begin{aligned} \dot{m_{out}} &= \dot{m_{cyl-out}} + \dot{m_{slip}} \\ &= \dot{m_{left}} + \dot{m_{exp}} + \dot{m_{bld-out}} + \dot{m_{slip}} \end{aligned} \tag{C.35}$$

C.0.6 FRICTION

The fuel consumption can be calibrated by manipulating mechanical losses. For modeling the friction in diesel engine, Chen-Flynn[47] is used which demonstrate the

mean friction effective pressure depends on the in-cylinder maximum pressure(P_{max}) and mean engine speed(n).

$$FMEP = A + B \cdot P_{max} + C \cdot n + D \cdot n^2$$

where A, B and C are constants:

- A - accounts for auxiliary losses.
- B - accounts for load effect of the engine.
- C, D - account as a quadratic law for the effect of the engine speed.

C.0.7 INLET AND OUTLET RECEIVER

The flow in and from the cylinder is divided into discrete flows (as explained in section 2.9), which mixed in the inlet and outlet receiver using standard volume element equations.

C.0.8 EXHAUST VALVE TEMPERATURE

Harsh et. al showed in his simulations that exhaust valve temperature is a critical parameter while finding the thermal limits for the diesel engine subjected to static back pressure. Exhaust valve temperature is estimated an exhaust valve estimator block modeled in the adopted model. The total heating of exhaust valve depends on the heating during the blow down process and cooling during the scavenging. The temperature of the exhaust valve is estimated with the help of in cylinder Sieliger parameters. It is a combination of cylinder temperature just before the opening of the exhaust valve (T6), representing heating during blow down, and inlet receiver temperature (T1), which represents cooling temperature during scavenging. Following equation is used to estimate the exhaust valve temperature.

$$T_{ev,est} = \frac{T_6 + r.T_1}{1 + r} \tag{C.36}$$

$$r = s^{0.8}.\left[\frac{T_1}{T_6}\right]^{0.25}.\left[\frac{EC - IO}{IO - EO}\right]^{0.2} \tag{C.37}$$

where

- s - Scavenge factor, defined as the ratio of the mean mass flow that goes through the engine during scavenging and the mean mass flow required for combustion.
- T_1 - blow down temperature
- T_6 - Inlet receiver temperature.
- EC - Angle at which exhaust closes
- IO - Angle at which inlet valve opens
- EO - Angle at which exhaust opens

ACKNOWLEDGEMENT

I am grateful to my supervisors, Rear-Admiral (ret.) Ir. K. Visser (TU Delft), and Mr. Harsh D. Sapra (Phd candidate, TU DELFT) for giving me the opportunity to work on this project and guiding me through out the tenure of the research project. I also thank them for their patience and relentless efforts. This work would be incomplete without the constant motivation and assistance provided by Chris Dijkstra, Marcel Roberscheuten, Arie V. Oord, Youri Linden at NLDA who provided me an opportunity to use their research laboratory and guided me during experiments. My acknowledgement would be incomplete without expressing the simple fact that where I stand today is solely due to my parents. I am truly grateful to my Father, S. Harjeet Singh, for his wisdom and inspiration. Alongside, my Father, I find myself truly blessed every time I think of my Mother, Manjit Kaur, for she is the bed-rock of my life and my family. Besides my parents, I am profusely in debt of my Brother, S. Pervinder Singh, and my Bhabhi, Simarjeet Kaur, for bestowing upon me the strength to keep going, no matter what. I also wish to thank my dearest nephew, Anhad Singh, who is my constant source of smiles and un-parallel happiness. With equal sincerity, I would also like to express my undying gratitude towards my very special friends, Arvind Poonia, Keshav Kala, Tushar Sharma, Vishwamber, Dhilshad ali, Ankit Shekhar. All of them stood beside me as the tides passed by, during the highs and the lows. Last but not the least, I would like to give a special thanks to my girlfriend Ravinder Kaur who motivated me whenever I was feeling lost. She stood with me and supported me during the master thesis project. Each and every one of them has contributed to my life and my work either through their words or their actions, and sometimes even both.

REFERENCES

[1] John Carlton. *Marine Propellers and Propulsion*. Butterworth-Heinemann, 2012.

[2] WOCE. Woce upper ocean thermal data. Available at https://www.ndbc.noaa.gov/view_text_file.php?filename=41001h2017.txt.gz&dir=data/historical/stdmet/ (2002).

[3] Harsh Sapra, Milinko Godjevac, Klaas Visser, Douwe Stapersma, and Chris Dijkstra. Experimental and simulation-based investigations of marine diesel engine performance against static back pressure. *Applied Energy*, 204:78 – 92, 2017.

[4] S. Chakrabarti. *Handbook of Offshore Engineering (2-volume set)*. Elsevier Ocean Engineering Series. Elsevier Science, 2005.

[5] D. Stapersma. *Diesel Engines: A Fundamental Approach to Performance Analysis, Turbocharging, Combustion, Emissions and Heat Transfer : Including Thermodynamical Principles. Pt. 1. Diesel Engines A : Performance Analysis and Turbocharging : WB4408A. Turbocharging, Volume 2*. TU Delft, 2010.

[6] D. Stapersma. *Diesel Engines: A Fundamental Approach to Performance Analysis, Turbocharging, Combustion, Emissions and Heat Transfer : Including Thermodynamical Principles. Pt. 1. Diesel Engines A : Performance Analysis and Turbocharging : WB4408A. Performance analysis, Volume 1*. TU Delft, 2009.

[7] International Maritime Organization. Resolution Mepc. Technical report, 2008.

[8] Jerzy Herdzik. Emissions From Marine Engines Versus Imo Certification and Requirements of Tier 3. *KONES Powertrain and Transport*, 18(2):162–167, 2011.

[9] M. I. Lamas and C. G. Rodríguez. Emissions from marine engines and NOx reduction methods. *Journal of Maritime Research*, 2012.

[10] Domkundwar V M. *Course in Internal Combustion Engines*. 2005.

[11] Richard Michael Avery Jr, Matthew Thomas Baird, Brian Andrew Lewallen, Tomislav Golub, and Peter Zagone. Engine control based on exhaust back pressure, March 16 2004. US Patent 6,708,104.

[12] Peter Hield. The effect of back pressure on the operation of a disel engine. Technical report, DEFENSE SCIENCE AND TECHNOLOGY ORGANIZATION VICTORIA (AUSTRALIA) MARITIME PLATFORMS DIV, 2011.

[13] Youssef Ismail, David Durrieu, Pascal Menegazzi, Pascal Chesse, and David Chalet. Potential of exhaust heat recovery by turbocompounding. Technical report, SAE Technical Paper, 2012.

[14] Jay A. Bolt, Stephen P. Bergin, and Frederick J. Vesper. The influence of the exhaust back pressure of a piston engine on air consumption, performance, and emissions. In *1973 International Automotive Engineering Congress and Exposition*. SAE International, feb 1973.

[15] Prof. R.Y.Patil Prashant P. Bornare, Dr. D. S. Deshmukh. Experimental investigation of backpressure variation on a single cylinder c.i engine system performance. *International Journal of Science, Spirituality, Business and Technology*, 2(2), may.

[16] Mohammad Uzzal Hossain Joardder, Md Uddin, Murari Mohaon Roy, et al. Effect of engine backpressure on the performance and emissions of a ci engine. International Conference on Mechanical Engineering 2011 (ICME2011), 2011.

[17] Nicolae Burnete, Dan Moldovanu, Doru-Laurean Baldean, and Levente Kocsis. Studies regarding the influence of exhaust backpressure on the performances of a compression ignited engine. In *Proceedings of the European Automotive Congress EAEC-ESFA 2015*, pages 141–149. Springer, 2016.

[18] S Cong, CP Garner, and GP McTaggart-Cowan. The effects of exhaust back pressure on conventional and low-temperature diesel combustion. *Proceedings of the Institution of Mechanical Engineers, Part D: Journal of Automobile Engineering*, 225(2):222–235, 2011.

[19] Mayank Mittal, Ron Donahue, and Peter Winnie. Evaluating the influence of exhaust back pressure on performance and exhaust emissions characteristics of a multicylinder, turbocharged, and aftercooled diesel engine. *Journal of Energy Resources Technology*, 137(3):032207, 2015.

[20] Constantine N Michos, Simone Lion, Ioannis Vlaskos, and Rodolfo Taccani. Analysis of the backpressure effect of an organic rankine cycle (orc) evaporator on the exhaust line of a turbocharged heavy duty diesel power generator for marine applications. *Energy Conversion and Management*, 132:347–360, 2017.

[21] X Tauzia, P Chessé, and A Maiboom. Simulation study of a ship's engine behaviour running with a periodically immersed exhaust. *Proceedings of the Institution of Mechanical Engineers, Part M: Journal of Engineering for the Maritime Environment*, 222(4):195–205, 2008.

[22] Ed Swain. Turbocharging the submarine diesel engine. *Mechatronics*, 4(4):349 – 367, 1994.

[23] Marek Idzior, Wojciech Karpiuk, and Maciej Bieliński. Operating problems of turbocharging systems in compression-ignition engines.

[24] Rowland S Benson and Norman Dan Whitehouse. *Internal combustion engines: a detailed introduction to the thermodynamics of spark and compression ignition engines, their design and development*, volume 1. Elsevier, 2013.

[25] Blair Kinsman. *Wind Waves: Their Generation and Propagation on the Ocean Surface (Dover Phoenix Editions) (Dover Phoneix Editions)*. Dover Pubns, 2002.

[26] C.A. Brebbia and S. Walker. *Dynamic Analysis of Offshore Structures*. Elsevier Science, 2013.

[27] Alan S Trenhaile and V Chris Lakhan. *Applications in coastal modeling*, volume 49. Elsevier, 1989.

[28] R.D. Geertsma, R.R. Negenborn, K. Visser, M.A. Loonstijn, and J.J. Hopman. Pitch control for ships with diesel mechanical and hybrid propulsion: Modelling, validation and performance quantification. *Applied Energy*, 206:1609 – 1631, 2017.

[29] SA Miedema and Z Lu. The dynamic behavior of a diesel engine. In *Proceedings of the WEDA XXII technical conference and 34th Texas A&M dredging seminar, Denver, Colorado, USA*, 2002.

[30] Francesco Baldi, Gerasimos Theotokatos, and Karin Andersson. Development of a combined mean value–zero dimensional model and application for a large marine four-stroke diesel engine simulation. *Applied Energy*, 154:402 – 415, 2015.

[31] A Aziz Hairuddin, Talal Yusaf, and Andrew P Wandel. Single-zone zero-dimensional model study for diesel-fuelled homogeneous charge compression ignition (hcci) engines using cantera. *International Journal of Automotive & Mechanical Engineering*, 13(2), 2016.

[32] Kenan Murić, Ola Stenlåås, and Per Tunestål. Zero-dimensional modeling of nox formation with least squares interpolation. *International Journal of Engine Research*, 15(8):944–953, 2014.

[33] S Galindo Lopez. Three-zone in-cylinder process model for di diesel engines. 2014.

[34] Paulus Johannes Maria Schulten. *The interaction between diesel engines, ship and propellers during manoeuvring*. PhD thesis, TU Delft, Delft University of Technology, 2005.

[35] Dileep N Malkhede, Bhartendu Seth, and HC Dhariwal. Mean value model and control of a marine turbocharged diesel engine. Technical report, SAE Technical Paper, 2005.

[36] H Grimmelius, EJ Boonen, H Nicolai, and D Stapersma. The integration of mean value first principle diesel engine models in dynamic waste heat and cooling load analysis. In *CIMAC Congress, Bergen, Norway*, volume 31, page 51, 2010.

[37] Gerasimos Theotokatos and Vasileios Tzelepis. A computational study on the performance and emission parameters mapping of a ship propulsion system. *Proceedings of the Institution of Mechanical Engineers, Part M: Journal of Engineering for the Maritime Environment*, 229(1):58–76, 2015.

[38] GG Dimopoulos, Ch A Georgopoulou, and NMP Kakalis. Modelling and optimisation of an integrated marine combined cycle system. *ECOS*, pages 4–7, 2011.

[39] D. Stapersma. Calibrating and matching the mean value first principle diesel engine model. *(KIM-PFS-2011-188)*, Issue A and Isuue B, 2015.

[40] HT Grimmelius and D Stapersma. Control optimisation and load prediction for marine diesel engines using a mean value simulation model. In *Conference proceedings ENSUS 2000, September 4-6*, pages 212–229. University of Newcastle upon Tyne, 2000.

[41] Sangram Kishore Nanda, Boru Jia, Andrew Smallbone, and Anthony Paul Roskilly. Fundamental analysis of thermal overload in diesel engines: Hypothesis and validation. *Energies*, 10(3), 2017.

[42] F. Cardarelli. *Materials Handbook: A Concise Desktop Reference*. Springer International Publishing, 2018.

[43] By Tim Johnson. Diesel engine emissions and their control. *Platinum Metals Review*, 52(1):23–37, 2008.

[44] Ibrahim S Seddiek and Mohamed M Elgohary. Eco-friendly selection of ship emissions reduction strategies with emphasis on sox and nox emissions. *International Journal of Naval Architecture and Ocean Engineering*, 6(3):737–748, 2014.

[45] HT Grimmelius and P Baan. *Doorontwikkeling modulair simulatiemodel van een dieselmotor*. WbMT, 1998. OVS 98/25.

[46] C Dijstra. Description of simulink mean value diesel engine model 'deii', dms 04/10, internal report.

[47] Simon K Chen and Patrick F Flynn. Development of a single cylinder compression ignition research engine. Technical report, SAE Technical Paper, 1965.